Università degli Studi di Cagliari

Scienze e Tecnologie Chimiche

XXVIII CICLO

CRYSTAL ENGINEERING OF MOF BASED ON POLYPYRIDYL LIGANDS AND COORDINATIVELY UNSATURED Ni^{II} IONS

CHIM/03

Presentata da: Romina Lai

Coordinatore Dottorato: Prof. Mariano Casu

Tutor: Prof. M.Carla Aragoni

Esame finale anno accademico 2014 – 2015

Ringraziamenti

La prima persona che vorrei ringraziare è la Professoressa M.Carla Aragoni, per avermi dato questa opportunità, per il suo incommensurabile contributo scientifico a questo lavoro di ricerca, per la sua disponibilità, per avermi sempre incoraggiata e per tutti i suoi preziosi consigli.

Grazie a tutto il gruppo di ricerca, al Professor Vito Lippolis, alle Dottoresse Claudia Caltagirone ,Alessandra Garau, al Prof Franco Isaia e ad Antonio Sabeddu per il quotidiano supporto.

Un grazie particolare al Professor Massimiliano Arca per la sua consueta disponibilità e per aver spesso e volentieri risolto in un click tanti dei miei dubbi.

Un ringraziamento sentito va alla Dottoressa nonchè grande amica Anna Pintus, perchè senza di lei non sarei quella che sono oggi. Grazie al suo coraggio, caparbietà e ad avermi esortata a non mollare mai e a scegliere spesso le strade più difficili per poi uscire vittoriosi e orgogliosi di se stessi.

Grazie al Professor Simon Coles e a tutto il suo gruppo di ricerca, per avermi dato la possibilità di trascorrere un periodo altamente produttivo presso il National Crystallography Service dell'Università di Southampton.

Grazie alla Professoressa Maura Monduzzi per essere sempre stata presente e al Professor Guido Ennas per la sua preziosa collaborazione.

Un ringraziamento speciale alla Dottoressa e grande amica Martina Olivari, per avermi supportata nei momenti di sconforto per aver riso a crepapelle durante i miei disastri in laboratorio e per aver addolcito i miei momenti no con dei cioccolatini.

E un grazie alle dottoresse Patrizia Pitzanti Laura Maiore ed Enrica Tuveri per tutte le risate e per i momenti passati insieme in studio..

Grazie a tutti i colleghi Dottorandi e Post-doc della sala dottorandi. Per tutti i momenti passati assieme e in particolare al Dottor Luca Medda e alla dottoressa Francesca Cugia siete stati una parte importantissima del mio percorso. Grazie ai Dottori Arianna Casula, Valentina Cabras e Nicola Melis con cui ho condiviso tanti momenti che porterò sempre con me.

Un grazie grande a tutti gli studenti studenti, Walter, Carlo, Gabriele, Enrico e Matteo per tutte le volte che mi hanno fatto arrabbiare, sorridere e urlare "svuotate la potassa!" ma soprattutto perchè sono cresciuta professionalmente anche grazie a loro.

Il grazie più importante va ovviamente alla mia Famiglia e ai miei Amici perchè continuano ad esserci in ogni istante della mia vita.

Summary

List of Tables

List of Schemes

List of Figures

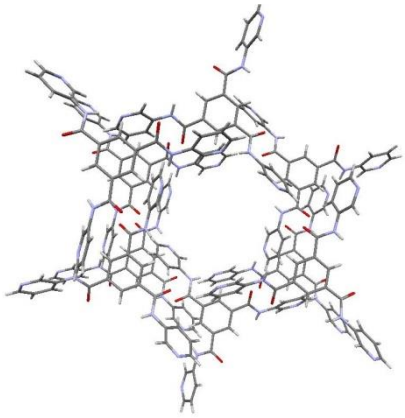

What is Supramolecular Chemistry?

J. M. Lehn ***"Supramolecular chemistry is the chemistry of the intermolecular bond, covering the structures and functions of the entities formed by the association of two or more chemical species"***

F. Vögtle ***"In contrast to molecular chemistry, which is predominantly based upon the covalent bonding of atoms, supramolecular chemistry is based upon intermolecular interactions, i.e. on the association of two or more building blocks, which are held together by intermolecular bond"***

1 Introduction

1.1 Supramolecular Chemistry

Supramolecular chemistry is a branch of chemistry that embraces many different research areas of chemistry such as organic and inorganic chemistry, biochemistry, material chemistry and studies the properties of different compounds for possible practical applications. Supramolecular chemistry was first described by J.M Lehn as the chemistry beyond the molecule.[1] Fig. 1.1, illustrate an example of the differences among molecular and supramolecular chemistry: whilst traditional chemistry focuses on the covalent bond, supramolecular chemistry is concerted only with weak and reversible non covalent intermolecular interactions that occur between, rather than within molecules. Intermolecular interactions include metal-ligand (M-L) coordination bonds, hydrogen-bonding, π-π donor-acceptor interactions, van der Waals (vdW), electrostatic and hydrophobic forces. These non-covalent interactions differ in strength and directionality ranging from hundreds kilojoules per mole for the strongest ones (typically ~200 $kJ \cdot mol^{-1}$ for M-L coordination bonds) to a few kilojoules per mole for the weakest ones (2-25 $kJ \cdot mol^{-1}$ for hydrogen bonds or π-π interactions). Supramolecular chemistry embraces important concepts and construct mechanisms that include host-guest chemistry, molecular recognition and self-assembly, molecular folding, mechanically-interlocked molecular architectures, and reversible and dynamic covalent chemistry.[2] These interactions and assembly processes are reversible and under thermodynamic control, and gaining control over the forces responsible for the formation of these supramolecular entities that possess the capability of "self-correction" is challenging and difficult.[3] Anyway many efforts have been made to control the assembly processes to create deliberate supramolecular networks starting from properly designed building blocks. When these methods are specifically applied to crystalline solids, it leads to the area of crystal engineering.[4]

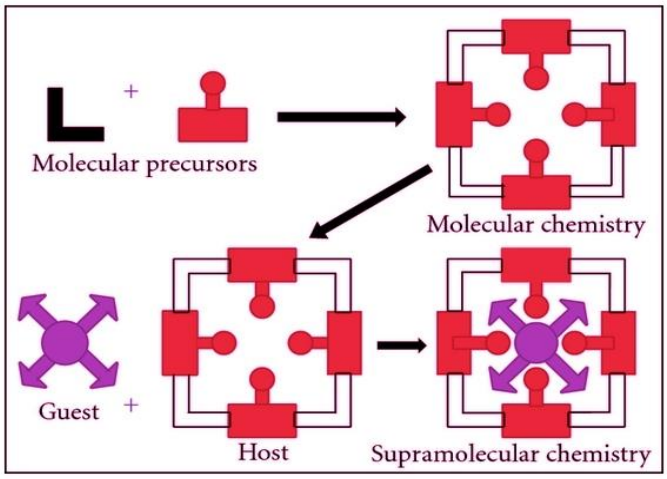

Figure 1.1 A Schematic Illustration of the Difference among Molecular and Supramolecular Chemistry in Structural Terms.[1]

1.1.1 Crystal Engineering

Crystal Engineering is an important area of supramolecular chemistry which aims to design and synthesize new solids with desired structural, chemical, and physical properties,[4] by applying the knowledge of the steric, topological and intermolecular bonding capabilities of the constituent building blocks. The term crystal engineering was introduced by Pepinsky in 1955 when he revealed controllable unit cell dimensions and symmetries with metal organic complexes, identifying the importance of intermolecular interactions in determining the solid-state structure of crystals.[5] Consideration of all types of interactions present within the crystal is needed in order to design and build a desired structure since during the crystallization process the individual synthons 'find' and interact with each other in solution to form the final structure in a spontaneous way. Desiraju firstly defined the term supramolecular synthon as "structural units within supermolecules which can be formed and/or assembled by known or conceivable synthetic operations involving intermolecular interactions".[6] A synthon is therefore derived from designed combinations of interactions. As an example, the complementary hydrogen bonds between two carboxylic acid moieties form the well-known carboxylic acid dimer,[7] and this spatial arrangement coming from an intermolecular interaction is termed a supramolecular synthon.[8]

[1] Image from website: http://www.hindawi.com/journals/isrn/2012/474830/fig1/

These supramolecular synthons are dependent on the types of intermolecular interactions that occur in the solid state. Recurring motifs between functional groups are termed supramolecular synthons and the molecular building blocks of the structure are referred to as tectons (Fig. 1.2). Crystal engineering is an emerging discipline whereby practitioners aim to arrange molecules, both organic and metal-organic, in the crystalline phase by rational design. This challenge requires the exploitation of well-known supramolecular glues such as hydrogen bonding and coordinate bonding. These are augmented by a myriad of nominally weaker and less directional noncovalent interactions that, increasingly, are being demonstrated as important in crystal structure design. Applications in fields as diverse as pharmaceuticals, photoluminescent materials, and metal-organic frameworks for gas storage are some of the motivations for crystal engineering that draw together scientists from a wide range of disciplines. Applications of crystal engineering span from organic to metal-organic and inorganic realms and include co-crystal formation, solid-state reactions, and metal-organic framework structures.

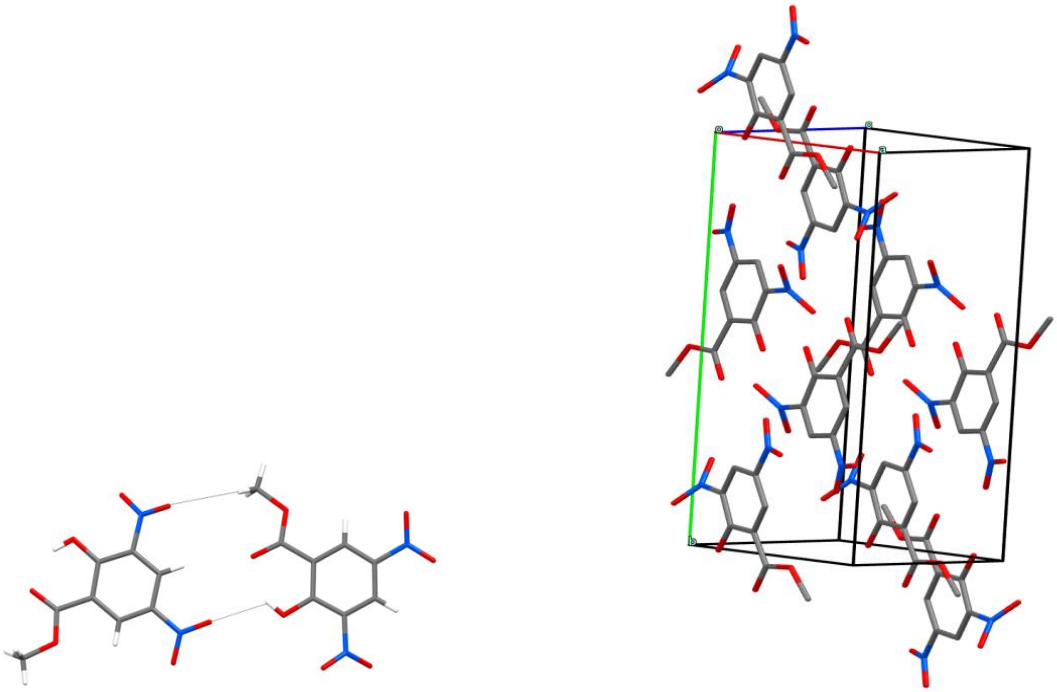

Figure 1.2 (a) Hydrogen Bonding and (b) Crystal Packing for methyl 3,5-dinitrosalicylate.

1.1.2 Self-Assembly

Molecular self-assembly is the spontaneous self-organization[9] of building blocks into ordered structures, held together through weak intermolecular forces. Therefore this implies that the interacting tectons are previously designed and capable to assemble without any external assistance. This type of approach has been named as reticular synthesis and involves supramolecular synthons, which

when combined, form 'molecular building blocks' (MBBs), forming the final structure. To predict the structure that forms, it is first necessary to have a knowledge of the interactions involved in the self-assembly processes. Because of the weakness of such binding interactions, the formation of supramolecular assemblies is often thermodynamically influenced, since results from spontaneous self-assembly processes, rather than from sequential bond-forming processes. Self-organization is the real driving force that leads to realization of supramolecular constructs.[10] After a first step, that involves the complementary molecular recognition among the structural subunits, the growth of a supramolecular structure progresses through sequential selective binding motifs, according to cooperative or linear behaviors. The crystallization is a self-assembly process, where the individual synthons interact with each other in solution to form the structure in a spontaneous way. There are two main kinds of self-assembly processes:

- Crystal self-assembly: A non-equilibrium process in which both kinetic and thermodynamic factors contribute to the structure construction. Structures that form faster may incurring polymorphism phenomena.
- Solution self-assembly: A thermodynamically controlled equilibrium where components assemble into the structure of maximum stability.

Therefore the choice of the structural motifs is crucial in supramolecular chemistry, because it goes to determine the specific physical and chemical properties of the final structure. Next paragraphs will present the main factors that dictate the ways followed by molecules to aggregate in the solid state, including a description of the diverse types of non-covalent interactions and other crystal packing principles that have being identified as being important in stabilizing crystal structure.

1.1.3 Ion-Ion Interactions

Ionic bonding is defined as an electrostatic attraction established between two ions of opposite charge. It is formed between atoms or groups of atoms where is occurred an exchange of electrons: the atom or the atomic group which provides electrons becomes a positive ion (cation), and the atom or the atomic group that acquires electrons turns into negative ion (anion). This bond typically occurs between metals and non-metals in salts where atoms with low ionization energy combines with atoms with high electron affinity. A common example of ionic compound is the sodium chloride salt. In this molecule the sodium loses an electron, forming a cation, and the chlorine atom gains an electron to form an anion. The resulting ions arrange in the solid state in order to maximize the electrostatic attraction by multiple ionic interactions so that each chloride anion is surrounded by six sodium cations and vice versa, in an infinite array of ions with the well-known face-centered

cubic (fcc) lattice.[11] Fig.1.3 shows two examples of synthons formed by ionic components held together through ion-ion interactions.

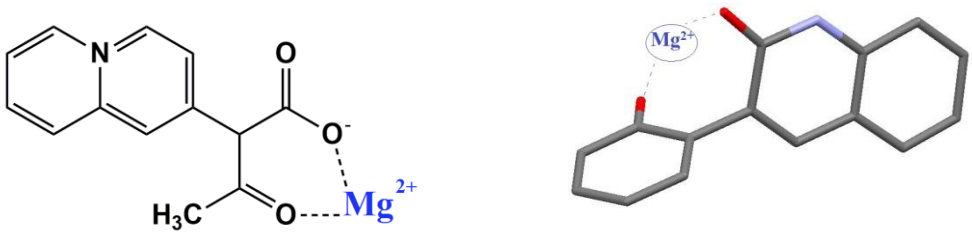

Figure 1.3 Two Examples of Ion-Ion Interaction between Oxygen and Magnesium Cation.

1.1.4 Ion–Dipole Interactions

Ion-dipole interactions are among the most intense and common interactions found in Supramolecular Chemistry and have great important in the solutions since they mainly involve solvents molecules polar in nature and the ionic species dissolved: cations and anions are always surrounded by solvent molecules. Ion-dipole interactions feature energies comprise in the range between 50 and 200 kJ·mol^{-1}, and became stronger with the increase of the ionic charge and the dipole moment, and depend on the temperature.[11] An illustrative example of ion-dipole interactions is that occurring between Na^+ and H_2O (Fig. 1.4a). Other peculiar examples, typical of the host-guest supramolecular branch, are provided by the inclusion complexes between metal cations and crown ethers (Fig. 1.4 b).

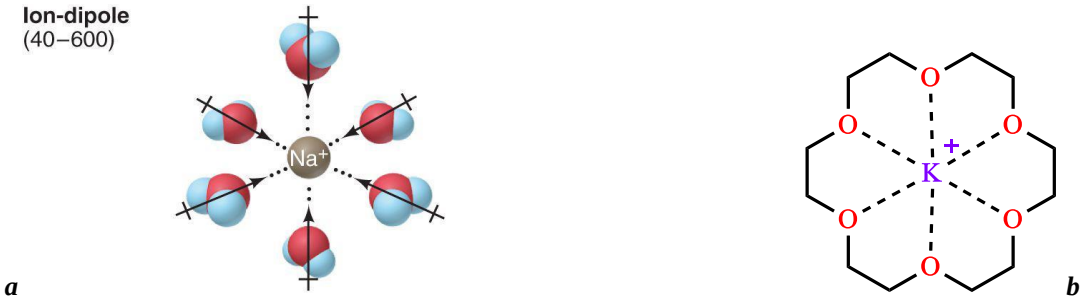

Figure 1.4 Examples of Ion-Dipole Interaction (a) Na^+ Hydrated Ion. (b) K^+ Crown Ether Complex.[2]

[2] Imagine from website: https://www.studyblue.com/notes/note/n/chem-1203-review/deck/5805625.

1.1.5 Dipole-Dipole Interactions

Dipole-dipole interactions are attractive forces quite weaker than ion-dipole forces that involve neutral polar molecules. This electrostatic attraction is established between a polar molecule bearing a partial positive charge δ^+ and another one featuring a partial negative charge δ^-. They are weak (5 - 20 kJ mol^{-1}) and short-range interactions electrostatic in nature, significant only if the dipoles are separated by short distances.[12] If two molecules have the same mass and size, dipole-dipole forces increase with increasing polarity.

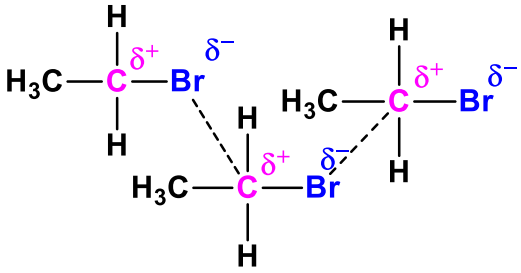

Figure 1.5 Example of Dipole-Dipole Interactions between Alkyl Halides.

1.1.4 Hydrogen-Bonds

Exhaustive reports on hydrogen bond can be found in the literature,[12] and a detailed description of this bond is far from the aims of this work, and we illustrate here just few peculiarities on these kinds of interactions. Hydrogen bonding is a particular type of dipole-dipole interaction featuring bond strength (4-120 kJ mol^{-1}) significantly higher than similar intermolecular forces. It is formed when one or more hydrogen atoms are covalently bonded to a more electronegative element such as Cl, O, N, thus creating a dipole D-H [where the D atom is named ***donor***] in which the hydrogen atom has a partial positive charge and can interact with a second electronegative atom called ***acceptor*** *(A)* that owns a lone pair available thus forming a D-H···A bond. Although they are weaker than conventional bonds, hydrogen bonds have great influence on the properties of hydrogenated compounds (eg. density, viscosity, vapor pressure and acid-base character etc.) and in contrast to covalent bonds, they are reversible and their strength depends on the chemical environment, and depending on the fact that donor and acceptor atoms are located on the same molecule on in different ones, they can be intramolecular or intermolecular respectively.

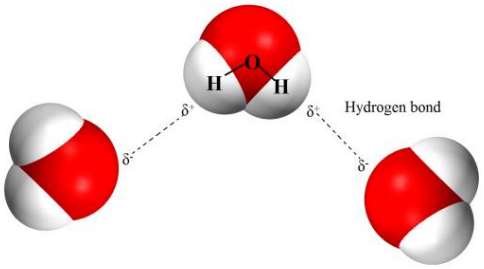

Figure 1.6 3D Model of Hydrogen-Bonds in Water.

Hydrogen bond is characterized by a specific directionality and great versatility therefore, a suitable setting of the external parameters permit to forecast chemical and physical properties of supramolecular molecule based on this kind of interaction.[13] Not by chance hydrogen bonds have been widely used in supramolecular chemistry in dendrimers and polymers synthesis (Fig. 1.7).

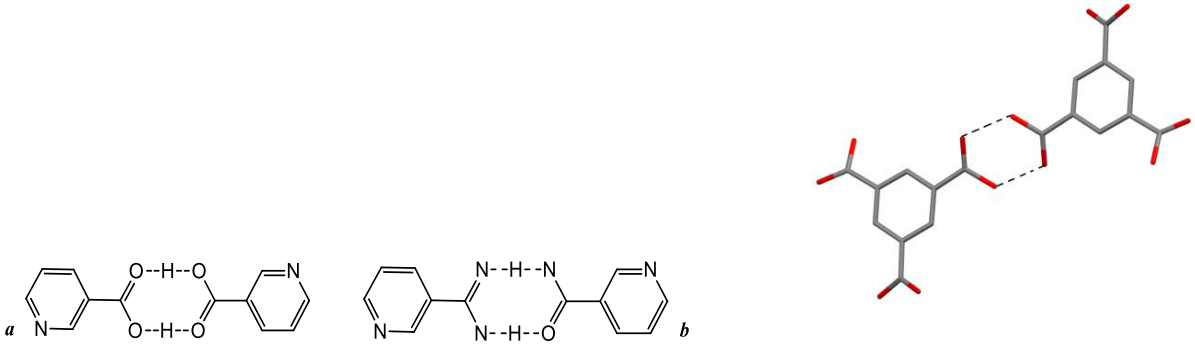

Figure 1.7 Self-Complementary Dimers of Carboxylic Acids (a), Carboxamides (b). An example of Intermolecular Hydrogen Bonding in a Self-Assembled Dimer Complex.

The hydrogen bond lengths (r) depend on many factors such as nature of the involved atoms, interaction strength, temperature, pressure, and varies from 1.2 to 2.3 Å. Based on their lengths and strengths, G.A Jeffrey and W. Saenger divided hydrogen bonds into three general categories: weak (0.01-0.02 kJ mol^{-1}), medium (0.63 kJ mol^{-1}), and strong (above 0.63 kcal mol^{-1}).[14] Hydrogen bonds are often rationalized in terms of geometric parameters[15] such as bond angles and D⋯A or H⋯A distances (Fig. 1.7). In a typical hydrogen bond the donor interacts with one acceptor forming a linear interaction (although experimentally, θ is normally smaller than 180°).

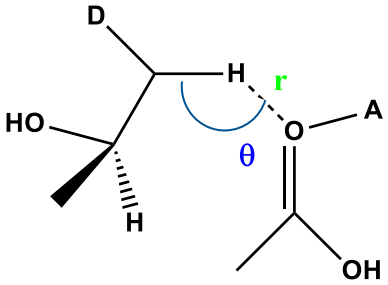

Figure 1.8 Representation of Hydrogen Bond.

1.1.6 *π-π* Interactions

These interactions are among the principal and most important non-covalent forces and play an important role in supramolecular host-guest system and in self-assembly processes.[16] π-π stacking is referred to as the ensemble of weak electrostatic interactions occurring between aromatic rings due to the intermolecular overlapping of p-orbitals in π-conjugated systems that determines stabilization in the system.[17] This charge re-distribution overall the whole π–π system also leads to a induced negative dipole above and below the plane of the conjugated carbon system, and a positive dipole inside of the hydrogen atoms system. The most important geometry types of aromatic π–π interactions are:

-Face-to-face (C···C) interactions are present when two or more aromatic rings are parallel disposed with distances in the range of 3.3-4.0 Å. Due to electrostatic repulsions, perfect facial alignments are quite uncommon, and slipped arrangements are more often found.

-Edge to face (C-H···π) interactions occur when the positive hydrogen rim of one conjugated system is directed towards the π-system of another.

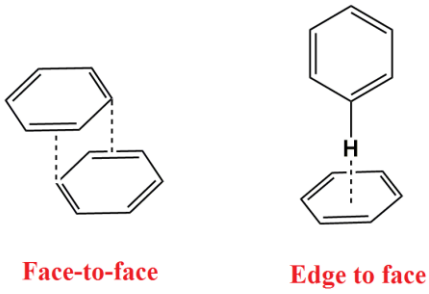

Figure 1.9 Face-to-Face and Edge-to-Face Aromatic π –π Interactions.

1.1.5 Van Der Waals Forces

Van der Waals Forces are weak attractive and repulsive forces between molecules generated by the presence of induced dipoles. They are very low magnitude (1 kJ mol^{-1}) and not directional intermolecular forces that act only at very short range since their strength is a function of r^{-6}. The origin of these forces can be sought in the electrostatic interaction between electron clouds of the involved atoms, which is modified by the presence of neighboring atoms molecules and the surrounding environment. As a consequence, van der Waals forces become very important during the crystallization processes when atoms and molecules have saturated their forming chemical bonds possibilities and interact each other packing in order to form the more stable solid structure. In supramolecular chemistry, they are important in the formation of inclusion compounds where organic molecules are incorporated within crystalline lattices or molecular cavities, e.g. the inclusion of toluene within the molecular cavity of the p-tert-butylphenol-based macrocycle, p-tert-butylcalix[4]arene.[18]

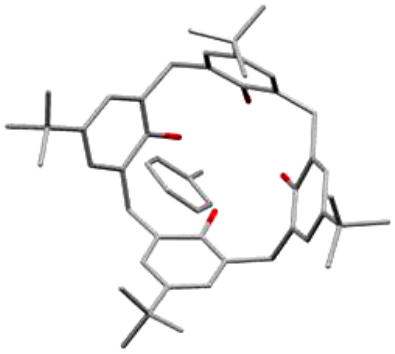

Figure 1.10 Two Examples of Inclusion Complex between Toluene and p-tert-butylcalix arene and between water and p-tert-butylcalix arene.

1.1.7 Metal-Ligand Bond Coordination

In a very simply and schematic way, we can describe a coordinative metal-bond as the donor-acceptor interaction between a Lewis acid (the central metal ion) and a Lewis base (ligand), Fig. 1.11. The atom of the ligand that directly participates in the formation of the bond with the metal ion is called donor atom; the metal ion is the atom acceptor by using its empty or partially filled d-orbitals.

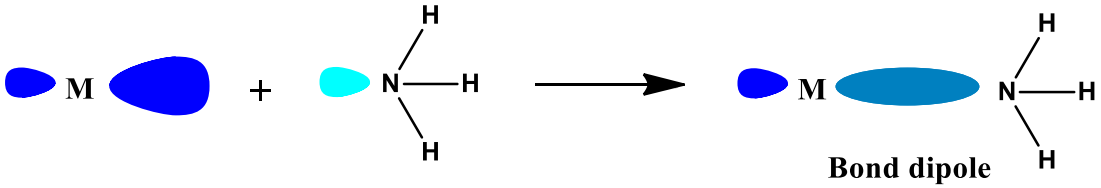

Figure 1.11 Representation of the Metal-Ligand Bond Formation. The ligand ammonia donates electron to the metal through sp^3 hybrid orbital.

Without getting in the details of the nature of this bond, we just want to evidence here that coordination bonds are particularly interesting in the field of supramolecular chemistry, and in particular in the crystal engineering, thanks to the high grade of control obtainable by using metal ions or metal complexes as building blocks in the construction of extended structures usually referred to as coordination polymers (see below). In fact coordination bonds are high directional and lead to geometries predictable on the bases of the metal ion used coordination, and a large variety of metals having different coordination numbers and geometries are known and easily available. Moreover the coordination bond is strong (100-500 kJ mol^{-1}) thus warranting the formation of robust networks, but it is governed by thermodynamic equilibria and can be reversibly replaced and/or modify by varying the ligands or the experimental condition used. Moreover, the impressive number of existing coordination compounds provides a very rich library of different metal-ligand synthons that can be used to design and prepare coordination polymers.[19]

1.2 Coordination Polymers and Metal-Organic Frameworks

Coordination Polymers are infinite systems built up by metal ions and organic ligands through coordination bonds and weak interaction. They are usually crystalline compounds and can extend infinitely into one, two or three dimensions by covalent metal-ligand bonding. The self-assembly processes involving metal ions and well-designed organic ligands is became the most employed approach in the construction of coordination polymers with predetermined molecular architecture. [20]

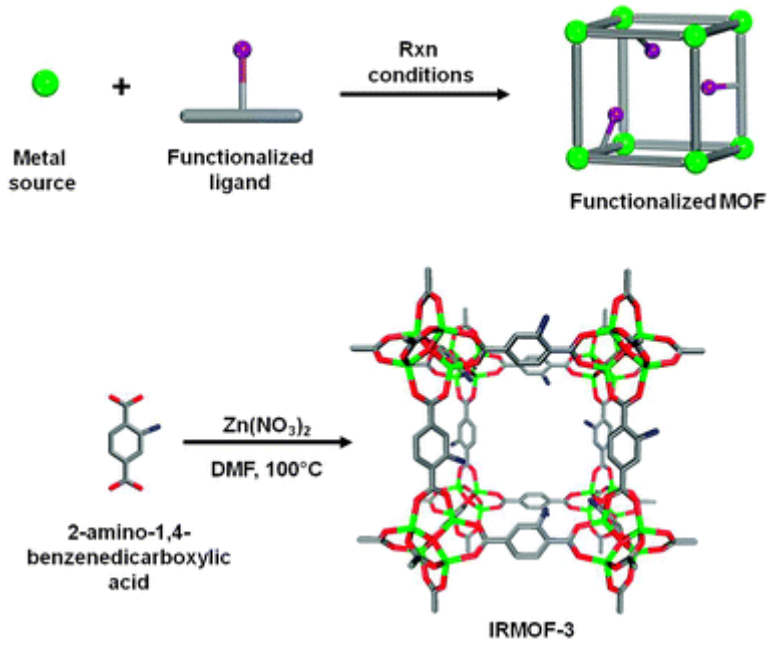

Figure 1.12 Coordination Polymers Assembly.[3]

1.2.1 Dimensionality and Motifs

Coordination polymer architectures certainly depend from characteristic and self-assembly capabilities of the molecular building blocks. In fact crystal structure and dimensionality of the polymeric networks are strongly influenced by the coordination geometry of the metal node and by organic ligand features such length, rigidity, geometry and nature, number, and position of the donor atoms. Transition metals are widely used as nodes since they provide various and easily predictable features such as oxidation state, coordination numbers and geometries (linear, square-planar, tetrahedral, square-pyramidal, trigonal-bipyramidal, octahedral, trigonal-prismatic, pentagonal-bipyramidal) that can be used to direct a particular desired assembly. As an example, metals such as Ag^{I}, which adopt linear coordination geometries, can be used to form one-dimensional polymers combined with linear ligands; whereas metal ions such as Zn^{II} and Ni^{II} that usually adopt tetrahedral or octahedral coordination geometries can be employed to form three-dimensional networks (Fig. 1.13

[3] Image from K.K.Tanabe, S.M. Cohen, *Chem. Soc. Rev.*, **2011**, 40, 498-519.

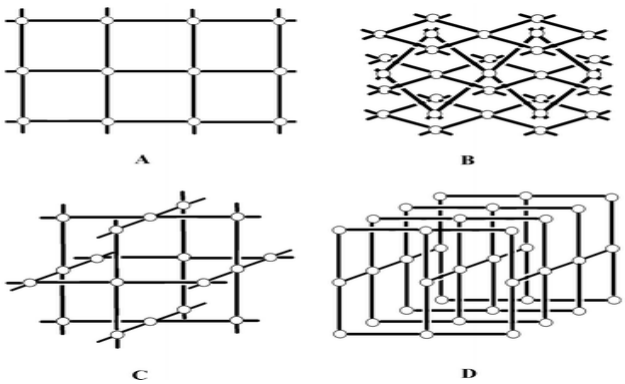

a

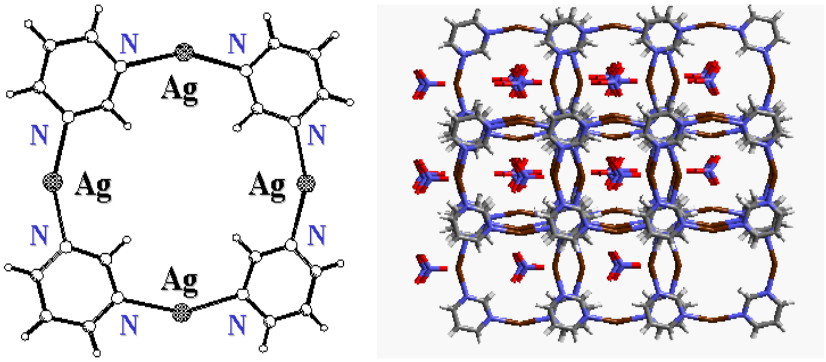

b

Figure 1.13 Topology of Frameworks observed for Coordination Polymers based upon linear, octahedral or square-planar nodes and linear bridging ligands: A, square grid planar network; B, 3-D structure by inclined interpenetration of square grids; C, 3-D network of NbO type; D, 3-D network of $CdSO_4$ type.[4]

The topology of coordination polymers also depends on the ligand, and when different conformations and binding modes are possible for the same ligand, unexpected and unpredictable structures can be obtained. This is the reason why rigid spacers such for example 4,4'-bipyridine are often preferred in order to overcome this problem. Many of the organic ligands exploited in the construction of coordination polymers contain oxygen and nitrogen donor atoms, in particular carboxylate- and piridyl-based spacers. Some common examples of N-donor and O-donor ligands are given in figure below.

---

[4] Image from: I. Boldog, E B. Rusanov, A.N.Chernega, J. Sieler, K. V. Domasevitch, *J. Chem. Soc., Dalton Trans.*, **2001**,12, 893-897(a), M.Hakansson, H.Eriksson, S.Jagner, *Inorganica Chimica Acta*, **2006**,359, 2519-2543(b).

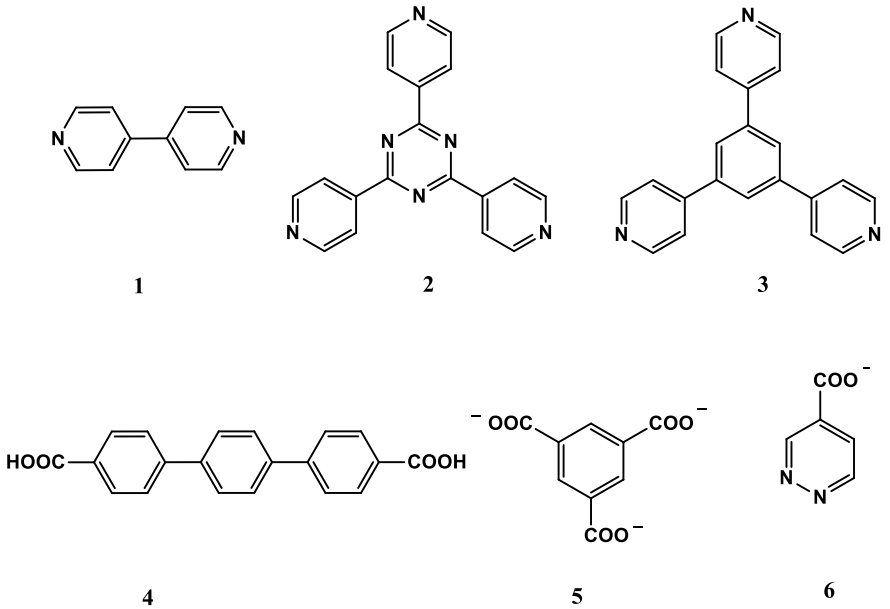

Figure 1.14 Formula Structures of Common Organic Ligands used in Coordination Polymers Synthesis. Pyridine ligands (1,2,3). Carboxylic ligands (4,5,6,).

One of main interests in the construction of coordination polymers is the obtaining of new functional materials, with modulated properties. Coordination polymers in fact, have potential applications in various sectors, such as gas storage, ion exchange, catalysis, conductivity, luminescence, chirality, magnetism, nonlinear optics or deposition of thin layers, often related to the existence of empty cavities inside the network (see also § 1.2.3).[21]

1.2.2 Synthesis

To realize a certain desired framework, is very important a clever choice of metals ions, ligands, and framework motifs. Typically, coordination polymers and MOF are synthesized by combining organic ligands and metal salts in solvothermal conditions (usually 120–260° C) in high-pressure chambers (autoclave). During the reaction it is also necessary to control the temperature, the concentrations and the extent of solubility of the reactants in the solvent, and finally the pH of the solution, in order to obtain single crystals suitable for X-ray diffraction. Other different synthetic methods are reported in literature such as reactions in non-miscible solvents,[22] electrochemical reactions,[23] while ultrasonic and microwave methods are less used at this time. In order to obtain the solid product saturation methods are applied. In this process crystals grow from the saturated solution by slow evaporation of the mother liquor. Diffusion methods are preferred to get single crystals suitable for X-ray diffraction analysis especially if the products are poorly soluble. Various methods

can be applied for such a process like solvent liquid diffusion, slow diffusion of reactants etc. Crystallization processes are very hard to predict and isomerism phenomena may occur leading super structural diversity for a given molecule.[24]

Polymorphism : is generally defined as the possibility of a given compound to exist in different molecular arrangements and or different conformations, Fig. 1.15. In this context thermal and kinetic effects play an important role into determine which crystal structures can be isolated.[25]

Structural Isomerism : it has been defined by B. Moulton and M. J. Zaworotko[26] as the existence of different superstructures obtained by the same building blocks. The resulting supramolecular networks can be described as effectively different compounds even though their empirical formula and chemical components are identic.

Conformational polymorphism : is closely related to building blocks conformation and occurs when different supramolecular structures are formed due the different conformations of flexible ligands and/or in some cases caused from solvent molecules present in the structure.[27]

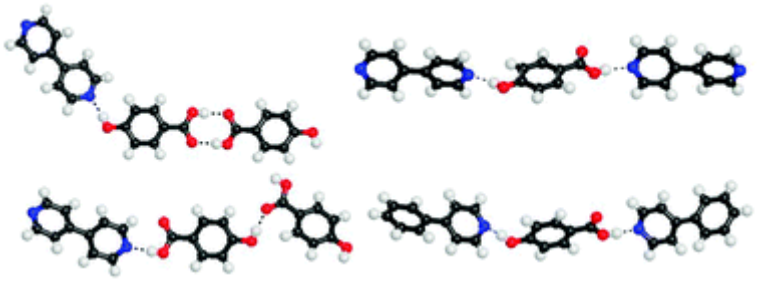

Figure 1.15 Example of Polymorfism in in Co-crystals of 4,4′-bipyridine and 4-hydroxybenzoic acid.[5]

1.2.3 Metal Organic Frameworks

Metal-organic frameworks (MOFs) represent a relatively new class of inorganic-organic hybrid compounds containing metal ions connected by organic bridging ligands through coordinative bond and weak interactions, in extended structures. MOF are characterized by robust networks built up through strong coordinative bonds (energies of about 360 kJ mol^{-1}), comparable to those of C-C single bonds. The structures can contain different metal-ligand linkages and can be mono-dimensional (1D), bi-dimensional (2D) or three-dimensional (3D), and are usually characterized by the presence of voids within the framework able to accommodate organic guest molecules for a number of applications (§ 1.2.3.1).[28] In the ligand structure is possible identify two basic components: the functional groups coordinating (linker), which connect the metal nodes in a determined

[5] Image from: A. Mukherjee,G.R. Desiraju, *Chem. Commun.*, **2011**,47, 4090-4092.

geometry, and the spacer fragment linking together different centers which may contribute to the geometry of the structure, influencing the distance between the nodes. One of the principle advantages of MOFs is the possibility to modify characteristic of the pores such as dimension and topology by varying, through organic synthesis, the molecular structure of the organic ligands. In this way it is possible prepare structures featuring the same topology where only the distance between the nodes changes in the framework by using, for example, the same linker and spacers of different lengths. An example is the series called IRMOF (IsoReticular Metal Organic Framework) made by the research group of O. Yaghi.[29] One of the first examples of isoreticular metal-organic frameworks is the IRMOF-1 MOF (Fig.1.16) formed by benzene-1,4-dicarboxylic acid coordinated to Zn_4O to form a porous cubic framework. On this example, a great number of IRMOFs have been developed, which preserve the isoreticular cubic structure as shown in Fig. 1.16. Moreover, if linear naphthyl, biphenyl dicarboxylate, pyrene or triphenyl dicarboxylic acids are used in place of benzene, the final structure can be expanded without altering the cubic structure of the resulting MOFs.[30]

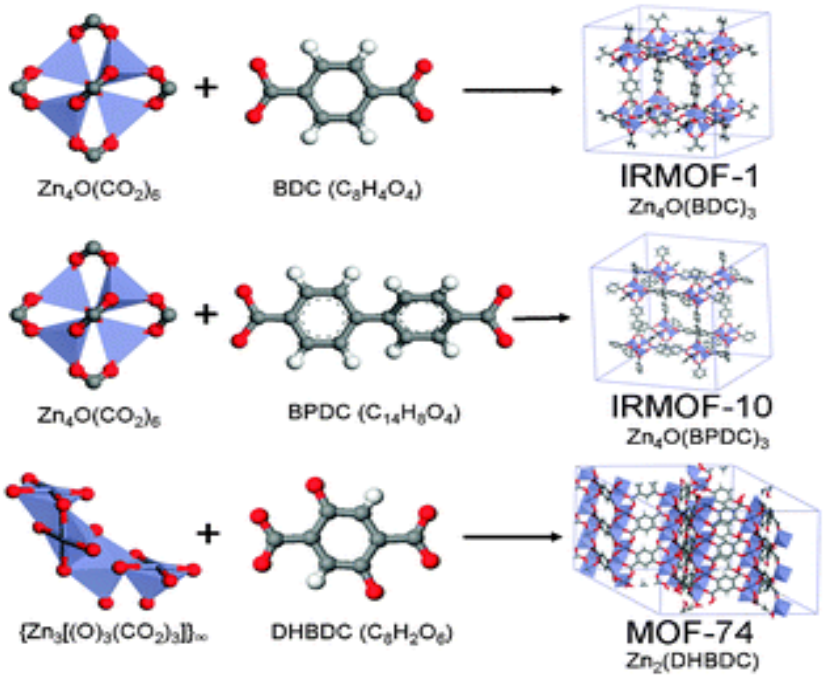

Figure 1.16 Structures of IRMOF-1, IRMOF-10, and MOF-74 respectively with, 4-benzene-1dicarbo= =xylate, 4,4′-biphenyldicarboxylate, and 2,5-dichydroxybenzene-1,4-dicarboxylate.[6]

[6] Image from: S.S. Han, SH.Choi A.C.T. Van Duin, *Chem. Commun*., **2010**, 46, 5713–5715.

1.2.3.1Application of Coordination Polymers and MOF

The interest on coordination polymers and metal organic frameworks has exponentially grown in the last twenty years, given the potential applications that they have shown, especially related to the caves formed inside them. Following some examples are synthetically listed.

- *Gas Adsorption:* The MOFs selective adsorption, can allow storage of large amounts of gas at constant volume occupied rather than the pressurized storage. This is due to the presence of specific interactions adsorbent/adsorbate, that limiting the interactions between molecules of the adsorbate, unlike compression systems where the storage capacity depends only on the PVT characteristic gas parameters. The IRMOF-1 was the first metal organic framework to be used for these investigations because it was cheap and with a large surface area. Afterwards, many papers have been reported on the hydrogen adsorption of MOFs that demonstrated that the bigger is the surface area of the framework, the greater the gravimetric uptake of hydrogen by weight at 77K.[31]
- *Luminescence:* Coordination polymers containing lanthanide ions are mainly used as electroluminescent devices or sensors because of their photophysical properties.[32] Coordination polymers are interesting luminescent materials because they exist in a crystalline form and have predictable topologies. Removal of solvent molecules from the framework allows for greater luminescence intensity because the solvent molecules can quench emission. Permanent porosity, combined with the rigidity of the framework, may also lead to increased luminescence lifetimes and other features not inherent in traditional inorganic complexes. Permanent porosity allows the framework to adsorb certain molecules into the pores with close proximity to the metal centers, which may lead to a red shift in their spectra and/or help to increase the luminescence intensity of the material.
- *Catalysis:* Coordination polymers have been studied for their heterogeneous catalytic properties.[33] Differently of zeolites that can be used as catalytic materials just for small organic molecules. Due to their high thermal stability they can be used to catalyze certain reactions under extreme conditions, where a thermally stable material is needed. Some MOFs based on CuI can be used as catalysts for the reaction of benzaldehyde cyanosilylation .[34] In this case the compound is previously activated by treatment under vacuum, removing the solvent molecules coordinates in senior positions, making the metal center accessible to the substrate.

- *Magnetism:* The coordination polymers of ligands such as cyanide, azide and thiocyanate have long been studied for their interesting magnetic properties.[35] Actually they exhibit many kinds of magnetism: antiferromagnetism, ferromagnetism which are cooperative phe-

nomena of the magnetic spins within a solid arising from coupling between the spins of the paramagnetic centers due they are able work as magnets, by using bridging ligands to translate magnetic moments between metal centers many types of coordination polymers have been synthesized.

1.4 Aim of the research

The design and synthesis of new coordination polymers and molecular crystals of different dimensionality and topology is an area of research in great expansion. One of the most common synthetic approaches for the construction of polymers is the use of covalent coordinative bonds between transition metal ions, usually referred to as nodes, and suitable coordinating polydentate organic ligands referred to as spacers or linkers. Since the use of "naked" metal ions enlarges the number of products potentially available and therefore introduces a certain grade of uncertainty, preformed coordination compounds are used as nodes. In order to be suitable to be used as building blocks, complexes metal ions must feature coordinative unsaturation and therefore be able to coordinate additional neutral donor molecules. An example is the construction of coordination polymers through the interaction between the metal porphyrins or metal phthalocyanines and appropriate donors that can able to act as a bridge, as cyanides, thiocyanates and di- or poly-pyridine derivatives.[36]Our research group has gained a certain experience in this research field working on the construction of coordination polymers based on square-planar Ni(II) complexes able to interact with multi-dentate donor molecules.[37] In particular, neutral square planar dithiophosphonato [$Ni(RO dtp)_2$] and dithiophosphato [$Ni(PS_2(OR)_2)_2$] complexes of nickel(II) [dtp = ($(CH_3O\text{-}C_6H_4)(RO)PS_2$); R = Me, Et, Pr, Pr^i] have shown an high tendency to form octahedral complexes with pyridine and its derivatives either in the solid state or in solution.[38] Following this result, studies on the interaction between neutral dithiophosphonato complexes of nickel(II) and poly-pyridyl ligands as building blocks in the construction of neutral coordination networks have been started.[39] The idea is to obtain solid materials with programmed micro-porous structures that can be used for the recognition and selective absorption of small molecules. It is worth to underline that the preparation of polymeric microporous materials by using neutral building blocks presents the advantage of the absence of counter-anions which otherwise would occupy the micro-cavities defined by the polymeric structure.

1.5 Organodithiophosphorous Compounds

Dithiophosphoric ligands of the type $RR'PS_2^-$, such as phosphoro- (1) phosphino- (2), phosphono- (3) and amidophosphono-dithioates (4), in Fig. 1.17, and their metal complexes, are well known for

their application in industrial and agricultural fields, and widely used as additives to lubricant oils,[40] antioxidant agents, extraction reagents for metals, flotation agents for mineral ores, insecticides, rodenticides, and pesticides.[41]

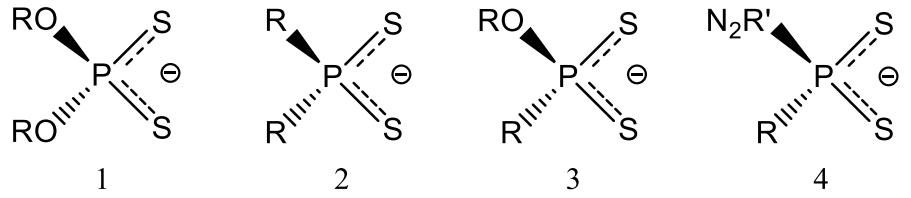

Figure 1.17 Organodithiophosphorous derivates structures.

Organodithiophosphorous derivatives are mononegative anions of the type $(RR´PS_2)^-$ formally derived from the corresponding monoprotic acids; they are versatile ligands since the sulphur atoms have the potential to bind either in a monodentate or bidentate form, in this last case yielding inorganic chelate rings. The phosphor-1,1,-dithio- set of ligands can coordinate to virtually all main group and transition metals, giving rise to a wide variety of coordination patterns. Fig. 1.18 shows the coordination patterns for dithio-organophosphorus ligands: monometallic mono- and biconnective, aniso- or iso-bidentate coordination.

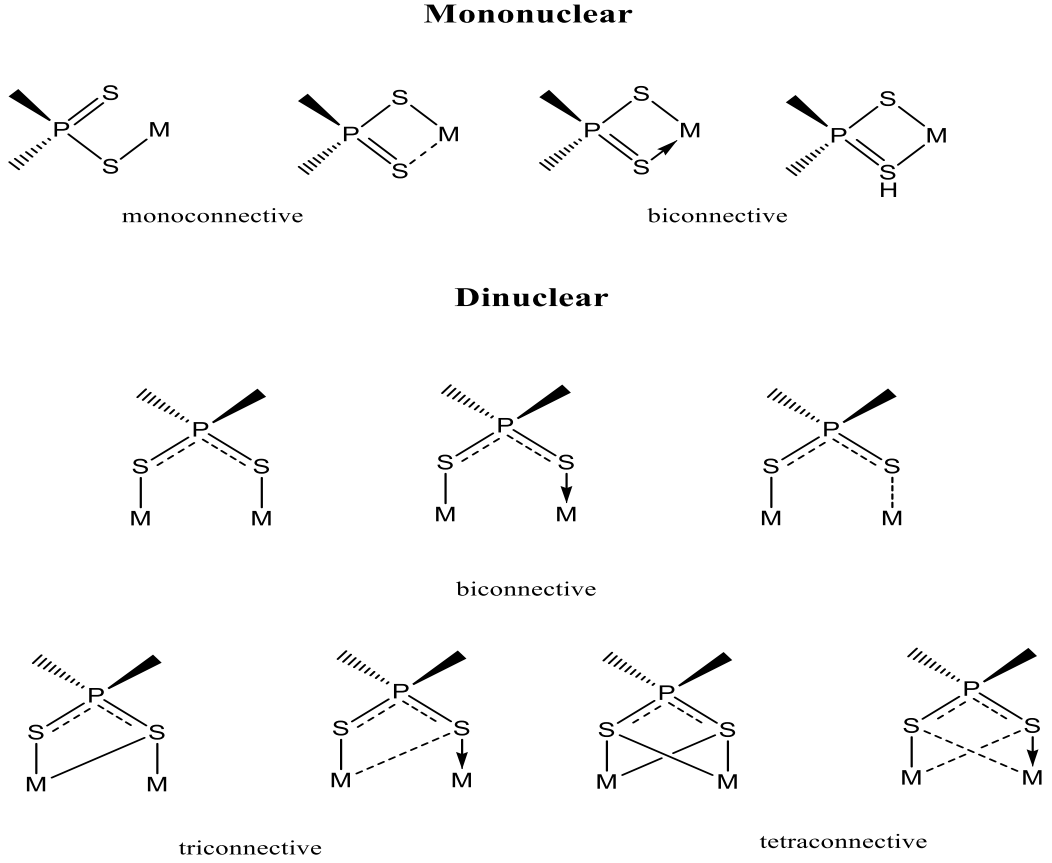

Figure 1.18 Coordination Modes of Organodithiophosphorous Ligands. Bi-, tri- and tetra-connective.

The kind of coordination that is preferred by a particular metal and organodithiophosphorous ligands depends upon the predominance of one resonance structure of the deprotonated dithiophosphorous acid over another, both of which are shown above.

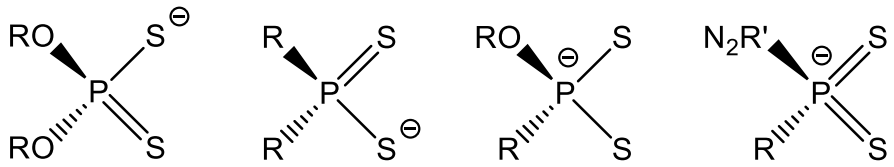

Figure 1.19 Contributing Resonance Structures for Dithiophosphonato Ligands.

Depending on type, oxidation state and coordination geometry of the metal ion, resonance structures 5, 6 or 7 typically predominate. Resonance structures 5 and 6 have been observed for complexes where the ligand binds in a μ^1-fashion (monodentate) with one sulfur atom only, examples can be found in many Pb(II), Hg(II), and Zn(II) complexes.[42] Resonance structure 7 predominates in many dinuclear Au(I) complexes, as well as in the common Ni(II) isobidentate chelating mononuclear complexes. Evidence of 7 is usually shown by the two equal P-S bond lengths in the solid state. Structure H is actually unknown for metal dithiophosphonates but included here for completeness.[43] Following a new reaction path which exploits 1,3-dithia-2,4-diphosphetane-2,4-disulfide derivatives, including the most known Lawesson's Reagent (LR), several metal complexes with dithiophosphates, dithiophosphonates and amidophosphonodithioates with several metal ions have been prepared by our research group.[44]

1.5.1 Dithiophosphato Complexes

Nickel(II) dithiophosphates consist of centrosymmetric units in which the two dithiophosphato units are coordinated to the central nickel atom through the sulfur atoms in a square-planar environment as exemplified in Fig. 1.20.

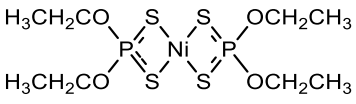

a

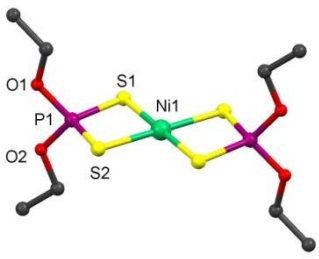

b

Figure 1.20 Formula (a), and Ball-and-stick Model (b) of the Complex Diethyldithiophosphate Nickel(II), $[((EtO)_2PS_2)_2Ni]$; hydrogen atoms are omitted for clarity.

1.5.2 Synthesis

The opening of the P_2S_2 tetra-atomic ring of Phosphorus Pentasulfide has proven to be a versatile way to synthesize dithiophosphato mononuclear complexes of Ni^{II}.[45] Following the synthetic route showed in the following scheme, we prepared metal the dialkyl dithio-phosphates $[((MeO)_2PS_2)_2Ni]$ (**D1)** and $[((EtO)_2PS_2)_2Ni)]$ (**D2)** by directly reacting phosphorous pentasulfide (P_4S_{10}) in Methanol and Ethanol, respectively, in the presence of the metal salt.

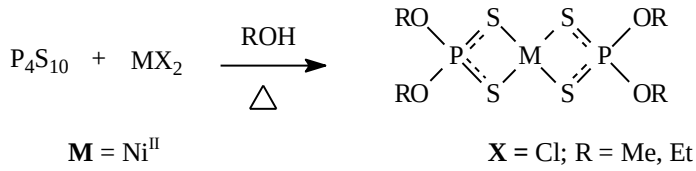

Scheme 1.1 Synthesis of Dithiophosphato Ni^{II} Complexes in Solvothermal Conditions.

1.5.3 Dithiophosphonato Complexes

Afore our work published in 1997, the chemistry of dithiophosphonates was quite scarce probably due to synthetic difficulties. In fact, many routes have been tried like for example the synthesis developed by Martin et al. which uses Grignard's reagent and 2-chloro-1,3,2-dithiaphospholane,[46] but all the ways were difficult and required several reactions steps, leaving this class of ligands quite unexplored. In the late nineties, in an attempt to optimize the syntheses of a new class of nickel dithiolenes using LR as a sulfuring agent,[47] incidentally Ni^{II} and Pd^{II} dithiophosphonato complexes were obtained, and among them the trans-bis[O-ethyl-(4-methoxyphenyl)dithiophosphonato]Ni complex [Ni(EtOdtp)2], dtp = $(CH_3O\text{-}C_6H_4)PS_2$,was structurally characterized.(Scheme 3). It was then clear that under the appropriate conditions 1,3-dithia-2,4-diphosphetane-2,4-disulfide derivatives, such as the well-known Lawesson's reagent (LR), and analogous compounds (Fig. 1.21) undergo to P_2S_4 ring opening, by leading to the corresponding metal complexes in the presence of the metal ion (Scheme 1.2).[48]

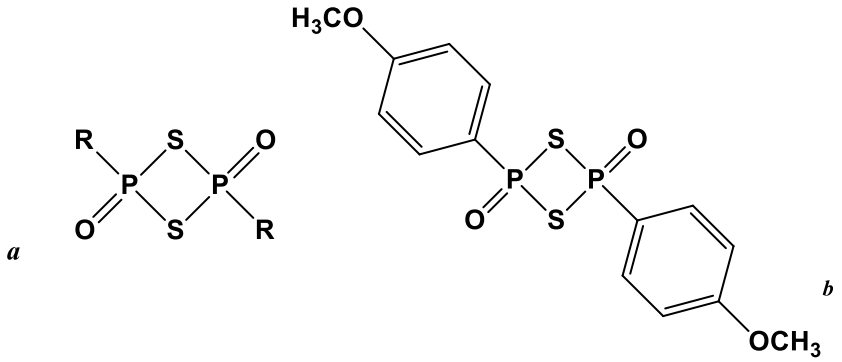

Figure 1.21 The General Structure of Organodithiophosphonic Anhydride Cyclic Dimers (a), and Lawesson's Reagent (LR) (b).

Using this synthetic method, many dithiophosphonates, and their corresponding metal complexes have been prepared and fully characterized.

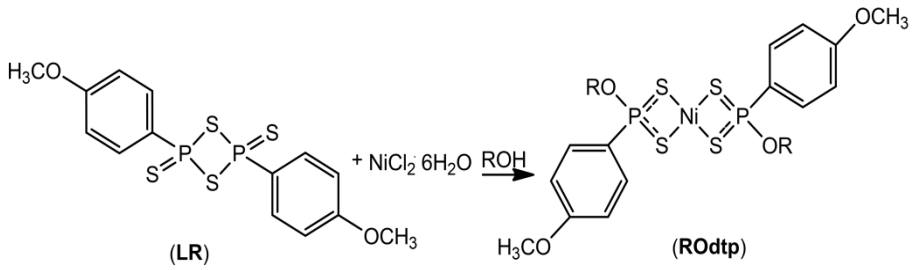

Scheme 1.2 Synthetic Route to Dithiophosphonato Complexes starting from Lawesson's reagent; R= Me, Et.

Nickel(II) dithiophosphonates [$(CH_3O\text{-}C_6H_4)(CH_3O))PS_2)_2Ni$] (**D3**) and [$(CH_3O\text{-}C_6H_4)(CH_2CH_3O)(PS_2)_2Ni$] (**D4**), consist of centrosymmetric units in which the two dithiophosphonato units coordinated to the central nickel atom as S,S-bidentate ligands. The phosphorus atoms reside in a square-planar sphere with the 4-methoxyphenyl (anisole) and the –OR groups *trans* disposed with respect to the coordination plane define by the P(1), S(1) and S(2) atoms (Fig. 1.22).

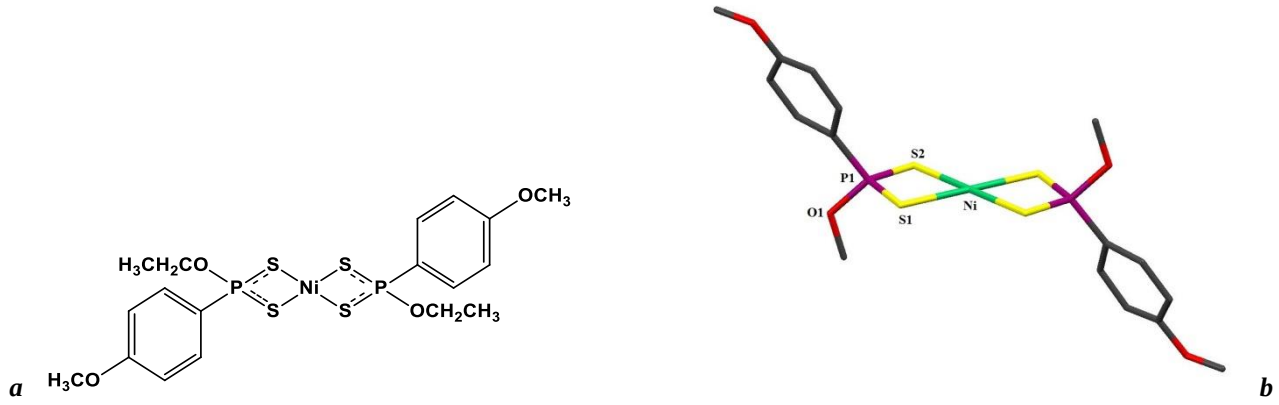

Figure 1.22 (a) Chemical Structures of [$Ni(MeOdtp)_2$] ,dtp=$(CH_3O\text{-}C_6H_4)PS_2$; (b) Capped sticks representation, hydrogen atoms are omitted for clarity.

1.5.4 Reactivity of Ni^{II} Dithiophosphato and Dithiophosphonato Complexes towards Nitrogen Donors

Square-planar Ni^{II} dithiophosphato and dithiophosphonato complexes [$Ni(RODtp)_2$] react with various nitrogen donors, both conjugated, such as pyridine and unconjugated.[49] The reaction between these complexes and nitrogen neutral donors such pyridines leads to complexes where the donors bind the central metal ion which thus assume a local octahedral geometry.[50] The tendency of these

square planar metal complexes to form octahedral complexes with pyridine, has led to further investigations into the propensity of these complexes to be axially coordinated by N–R–N bidentate ligands.

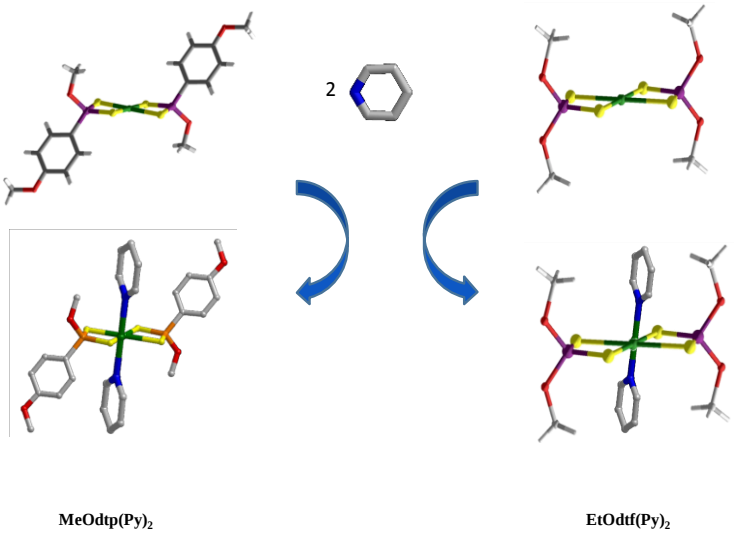

Figure 1.23 Formation of trans-bis (O-methyl-(4-methoxyphenyl)dithiophosphonato)-bis-(pyridyl) nickel(II) [Ni(MeOdtp)$_2$(Py)$_2$], and bis-(bis-(O-methyl)dithiophosphato)-bis-(pyridyl) nickel(II) [Ni((MeO)$_2$PS$_2$)$_2$(Py)$_2$] Complexes.

By using suitable bidentate ligands such as 4,4'-bipyridine that for topology reasons are not allowed to chelate the metal ion, polymeric structures were obtained where the bipyridine molecules coordinates two independent complex units acting as linkers. (Fig.1.24).

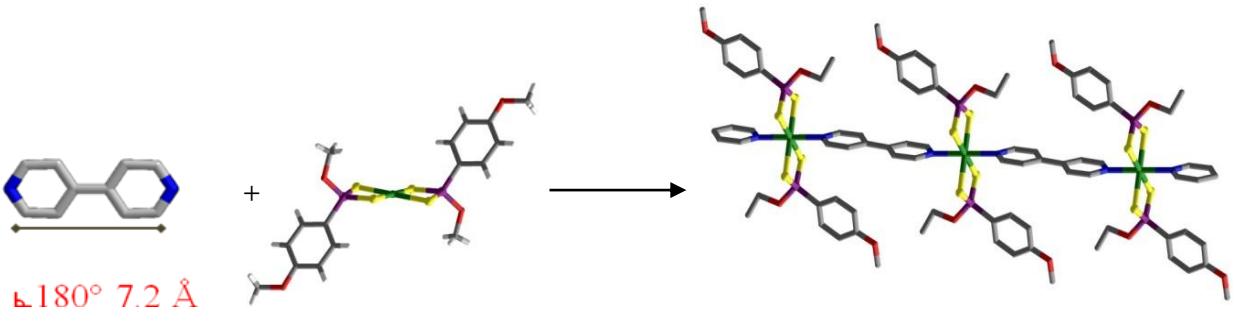

Figure 1.24 1D Polymer Synthesis from Bipyridine Ligand and [Ni(EtOdtp)$_2$].

Starting from these results, a synthetic program has been developed based on the ability of neutral dithiophosphato and dithiophosphonato Ni^{II} complexes to act as building blocks for the predictable assembly of inorganic coordination polymers of the type [Ni(ROpdt)$_2$(N-L-N)]$_\infty$ by using suitable N-L-N bidentate bipyridyl-based spacers.[51] It has been demonstrated that the primary structural mo-

tif of the polymers depends mainly on the features of the pyridyl-based spacers such as length, rigidity, number and orientation of the donor atoms, whereas the substituents on the phosphorus atoms influence the final 3D-architecture through hydrogen bonds and face-to-face or edge-to-face π–π interactions.[52]

1.6 Objectives

Since the topology of the coordination polymer mainly depends on the nature of the metal ion, the geometric features of the donor, and the number and position of the donor atoms, the present research project has been focused on the following objectives:

- The deliberate construction of coordination polymers from rigid bidentate ligands with programmed topology that allows us to exactly predict the final structure of the resulting polymer.
- The synthesis of coordination polymers from polydentate spacers in order to expand the network dimensionality to the third dimension, in view to construct MOF's with micro cavities in the final network.

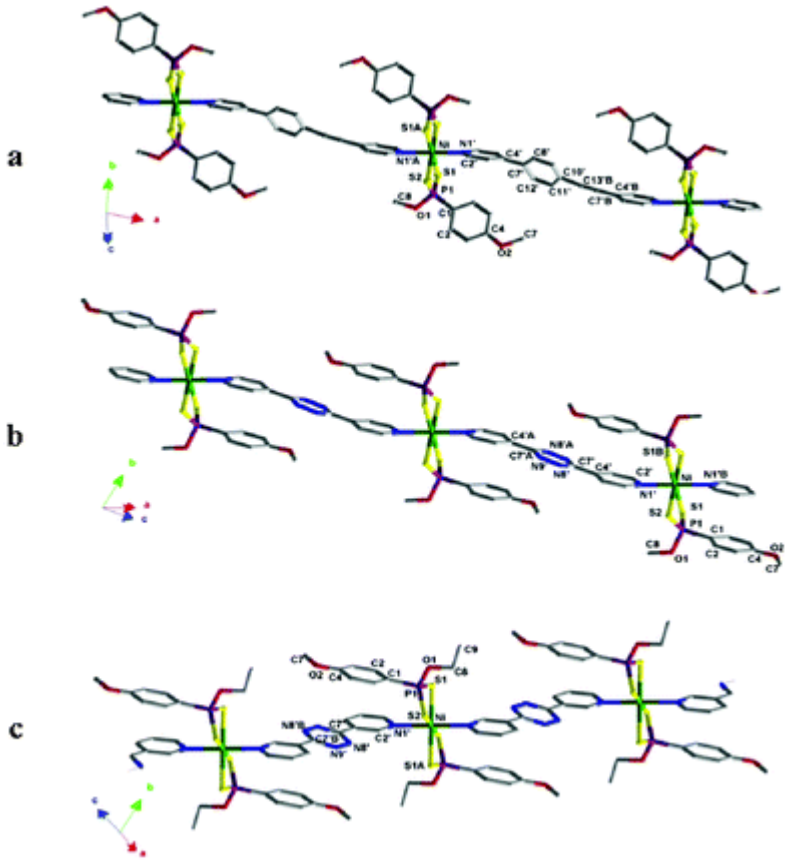

Figure 1.25 Polymers obtained using [Ni(MeOdtp)$_2$] and different Spacers: (a) 1-pyridyl-4-(4'-pyridyl-ethynyl)-benzene; (b) 3,6-bis(3-pyridyl)-1,2,4,5-tetrazine; (c) 3,6-bis(3-pyridyl)-1,2,4,5-tetrazine.

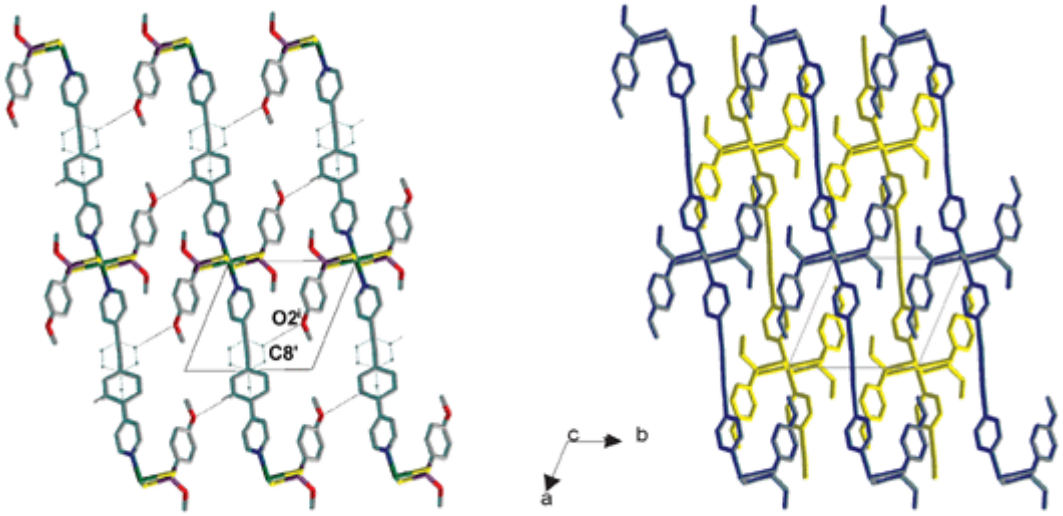

a b

Figure 1.26 2D Packing View along Crystallographic Axis *b* of the Polymer [Ni(MeOdtp)$_2$(1-pyridyl-4-(4'-pyridyl-ethynyl)-benzene)] showed in Fig. 1.25 (a).

2 Results and Discussion

The design and synthesis of oligomeric or polymeric complexes by using neutral coordination complexes held together by additional donor molecules or secondary-bonding interactions is acquiring increasing importance in the field of crystal engineering.[53] Following the research lines previously discussed, we have developed a program of synthesis and characterization of new coordination polymers using as molecular building blocks the dithiophosphato and dithiophosphonato Ni^{II} complexes schematized in Fig. 2.1 and various polydentate ligands represented in Table 2.3.

2.1. Building Blocks

The decision of using square planar Ni^{II} phosphorodithioato complexes as the metal nodes comes from the well-known tendency of these coordinatively unsaturated complexes to axially bound two additional donor molecules by reaching an octahedral coordination geometry in a quite predicable way, thus limiting the number of possible out-coming products and therefore the phenomenon of isomerism.[54] Moreover, by using neutral nitrogen donors as spacers the resulting coordination polymers are neutral in charge and do not need the presence counter ions that could participate and interfere in the final supramolecular network. The four square planar nickel complexes $[((MeO)_2PS_2)_2Ni]$ (**D1**); $[((EtO)_2PS_2)_2Ni]$ (**D2**); $[((MeO\text{-}C_6H_4)(MeO))PS_2)_2Ni]$ (**D3**); $[((MeO\text{-}C_6H_4)(EtO))PS_2)_2Ni]$ (**D4**) have been synthesized and fully characterized. Crystallographic data and selected bond lengths and angles for (**D1**), (**D2**), (**D3**), (**D4**) are reported in Tables 2.1 and 2.2, respectively The synthetic procedure and characterization are reported in the experimental section (§ 3.2).

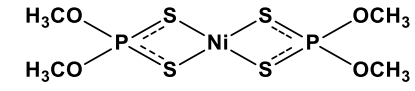

(**D1**)

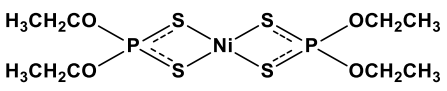

(**D2**)

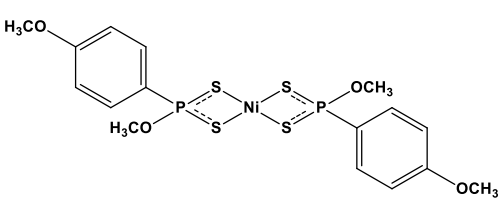

(**D3**)

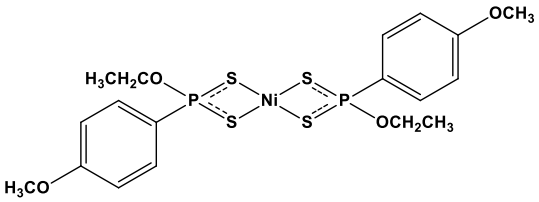

(**D4**)

Figure 2.17 Dithiophosphato and Dithiophosphonato Ni^{II} complexes formula structures.

As can be seen, the four complexes mainly differ for the P-substituents: dithiophosphato complexes are characterized by the presence of the symmetric *O*-alkyl substituents *O*-Me (**D1**) and *O*-Et (**D2**), whilst the dithiophosphonato complexes feature two aromatic p-methoxyphenyl substituents and two *O*-alkyl substituents *O*-Me (**D3**) and *O*-Et (**D4**), *trans* disposed with respect to central nickel ion. The different chemical nature of these substituents, and the different steric hindrance, are responsible for the different types of interactions experimented by the resultant polymeric chains and are of primary importance in controlling the packing and the final crystal structures.

Table 2.2 Summary of Basic Crystal Data for (**D1**),(**D2**), (**D3**) and (**D4**)

Empirical Formula	**$C_4H_1 Ni_1O_4P_2S_4$ (D1)**	**$C_8H_{20}Ni1O_4P_2S_4$ (D2)**	**$C_{16}H_{20}NiO_4P_2S_4$ (D3)**	**$C_{18}H_{24}Ni\ O_4P_2S_4$ (D4)**
Crystal system	Orthorhombic	Monoclinic	Monoclinic	Triclinic
Space group	P b c a	P 21/c	P 21/c	P -1
a, b, c (Å)	10.290(2); 8.640(2); 16.356(4)	10.493(5); 10.277(3); 8.754 (1)	11.823(3); 6.5091(15); 14.414(4)	6.5023(13); 7.6448(15); 13.109(3)
α, β, γ (°)	90;90;90	90;102.59(5);90	90, 110.464(7), 90	99.37(3); 99.72(3);104.09(3)
Volume ($Å^3$)	1454.14	919.49	1039.256	608.619
Z	4	2	2	1
Calculated density ($g\ cm^{-3}$)	1.68	1.54	1.68	1.51
R- factor %	7.5	3.06	2.4	7.37

Table 2.3 Selected Bond Lengths (Å) and Angles (°) for (**D1**),(**D2**), (**D3**) and (**D4**)

Atoms	**$C_4H_{12}Ni_1O_4P_2S_4$ (D1)**	**$C_8H_{20}Ni_1O_4P_2S_4$ (D2)**	**$C_{16}H_{20}NiO_4P_2S_4$ (D3)**	**$C_{18}H_{24}NiO_4P_2S_4$ (D4)**
Ni-S1	2.2182	2.2298	2.2330	2.225
Ni-S2	2.2250	2.2361	2.2413	2.227
S1-P1	1.984	1.9857	2.0048(7)	1.990(3)
S2-P1	1.9792	1.9934	2.0042(7)	2.007(3)
S1-Ni-S2	88.29	88.53	88.87	88.04
S1-P1-S2	102.66	103.14	102.77(3)	101.4(1)
Ni-S1-P1	84.49	84.33	82.58	84.18

The choice of the ligands used as spacers between the phosphonodithioato Ni^{II} complexes is essential to programming the topology of the out-coming polymer. In fact, as previously stated, the primary structure of the resulting coordination polymer directly depends on the geometry and topology of the molecules used as spacers. The following table shows the polydentate ligands whose reactivity towards organodithiophosphorous metal complexes has been here investigated. The nitrogen donors have been selected according to their rigidity, conformation, number and position of donor atoms. We used three different typologies of ligands: bidentate rigid spacers, semi-rigid bidentate spacers, and tridentate spacers. These molecules were synthesized optimizing the literature synthesis following the three different synthetic routes reported in Scheme 2.1: (a) cross coupling reactions; (b) nucleophilic substitution reactions; (c) esterification reactions. The ligand **L3** was synthesized and characterized in collaboration with Prof. Pasini in the laboratories of the University of Pavia (Italy).

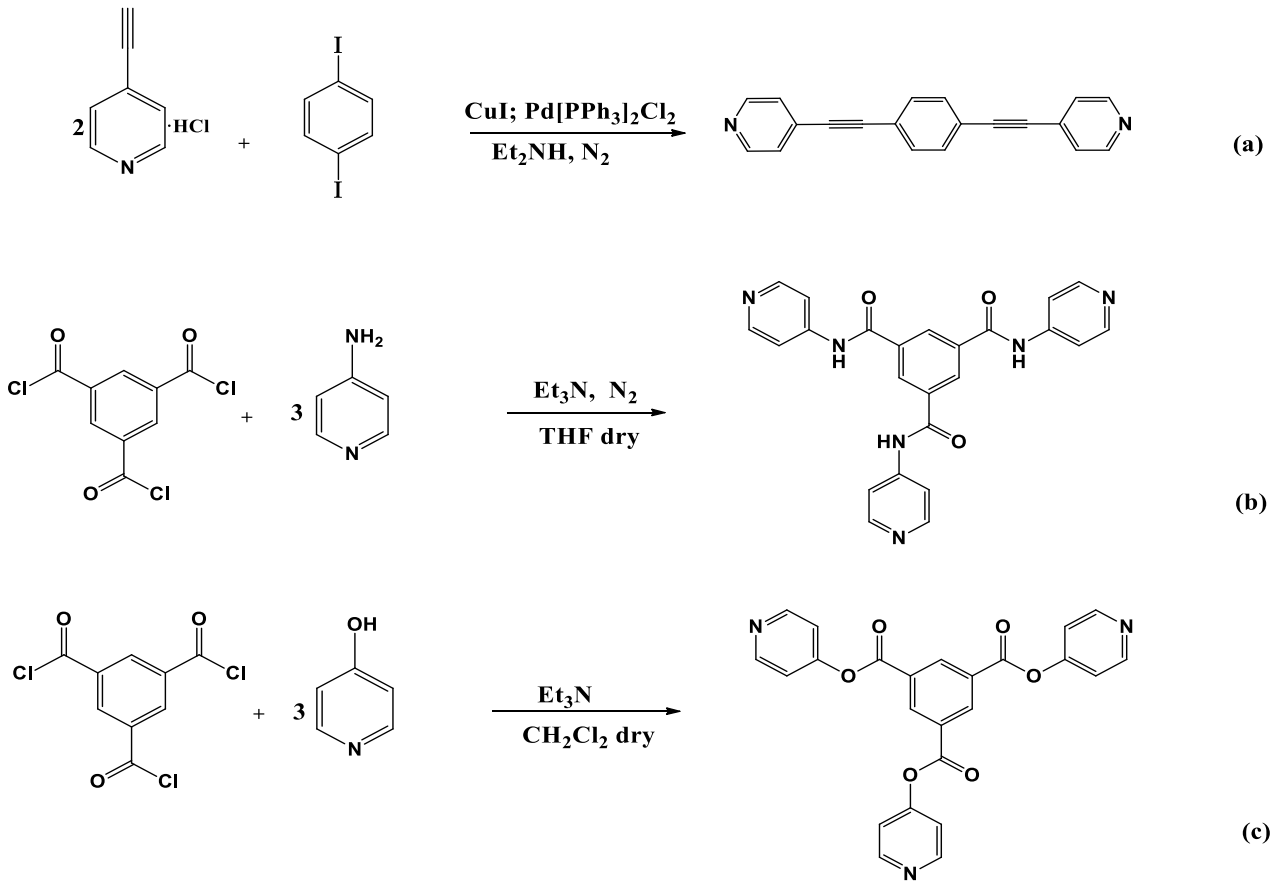

Scheme 2.1 The three synthetic procedures mainly used in this work here schematized for study cases: (a) 1,4-bis(4-pyridylethynyl)benzene (**L2**); (b) N,N',N''-tris(4-pyridin)benzene-1,3,5-tricarboxamide (**L8**); (c) 1,3,5-Benzene-tricarboxylic acid-1,3,5-tri-4-pyridinyl ester (**L10**).

Table 2.4 Polypyridyl Ligands used as Building Blocks

(1,4-bis(3-pyridyl)butadiyne

(L1)

1,4-bis(4-pyridylethynyl)benzene

(L2)

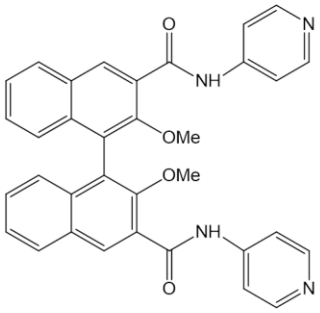

2,2'-dimetoxy-1,1'-binaphtyl-3,3'-bis(4pyridyl-amido)(R)**L**

(L3)

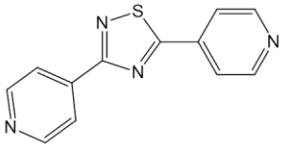

2,5-bis(3-pyridyl)-4-thia-1,3-thiazolidine

(**L4**)

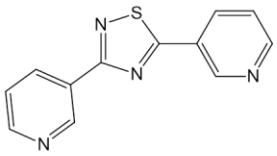

2,5-bis(4-pyridyl)-4-thia-1,3-thiazolidine

(**L5**)

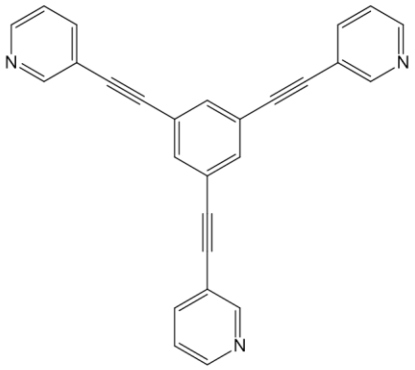

1,3,5-tris(3pyridylethynyl)benzene

(L6)

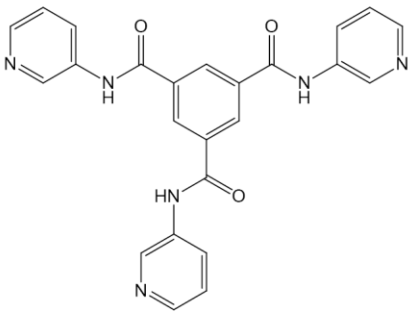

N,N',N''-tris(3-pyridin)benzene-1,3,5 tricarboxamide

(L7)

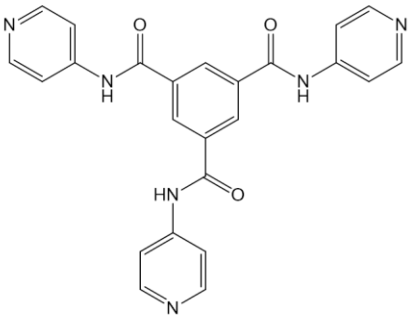

N,N',N''-tris (4-Pyridin)benzene-1,3,5-tricarboxamide

(L8)

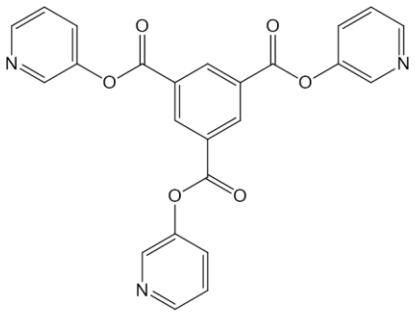

1,3,5-Benzenetricarboxylic acid, 1,3,5-tri-3-pyridinyl ester

(L9)

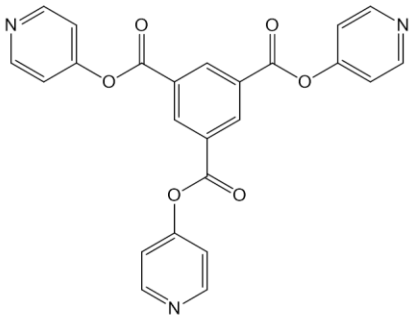

1,3,5-Benzenetricarboxylic acid, 1,3,5-tri-4-pyridinyl ester

(L10)

2.2 Building up of Coordination Polymers: Crystallization Techniques

The reaction between organodithiophosphorous metal complexes and polypyridinic donors leads to the formation of powder products due to their polymeric highly insoluble nature. Since a structural characterization performed on single crystals is fundamental to verify the polymeric nature of the resulting products and understand their supramolecular characteristics, several crystallization methods have been applied to obtain crystalline samples suitable for structural determination by X-Ray diffraction techniques. The formation of crystals is linked to the ability of molecules to organize themselves into crystalline lattices. This implies that the meeting between the building blocks has to be enough slow to allow the organization of molecules in an ordered structure. Many factors are involved in the process of crystallization such as pressure, temperature, solvent polarity, and the ideal conditions vary depending on the characteristics of the reagents and of the final product. During the PhD work many different crystallization techniques have been used, but only those we mainly used during the building up of coordination polymers are following described.

2.2.1 Solvothermic Reactions

One of the methods most frequently used for the crystallization of compounds takes advantage of the increasing of solubility in a given solvent by increasing of the temperature. In particular, if a compound is soluble in a solvent at high temperature values and insoluble in the same solvent at low temperatures, is possible to create suitable conditions for the formation of crystals by slow cooling of the solution. The synthesized polymers, however, are found to be insoluble in common solvents even at high temperatures. Because the solubility of solids usually increases as a function of the temperature, we thought to use high-pressure tubes where the solvents can be heated beyond their boiling temperature at atmospheric pressure. In fact, as can be seen from the diagram state in Fig.2.2 boiling temperature, which corresponds to the passage from the liquid phase to the vapor phase, in general, increases with increasing pressure. The method has been applied either to the compounds obtained as powders in a precedent reaction, or by directly reacting the starting synthons in sealed high pressure tubes in the presence of a pure solvent or a mixture of solvents. In this latter case, that we mainly used, we experimented two different behaviors: a) the final product can form immediately, precipitate as solid and then get dissolved with increasing of temperature; b) the reagents go in solution and combine in the product during the cooling of the reaction mixture.

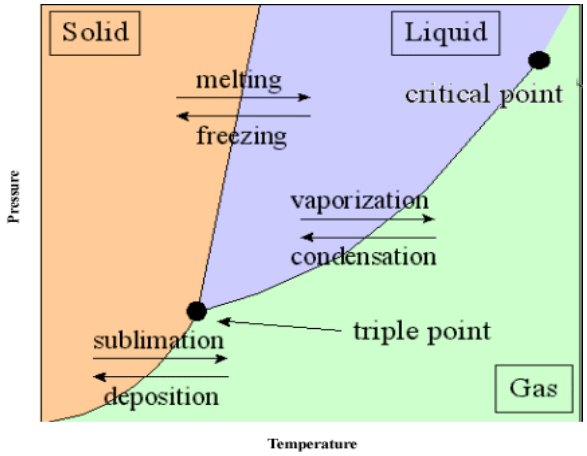

Figure 2.18 General Phase Diagram.[7]

2.2.2 Slow evaporation of a Solution of the Precursors

When the formation of the coordination polymers is not immediate and the reagents dissolve in the reaction mixture and do not give sudden precipitation of the product, it is possible to obtain the compound in crystalline form, by means of slow evaporation of the solvents of the reaction mixture. Crystals suitable for structural characterization can be obtained in a variable time ranging between a few days and a few weeks.

2.2.3 Layering of Solutions

This method is generally used when a coordination polymer is highly insoluble in almost every solvent and the two relevant reagents can be solubilized in different solvents with different density. The solution containing the reagent dissolved in the lighter solvent is carefully layered on the solution of the second reagent in the heavier solvent. The reagents slowly diffuse and crystals can be grown either at layer interface or in different places, usually close to the glass. A third solvent with intermediate density can be used to create a buffer zone in order to slow the diffusion rate, which controls the rate of crystallization.

---

[7] Image from website: http://wps.prenhall.com/wps/media/objects/3311/3391416/blb1106.html

2.2.3 Solvent Diffusion

This method can be used when the final product is not immediately formed by reaction of the precursors. In this case a solution of the reagents is placed in a vial and a different less dense solvent (in which where the reagents are insoluble such ether for example) is carefully layered on the reagent solution, and crystals can form by slow diffusion of the lighter solvent.

2.3 Structural Characterizations

Following the research objectives highlighted before, a synthetic program has been developed to prepare coordination polymers using the following three different categories of ligands:

- Bidentate rigid ligands for the construction of coordination polymers with programmed final structures.

- Bidentate semi-rigid ligands used to evaluate the role of the different factors, such as solvent, nature of the P-substituents in **D1**-**D4**, and nitrogen position in different structural isomers of the same ligand, in determining the final structure.

- Polydentate ligands featuring three pyridyl moieties projected with the intent of constructing three-dimensional networks.

As stated before, in order to exactly understand the nature of the reaction products obtained from the reaction between the phosphonodithioato Ni^{II} complexes and the polydentate pyridyl-based ligands, X-ray diffraction analysis on single crystal is mandatory. This is the reason why a part of my PhD period was spent at the EPSRC UK National Crystallography Service at the University of Southampton (U.K) under the supervision of Prof. Simon J. Coles in order to learn how to collect and analyze the crystallographic data. Unfortunately, the obtainment of the compounds as single crystals suitable for X-ray characterization is not easy. Moreover, the loss of solvent included in the crystal structure often leaded to decomposition of the samples, notwithstanding low temperature measurements, and rapid data collection diffractometers were used to avoid the problem. Divided on the base of the set objectives, we report here a brief description of the structures successfully recorded at the EPSRC UK National Crystallography Service at the University of Southampton (U.K) during my stage period. Most of the data were collected using a Bruker-Nonius Kappa CCD area detector situated at the window of a rotating anode (graphite Mo-K_α radiation, λ = 0.71073Å), processed using CrysAlisPro software, solved by direct methods procedure in SHELXL-97, and refined by full- matrix least squares on F2 using SHELXL-97 and Olex 2.

2.3.1 Bidentate Rigid Ligands

2.3.1.2 1,4-bis(3-pyridyl)-butadiyne (L1)

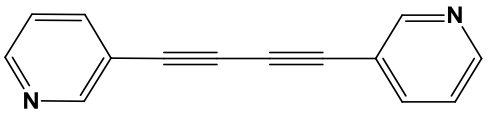

1,4-bis-(3-pyridil)-butadiyne (**L1**) has been prepared following the synthetic method described in Scheme 3.1 and following the procedure described in § 3.3.1. This ligand falls in the category of bis(aryl)diacetylenes, well known in literature as a building blocks and widely investigated due to the strong tendency of the diacetylene moiety to arrange into columnar systems thus leading to polymeric conjugated systems which display interesting optical and non-linear optical properties.[55] Due to the presence of the single C-C bond, two different orientations are allowed for the pyridyl moieties leading to a convergent and a divergent configurations depending on the relative orientation of the nitrogen donor atoms. Ligand **L1** has been reacted under solvothermal conditions in a 1:1 molar ratio with the nickel dithiophosphato and dithiophosphonato Ni^{II} complexes $[((MeO)_2PS_2)_2Ni]$ (**D1**), $[((EtO)_2PS_2)_2Ni]$ (**D2**), $[((MeO\text{-}C_6H_4)(MeO))PS_2)_2Ni]$ (**D3**), and $[((MeO\text{-}C_6H_4)(EtO))PS_2)_2Ni]$ (**D4**), using pure chloroform or a mixture of chloroform and the pertinent alcohol as solvent. The reactions afforded solid and crystalline compounds, which have been isolated and fully characterized as described in § **3.1-3.4**. Due to topology reasons, the two nitrogen atoms cannot bind to the same Ni^{II} ion, and therefore **L1** is expected to bridge two dithiophosphato or dithiophosphonato units acting as a rigid spacer. Single crystal X-ray diffraction performed on the resulting compounds confirmed their polymeric nature corresponding to the formulations $(\mathbf{D1}\cdot\mathbf{L1})_\infty$, $(\mathbf{D2}\cdot\mathbf{L1})_\infty$, $(\mathbf{D3}\cdot\mathbf{L1})_\infty$, and $(\mathbf{D4}\cdot\mathbf{L1})_\infty$. Crystallographic data and selected bond lengths and angles for $(\mathbf{D1}\cdot\mathbf{L1})_\infty$-$(\mathbf{D4}\cdot\mathbf{L1})_\infty$ are reported in Tables 2.4 and 2.5, respectively. As exemplified in Fig. 2.1, all compounds show the nickel ion lying in a distorted octahedral environment with the equatorial positions occupied by two dithiophosphoric units acting as isobidentate ligands with almost equivalent Ni-S and P-S bonds, featuring the P-substituents in the original *trans* configuration. The pyridine units of **L1** are axially coordinated to the Ni^{II} ion of two adjacent dithiophosphoric units, thus forming polymeric chains. The coordination of a neutral donor reduces the net positive charge on the central Ni^{II} ion leading to a lengthening of the Ni-S bond lengths and a consequent decrease in the S-Ni-S angle with respect to the corresponding Ni^{II} square planar complex, as can be observed by comparing the pertinent bond lengths and angles with those of the

corresponding square planar complexes reported in Table 2.5. At the same time the negative charge on the sulfur atoms increase with a consequent opening of the S-P-S angle.

Table 2.5 Summary of Basic Crystal Data for (**D1·L1**)$_\infty$, (**D2·L1**)$_\infty$, (**D3·L1**)$_\infty$, and (**D4·L1**)$_\infty$

Empirical Formula	$C_{18}H_{20}N_2$ Ni O_4 P_2 S_4 (**D1·L1**)$_\infty$	$C_{22}H_{28}N_2NiO_4P_2S_4$ (**D2·L1**)$_\infty$	$C_{30}H_{28}N_2$ Ni O_4 P_2 S_4 (**D3·L1**)$_\infty$	$C_{64}.H_{64}.N_4Ni_2O_8P_4S_8$ (**D4·L1**)$_\infty$
Formula weight (g mol^{-1})	1154.50	633.35	729.43	757.51
Temperature (K)	100 (2)	100 (2)	100 (2)	100 (2)
Crystal system	Orthorhombic	Monoclinic	monoclinic	Monoclinic
Space group	Pbca	P21/n (No.14)	I2/a	$P2_1/c$
a, b, c (Å)	11.9848(10); 13.8744(11); 14.6988(12)	8.9771(12); 11.9400(15); 13.6069(18)	13.877(3); 11.678(2); 23.433(6)	13.8002(9); 11.8644(8); 23.223(2)
α, β, γ (°)	90; 90; 90	90; 107.850(2); 90	90; 98.452(13); 90	90; 97.394(4);90
Volume (Å^3)	2444.1(3)	1388.3(3)	3756.2(14)	3770.7(5)
Z	2	2	4	2
Calculated density (g cm^{-3})	1.569	1.515	1.290	1.404
Reflections collected/Unique	16155/2783	9476 /2783	13255/4255	24705/8576
Wavelength	λ =71075	λ =71075	λ =71075	λ =71075
Final R indexes [I>=2σ (I)]	R_1 = 0.0209, wR_2 = 0.0593	R_1 = 0.0339, wR_2 = 0.0825	R_1 = 0.0686, wR_2 = 0.1863	R_1 = 0.0686, wR_2 = 0.1863

Table 2.6 Selected Bond Lengths (Å) and Angles (°) for (**D1·L1**)$_\infty$, (**D2·L1**)$_\infty$, (**D3·L1**)$_\infty$, and (**D4·L1**)$_\infty$

Atoms	$C_{18}H_{20}N_2$ Ni O_4 P_2 S_4 (**D1·L1**)$_\infty$	$C_{22}H_{28}N_2NiO_4P_2S_4$ (**D2·L1**)$_\infty$	$C_{30}H_{28}N_2$ Ni O_4 P_2 S_4 (**D3·L1**)$_\infty$	$C_{64}.H_{64}.N_4Ni_2O_8P_4S_8$ (**D4·L1**)$_\infty$
Ni-S1	2.4793(3)	2.4796(7)	2.4820(13)	2.4703(18)
Ni-S2	2.5081(3)	2.4710(7)	2.4590(13)	2.4933(10)
Ni-S3	-	-	-	2.4781(10)
Ni-S4	-	-	-	2.4733(10)
Ni-N1	2.0944(11)	2.1199(17)	2.110(4)	2.4802(18)
Ni-N2	-	-	-	2.117(3)
S1-P1	1.9883(5)	1.9878(8)	2.0018(18)	1.9980(14)
S2-P1	1.9884(5)	1.9877(8)	1.9971(17)	1.9997(13)
S3-P2	-	-	-	1.9995(14)

S4-P2	-	-	-	1.9973(13)
S1-Ni-S2	81.672(11)	82.50(2)	82.48(4)	82.05(6)
S1-Ni-S3	-	-	-	97.49(4)
S3-Ni-S2	-	-	-	178.85(3)
S4-Ni-S1	-	-	-	178.95(4)
S4-Ni-S2	-	-	-	98.85(3)
S4-Ni-S3				82.08(3)
S1-Ni-N1	91.36(3)	91.20(5)	90.72(11)	88.79(9)
S2-Ni-N1	88.92(3)	88.64(5)	88.69(11)	91.09(9)
S3-Ni-N1	-	-	-	88.19(9)
S4-Ni-N1	-	-	-	92.15(9)
S1-Ni-N2	-	-	-	91.18(8)
S2-Ni-N2	-	-	-	88.29(9)
S3-Ni-N2	-	-	-	92.43(9)
S4-Ni-N2	-	-	-	87.88(8)
S1-P1-S2	110.26(2)	110.38(4)	109.08(8)	108.77(10)
S3-P2-S4	-	-	-	114.12(14)
N-Ni-N	180.0	180.0	180.0	179.38(12)

All polymers (**D1**·**L1**)$_\infty$-(**D4**·**L1**)$_\infty$ present very similar features with a primary structure characterized by the endless repetition of metal centers and **L1** molecules in a zig-zag fashion where ligands **L1**, all featuring divergent configurations, bridge two Ni^{II} complex units with Ni···Ni distances of 13.87, 13.81, 13.88, and 13.80 Å for (**D1**·**L1**)$_\infty$, (**D2**·**L1**)$_\infty$, (**D3**·**L1**)$_\infty$, and (**D4**·**L1**)$_\infty$, respectively (Fig. 2.3). It is interesting to note that the alkoxy substituents at the phosphorous atoms point the hydrogens of the carbon atoms directly bound to the oxygen atoms point towards the pyridyl rings, see the example reported in the inset of Fig. 2.2a. This implies that OMe and OEt substituents are oriented towards and forwards the coordination plane, respectively, and therefore only OEt P-substituents are available to engage intermolecular interactions and contribute to the packing of the polymeric chains.

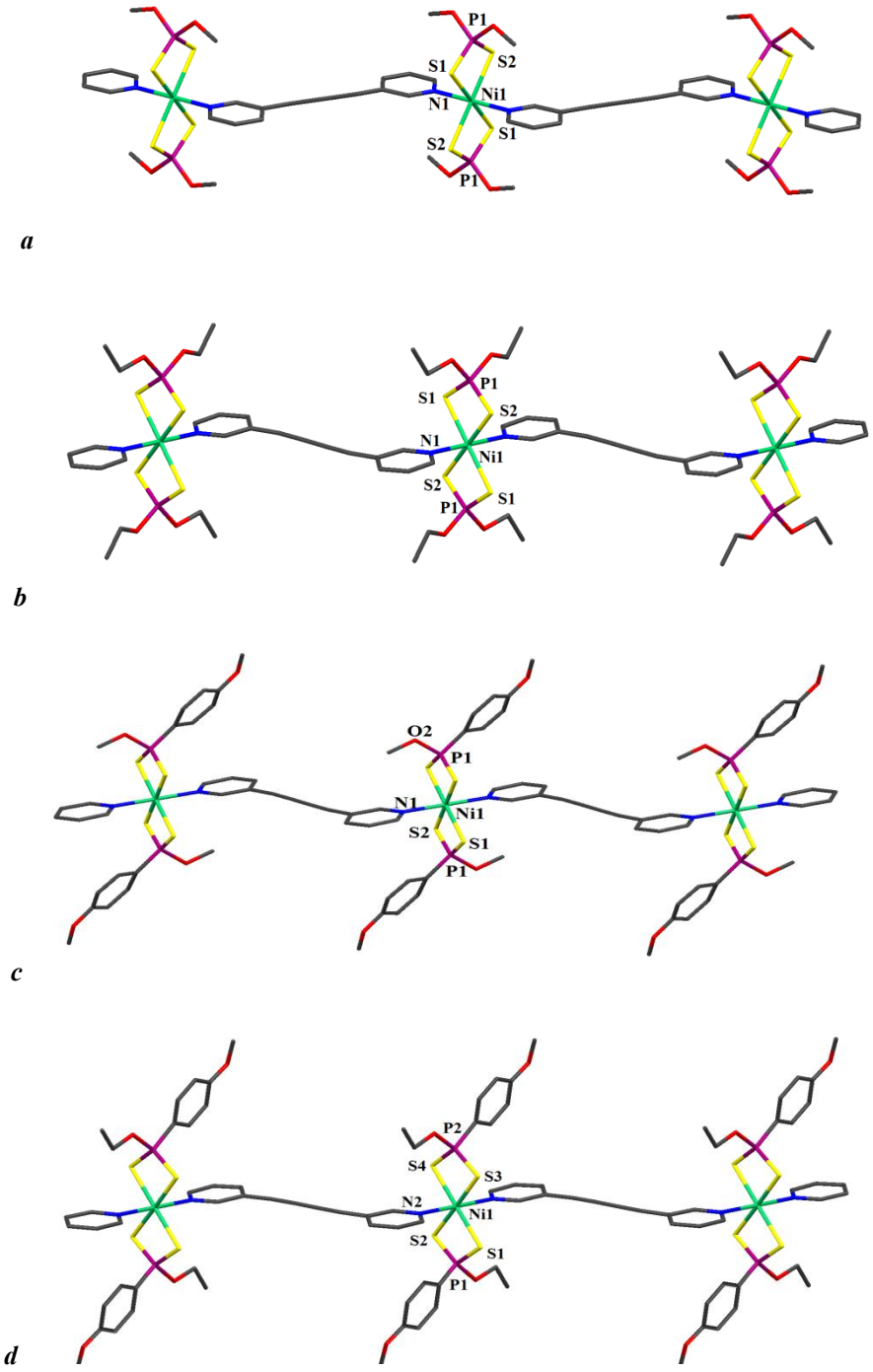

Figure 2.19 Zig-Zag Polymeric Chains of Compounds (a) (**D1·L1**)$_\infty$, (b) (**D2·L1**)$_\infty$, (c) (**D3·L1**)$_\infty$, and (d) (**D4·L1**)$_\infty$. Hydrogen atoms are omitted for clarity reasons.

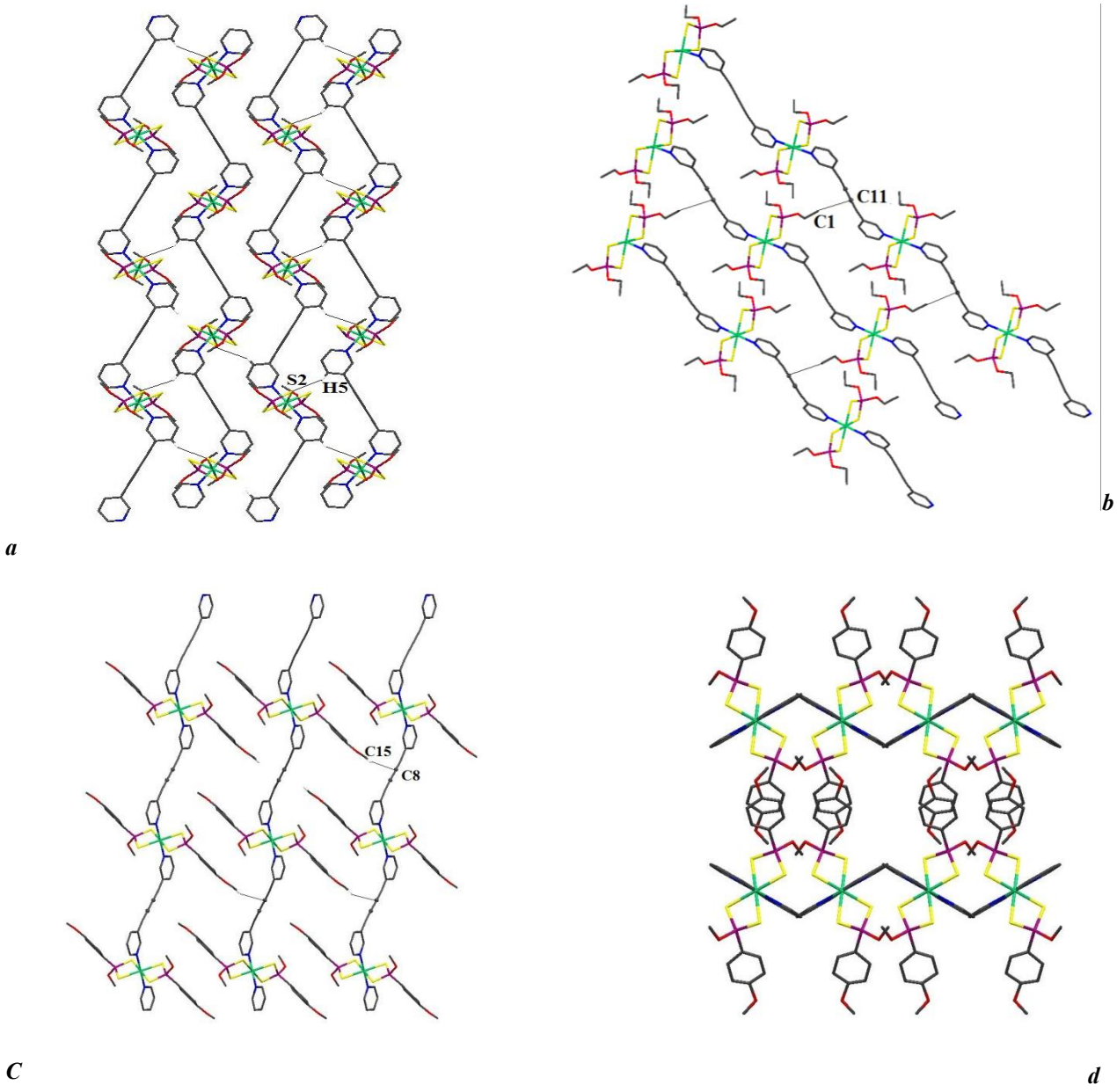

Figure 2.20 Packing Views and main Intra-Molecular Interactions: (a) view along *c* axis of $(\mathbf{D1{\cdot}L1})_{\infty}$; (b) $(\mathbf{D2{\cdot}L1})_{\infty}$,(c) view along b axis and along a axis (d) of $(\mathbf{D3{\cdot}L1})_{\infty}$ Polymers. Hydrogen atoms are omitted for clarity.

As shown in Fig. 2.2 (a) in the polymer $\mathbf{(D1{\cdot}L1)}_{\infty}$ the chains run along the axis *b* direction and are parallel disposed with metal nodes of adjacent chains shifted of b/2. As previously observed, the OMe P-substituents points towards the pyridine rings and do not contribute to link the chain that interact each other in the *ab* plane through weak hydrogen bonds involving the C5-H5 hydrogen

atom of pyridine and the coordinate sulfur atom S2 (Figure 2.4a, C5-H5···S2': H···S 2.75 Å, C···S 3.5881(14) Å, C-H···S 151°; ' 0.5+x, 0.5-y,1-z). Polymer chains of **(D2·L1)**$_\infty$ pack parallel interacting through weak hydrogen bonds involving the C7-H7 hydrogen atom of pyridine and the coordinate sulfur atom S2 (C7-H7···S2': H···S 2.83 Å, C···S 3.654(3) Å, C-H···S 146°; ' 0.5-x, -0.5+y, 1.5-z). It interesting to note that the ethyl substituents in **(D2·L1)**$_\infty$ are directed towards the acetylenic triple bond of the ligand, with short contacts (C1···C11 3.25 Å) between the chains that influenced the final crystal packing in **(D2·L1)**$_\infty$ (Fig. 2.2 b) In **(D3·L1)**$_\infty$ and (**D4·L1**)$_\infty$ polymers, the alkyl substituents are also oriented in a different manner, but the presence of methoxyphenyl rings on the phosphorus atoms engenders different interactions. In fact the methoxyphenyl appendages are engaged in a hydrogen bond with the acetylenic triple bond of the (C15-H15···C8 Å 2.77 Å) adjacent chain. The greater steric hindrance conferred by these different substituents at phosphorous atom in the dithiophosphonato complexes lead to the formation of cavities in the crystal structure that occupy a volume of 206.1 Å 5.5% of the the unit cell volume for **(D3·L1)**$_\infty$ and 198.2 Å 5.3 % of the unit cell volume for **(D4·L1)**$_\infty$. (Fig. 2.3).

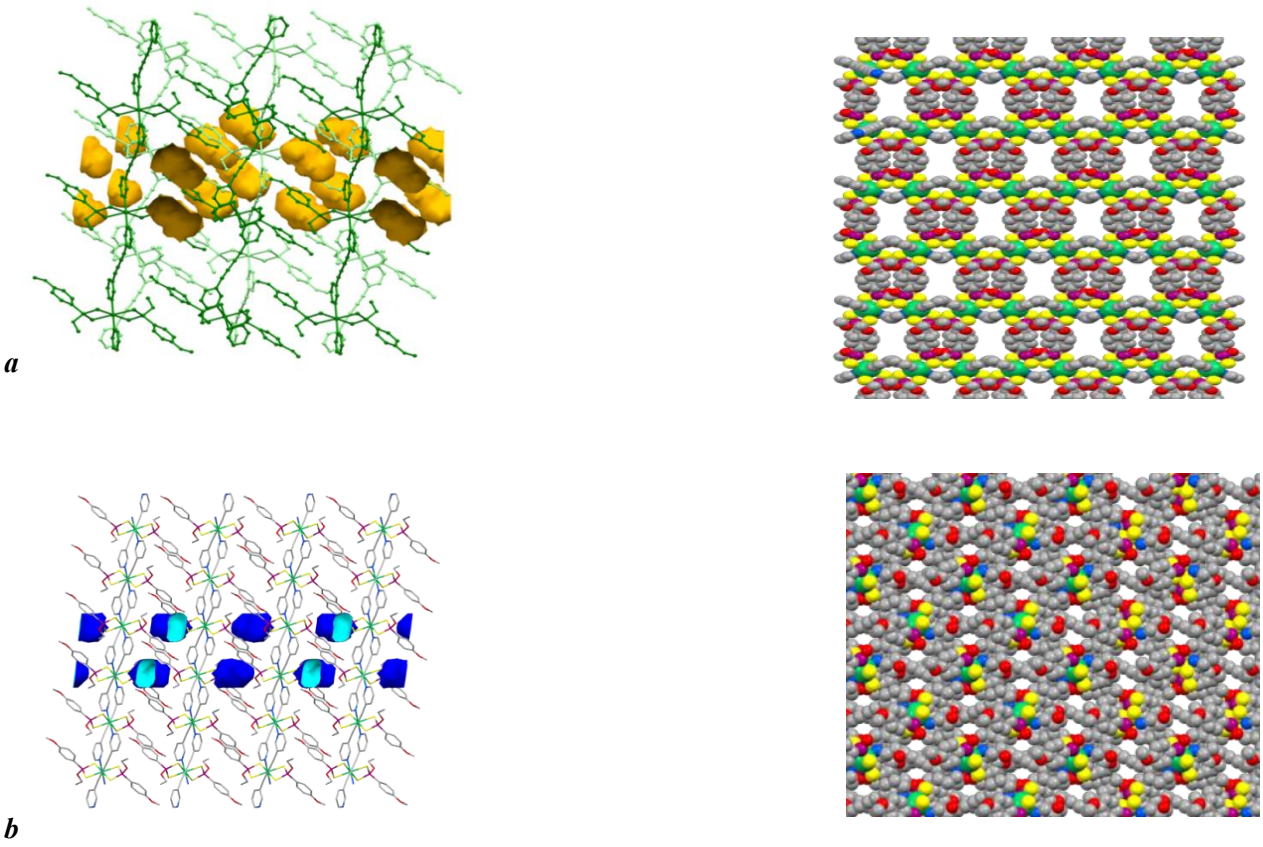

a

b

Figure 2.21 Crystal Packing Voids and Space Filled Representation of **(D1·L1)**$_\infty$ (a) and **(D3·L1)**$_\infty$ (b) polymers. Hydrogen atoms are omitted for clarity.

2.3.3 1,4-bis(4-pyridylethynyl)benzene (L2)

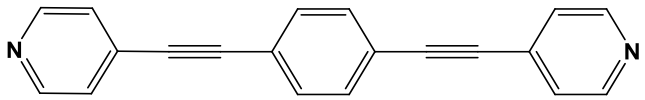

1,4-bis(4-pyridylethynyl)benzene has been prepared following the synthetic method described in Scheme 3.3 and following the procedure described in § 3.3.2. It is a rigid bidentate organic spacer with the two nitrogen donor atoms of the pyridine units separated by a distance of 16.52 Å. Ligand **L2** has been reacted under solvothermal conditions in a 1:1 molar ratio with the nickel dithiophosphato and dithiophosphonato Ni^{II} complexes $[((MeO)_2PS_2)_2Ni]$ (**D1**), $[((EtO)_2PS_2)_2Ni]$ (**D2**), $[((MeO\text{-}C_6H_4)(MeO))PS_2)_2Ni]$ (**D3**), and $[((MeO\text{-}C_6H_4)(EtO))PS_2)_2Ni]$ (**D4**), using pure chloroform or a mixture of chloroform and the pertinent alcohol as solvent. The reactions afforded solid compounds, which have been isolated and fully characterized as described in § 3.4.6- 3.4.8. Single crystals suitable for X-ray diffraction were obtained only from the reactions with **D2** and **D4**, which confirmed the expected polymeric nature of the compounds corresponding to the formulations $(\mathbf{D2}\cdot\mathbf{L2})_\infty$ and $(\mathbf{D4}\cdot\mathbf{L2})_\infty$. In fact, due to topology reasons, the two nitrogen atoms cannot bind to the same Ni^{II} ion, and **L2** is expected to bridge two dithiophosphato or dithiophosphonato units acting as a rigid spacer. Crystallographic data and selected bond lengths and angles for $(\mathbf{D2}\cdot\mathbf{L2})_\infty$ and $(\mathbf{D4}\cdot\mathbf{L2})_\infty$ are reported in Tables 2.6 and 2.7, respectively. As exemplified in Fig. 2.4, the two compounds show the nickel ion lying in a distorted octahedral environment with the equatorial positions occupied by two dithiophosphoric units acting as isobidentate ligands with almost equivalent Ni-S and P-S bonds, featuring the P-substituents in the original *trans* configuration. The pyridine units of **L2** are axially coordinated to the Ni^{II} ion of two adjacent dithiophosphoric units, thus forming polymeric chains. The coordination of a neutral donor reduces the net positive charge on the central Ni^{II} ion leading to a lengthening of the Ni-S bond lengths and a consequent decrease in the S-Ni-S angle with respect to the corresponding Ni^{II} square planar complex. At the same time increases the negative charge on the atoms of sulfur with a consequent opening of the S-P-S angle. The $(\mathbf{D2}\cdot\mathbf{L2})_\infty$ and $(\mathbf{D4}\cdot\mathbf{L2})_\infty$. compounds present very similar features with a primary structure characterized by the endless repetition of metal centers and **L2** molecules in smoothly undulating chains with Ni···Ni distances of 20.72 and 20.64 Å for $(\mathbf{D2}\cdot\mathbf{L2})_\infty$ and $(\mathbf{D4}\cdot\mathbf{L2})_\infty$, respectively (Fig. 2.4).

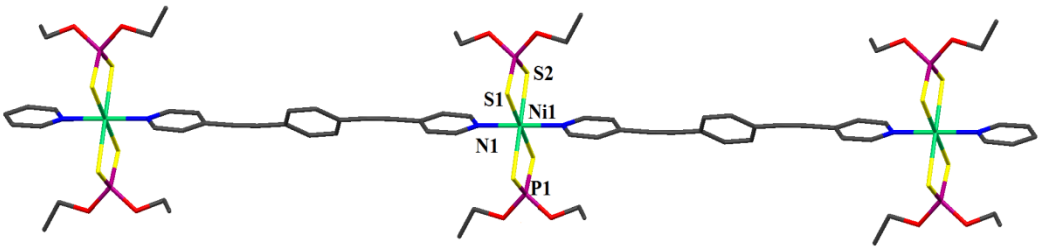

(D2·L2)$_\infty$

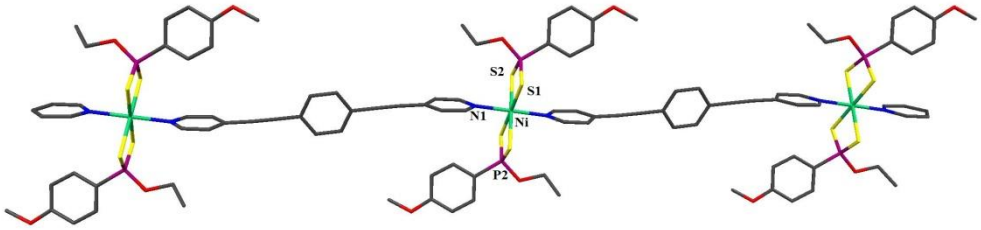

(D4·L2)$_\infty$

Figure 2.22 Undulated Polymeric Chains of (**D2·L2**)$_\infty$ and (**D4·L2**)$_\infty$. For clarity reasons, only non-carbon atoms have been labeled and hydrogen atoms omitted.

Table 2. 7 Summary of Basic Crystal Data for $(\mathbf{D2{\cdot}L2})_\infty$ and $(\mathbf{D4{\cdot}L2})_\infty$

Empirical Formula	$C_{28}\ H_{32}\ N_2\ Ni\ O_4\ P_2\ S_4$ $(\mathbf{D2{\cdot}L2})_\infty$	$C_{37}\ H_{36}\ N_3\ Ni\ O_4\ P_2\ S_4$ $(\mathbf{D4{\cdot}L2})_\infty$
Formula weight (g mol^{-1})	709.44	835.62
Temperature (K)	100	100
Crystal system	Monoclinic	Triclinic
Space group	P 1 21/c 1	P 1
a, b, c (Å)	8.7772(19) 12.607(3) 14.564(3)	9.0467(5) 10.5786(7) 11.1097(8)
α, β, γ (°)	90; 100.248(3); 90	111.970(11); 93.243(9); 93.874(9)
Volume (Å^3)	1585.9(6)	979.89(14)
Z	2	1
Calculated density (g cm^{-3})	1.486	1.423
Reflections collected/Unique	3294/ 3602	3111/ 4473
Wavelength	λ =71075	λ =71075
Final R indexes [I>=2σ (I)]	R_1 = 0.0323 wR_2= 0.0783	R_1 = 0.0586 wR_2 = 0.1517

Table 2.8 Selected Bond Lengths (Å) and Angles (°) for $(\mathbf{D2{\cdot}L2})_\infty$ $(\mathbf{D4{\cdot}L2})_\infty$

Atoms	$C_{28}H_{32}N_2NiO_4P_2S_4$ $(\mathbf{D2{\cdot}L2})_\infty$	$C_{37}H_{36}N_3NiO_4P_2S_4$ $(\mathbf{D4{\cdot}L2})_\infty$
Ni-S1	2.4706(5)	2.490(2)
Ni-S2	2.5062(7)	2.454(2)
Ni-N1	2.1039(13)	2.118(8)
S1-P1	1.9934(7)	1.9984(15)
S2-P1	1.9862(6)	2.0023(16)
S1-Ni-S2	81.835(12)	97.82(8)
S1-P1-S2	109.99(2)	108.62(16)
S1-Ni-N1	90.03(4)	87.9(2)
S2-Ni-N1	90.36(3)	90.9(3)
N1-Ni-N1	180.0	180.0

The polymeric chains of (**D2·L2**)$_\infty$ run parallel disposed along the 011 direction thus forming 2D layers through weak hydrogen bonds (Figure 2.5a): C2-H2···O2': H···O 2.53 Å, C···O 3.461(2) Å, C-H···O 166°; C12-H12B···S1'': H···S 2.86 Å, C···S 3.799(2) Å, C-H···S 161° (' 2-x, 0.5+y, 0.5-z; '' 2-x, -0.5+y, 0.5-z). The polymeric chains of (**D4·L2**)$_\infty$ run parallel disposed along the 101 direction thus forming 2D layers connected through weak hydrogen bonds involving the OEt appendages in the formation of a $R(6)_2^2$ motif (Figure 2.7b): C6-H6···O1': H···O 2.651(7) Å, C···O 3.415(7) Å, C-H···O 136°; ' 1-x, -1-y, 1-z. It is interesting to note that the 4-MeOPh P-appendages points towards the pyridyl rings being disposed approximately perpendicular (71.9°), thus allowing edge to face π-π intramolecular interactions with a $C_{Ph}\cdots C_{Py}$ distances of 3.7 Å, Figure 2.5b. .

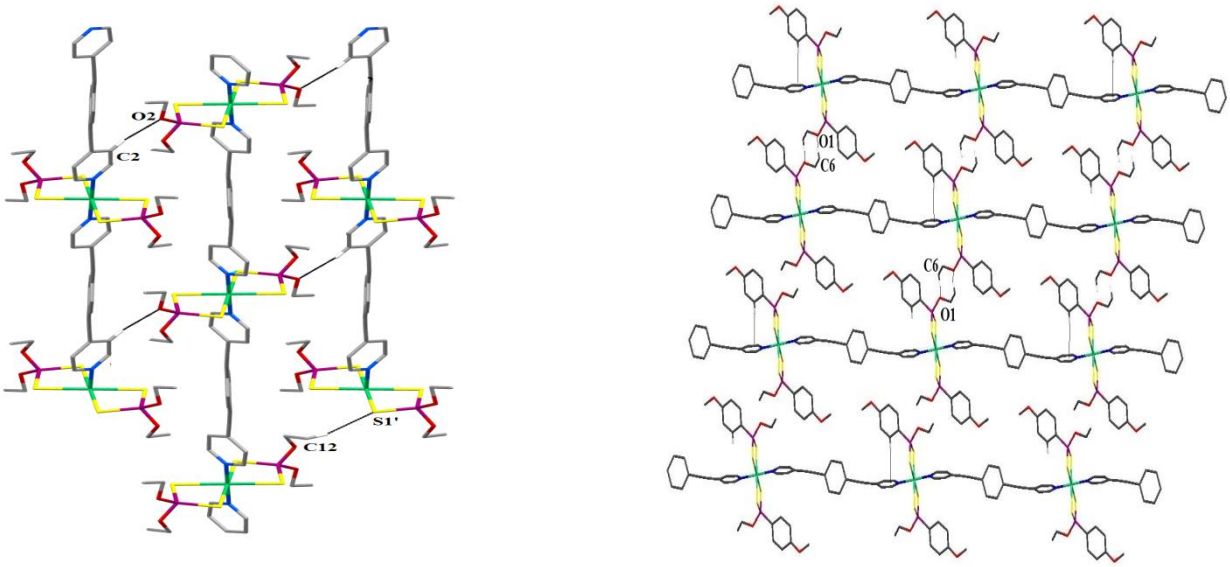

a ***b***

Figure 2.23 Packing Views and main Intra-Molecular Interactions for (**D2·L2**)$_\infty$ and (**D3·L2**)$_\infty$ polymers. Hydrogen atoms are omitted for clarity

2.3.2 Chiral and Semi-Rigid Bidentate Ligands

2.3.2.1 (R)-2,2′-dimethoxy-1,1′-binaphthyl-3,3′-bis(4-pyridyl-amido) (L3)

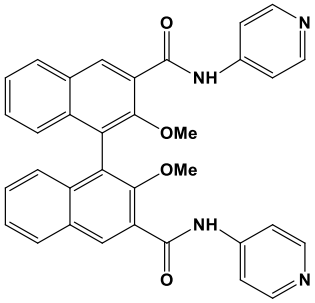

The enantiopure (*R*)-2,2′-dimethoxy-1,1′-binaphthyl-3,3′-bis(4-pyridyl-amido) **L3** was synthesized as described in § 3.3.3, in collaboration with the University of Pavia (Italy), since it was designed as an axially chiral spacer capable of bridging the metal connecting sites with the intent of introducing chirality and imparting a helicoidal shape to the resultant coordination polymer. The NH amide group is locked in an S(6)-type hydrogen-bonded system with the neighboring phenol ether in the 2,2' positions. This confers rigidity to the ligand in order to transfer the chiral information and twisting derived from the binaphthyl chiral axis to the overall coordination polymers. Ligand **L3** has been reacted under solvothermal conditions in a 1:1 molar ratio only with the nickel dithiophosphato Ni^{II} complexes $[((MeO)_2PS_2)_2Ni]$ (**D1**) and $[((EtO)_2PS_2)_2Ni]$ (**D2**), using pure chloroform or a mixture of chloroform and the pertinent alcohol as solvent. Dithiophosphonato complexes were not reacted in order to avoid the bulky aromatic appendages. The reactions afforded solid and crystalline compounds, which have been isolated and fully characterized as described in § 3.4.10 and 3.4.11. Due to topology reasons, the two nitrogen atoms cannot bind to the same atom Ni^{II}, therefore **L3** was expected to bridge two dithiophosphato units acting as a chiral spacer. Single crystal X-ray diffraction performed on the resulting compounds confirmed their polymeric nature corresponding to the formulations $(\mathbf{D1}\cdot\mathbf{L3})_\infty$ and $(\mathbf{D2}\cdot\mathbf{L3})_\infty$. Crystallographic data and selected bond lengths and angles for $(\mathbf{D1}\cdot\mathbf{L3})_\infty$ and $(\mathbf{D2}\cdot\mathbf{L3})_\infty$ are reported in 2.8 and 2.9 Tables, respectively. Polymer $(\mathbf{D1}\cdot\mathbf{L3})_\infty$ crystallizes in the monoclinic $P2_1$ chiral space group, with two independent **D1** units, two **L3** ligands, and one water molecule in the asymmetric unit. The pyridine units of **L3** are coordinated to the Ni^{II} ion of two adjacent dithiophosphoric units, thus forming polymeric chains. As exemplified in Fig. 2.6, both polymers show the nickel ion lying in distorted octahedral environments that anyway differ in term of configuration of the metal center, which is *trans* for $(\mathbf{D1}\cdot\mathbf{L3})_\infty$ and *cis* for $(\mathbf{D2}\cdot\mathbf{L3})_\infty$. The coordination of a neutral donor reduces the net positive charge on the central Ni^{II} ion leading to a lengthening of the Ni-S bond lengths and a consequent decrease in the S-Ni-S angle with respect to the corresponding Ni^{II} square planar complex. At the same time increases the negative charge on the atoms of sulfur with a consequent opening of the S-P-S angle. The $(\mathbf{D1}\cdot\mathbf{L3})_\infty$ and $(\mathbf{D2}\cdot\mathbf{L3})_\infty$. compounds consist of helically shaped polymers: right-handed helical chain for $(\mathbf{D1}\cdot\mathbf{L3})_\infty$ and left-handed helical chain for $(\mathbf{D2}\cdot\mathbf{L3})_\infty$, as shown in the Figure 2.7 with Ni···Ni distances of 20.66 Å for $(\mathbf{D1}\cdot\mathbf{L3})_\infty$ and 18.38 Å $(\mathbf{D2}\cdot\mathbf{L3})_\infty$.

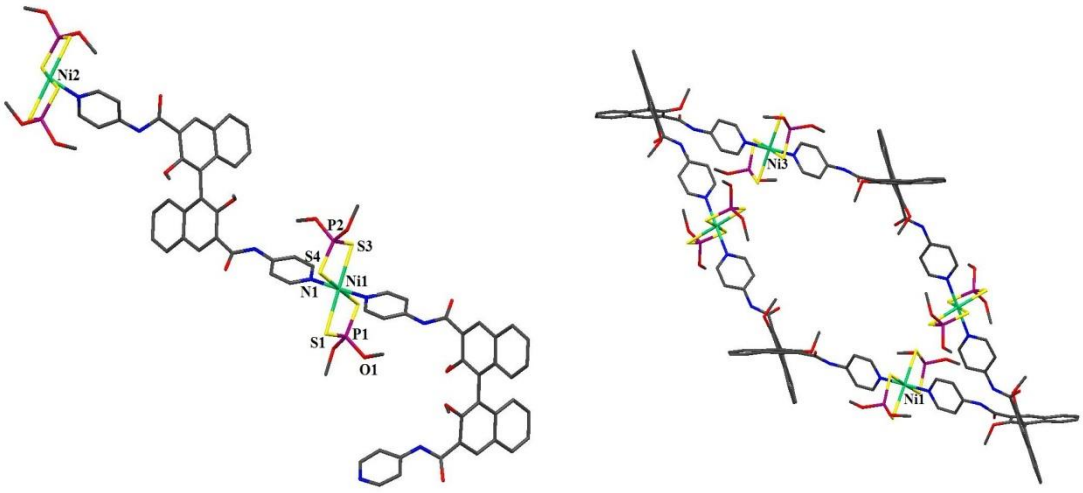

(D1·L3)$_\infty$

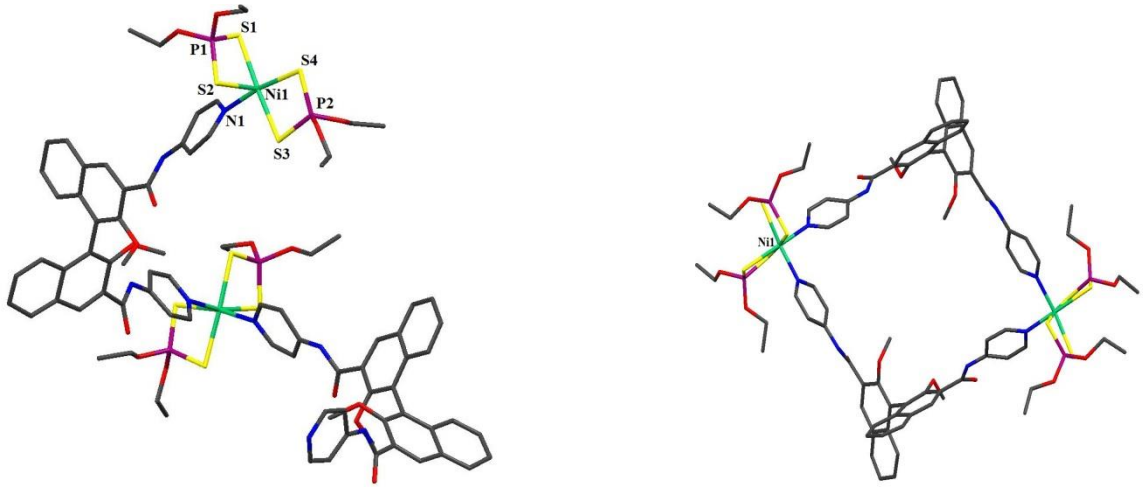

(D2·L3)$_\infty$

Figure 2.24 Helical Chains: view along the crystallographic axis *a* (left) and along the propagation direction *b* (right) of **(D1·L3)**$_\infty$ and view along the crystallographic axis *b* (left) and along the propagation direction *a* (right) of **(D2·L3)**$_\infty$ compounds. For clarity, only non carbon atoms have been labeled and hydrogen atoms omitted.

Table 2.9 Summary of Basic Crystal Data for **(D1·L3)**$_\infty$ and **(D3·L3)**$_\infty$

Empirical Formula	$C_{38}H_{38}N_4NiO_8P2S_4\ H_2O$ **(D1·L3)**$_\infty$	$C_{42}H_{46}N_4NiO_8P_2S_4$ **(D2·L3)**$_\infty$
Formula weight (g mol^{-1})	936.64	983.74
Temperature (K)	120	120
Crystal system	Monoclinic	Orthorhombic

Space group	P21	P212121
a, b, c (Å)	9.6133(2) 45.6542(12) 10.5801(3)	15.332(2) 8.6055(10) 34.795(4)
α, β, γ (°)	90; 113,202(1); 90	90; 90; 90
Volume (Å^3)	4267.92(19)	4590.8(10)
Z	2	4
Calculated density (g cm^{-3})	1.458	1.423
Reflections collected/Unique	44 414/18 504	26 414/7285
Wavelength	λ =71075	λ =71075
Final R indexes [I>=2σ (I)]	R_1 =0.0587 wR_2 = 0.1325	R_1 =0.1495 wR_2 = 0.3147

Table 2.10 Selected Bond Lengths (Å) and Angles (°) for (**D1·L3**)$_\infty$ (**D2·L3**)$_\infty$

Atoms	$C_{38}H_{38}N_4NiO_8P_2S_4·H_2O$ (**D1·L3**)$_\infty$	$C_{42}H_{46}N_4NiO_8P_2S_4$ (**D2·L3**)$_\infty$
Ni1-S1	2.5385(15)	2.513(6)
Ni1-S2	2.5001(15)	2.499(5)
Ni1-S3	2.5490(15)	2.514(5)
Ni1-S4	2.4900(15)	2.538(6)
Ni1-N1	2.093(4)	2.092(15)
Ni1-N3	2.085(4)	2.094(14)
Ni2-S5	2.5196(16)	-
Ni2-S6	2.4738(17)	-
Ni2-S7	2.4647(16)	-
Ni2-S8	2.5332(16)	-
Ni2-N2	2.074(5)	-
Ni2-N4	2.084(4)	-
S1-P1	1.983(3)	2.007(9)
S2-P1	1.9675(19)	1.949(7)
S3-P2	1.983(3)	2.010(7)
S4-P2	1.9731(3)	1.989(9)
S5-P3	1.985(2)	-
S6-P3	1.974(2)	-
S3-P4	1.986(2)	-
S4-P4	1.987(2)	-
S1-Ni1-S2	81.70(5)	79.66(19)
S1-Ni1-S3	178.74(5)	98.4(2)
S3-Ni1-S2	97.48 (5)	174.43(17)
S4-Ni1-S1	99.42 (5)	93.28(16)

S4-Ni1-S2	178.74(5)	93.99(19)
S4-Ni1-S3	81.40 (5)	80.86(19)
S1-Ni1-N1	89.70 (12)	87.4 (4)
S2-Ni1-N1	90.78 (12)	94.6 (4)
S3-Ni1-N1	89.48 (12)	90.6 (4)
S4-Ni1-N1	89.79 (12)	171.4(5)
S1-Ni1-N2	89.48 (12)	167.0(4)
S2-Ni1-N2	86.65 (12)	87.6 (4)
S3-Ni1-N2	89.96(12)	94.5 (4)
S4-Ni1-N2	90.77 (12)	89.7 (4)
S5-Ni2-S6	82.03 (5)	-
S5-Ni2-S7	96.23(53)	-
S5-Ni2-S8	178.42(6)	-
S6-Ni2-S7	178.25(6)	-
S6-Ni2-S8	99.43 (5)	-
S7-Ni2-S8	82.32 (5)	-
S5-Ni1-N2	91.19 (13)	-
S5-Ni2-N4	88.71 (12)	-
S6-Ni2-N2	90.38 (13)	-
S6-Ni2-N4	89.26(12)	-
S7-Ni2-N2	90.86 (12)	-
S7-Ni2-N4	89.26(12)	-
S8-Ni2-N2	89.50 (5)	-
S8-Ni2-N4	90.86(12)	-
S1-P1-S2	113.06 (9)	108.5(3)
S3-P2-S4	112.32 (9)	110.0(3)
S5-P1-S6	111.75 (10)	-
S7-P2-S8	111.49 (9)	-
N1-Ni2-N4	179.05 (16)	91.6 (5)

The spirals of (**D1**·**L3**)$_\infty$ run along the *b* direction involving crystallographic 2-fold screw axis, with a helical pitch of 45.65 Å coincident with the *b*-axis length, and intertwine with each other in both the *a* and *c* directions in a densely interlocked architecture stabilized by an intricate net of H-bonds, mainly involving the amido groups, the water molecules and both the P-methoxy substituents, Fig. 2.7. The spirals of (**D2**·**L3**)$_\infty$ run parallel along the *a* direction involving a crystallographic 2-fold screw axis with a helical pitch of 15.33 Å, coincident with the *a*-axis length, Fig. 2.8. Although the spirals are homochiral, they pack in the crystal with opposite screw sense: at the left side of Fig. 2.8 helices running along the -100 (top) and 100 (bottom) directions are shown. Spirals with the same

orientation intertwine with each other and pack in a quite compact arrangement formed by stacking planes formed by helices running either along 100 or −100 shown in blue and yellow in Figure 2.8 (right), respectively.

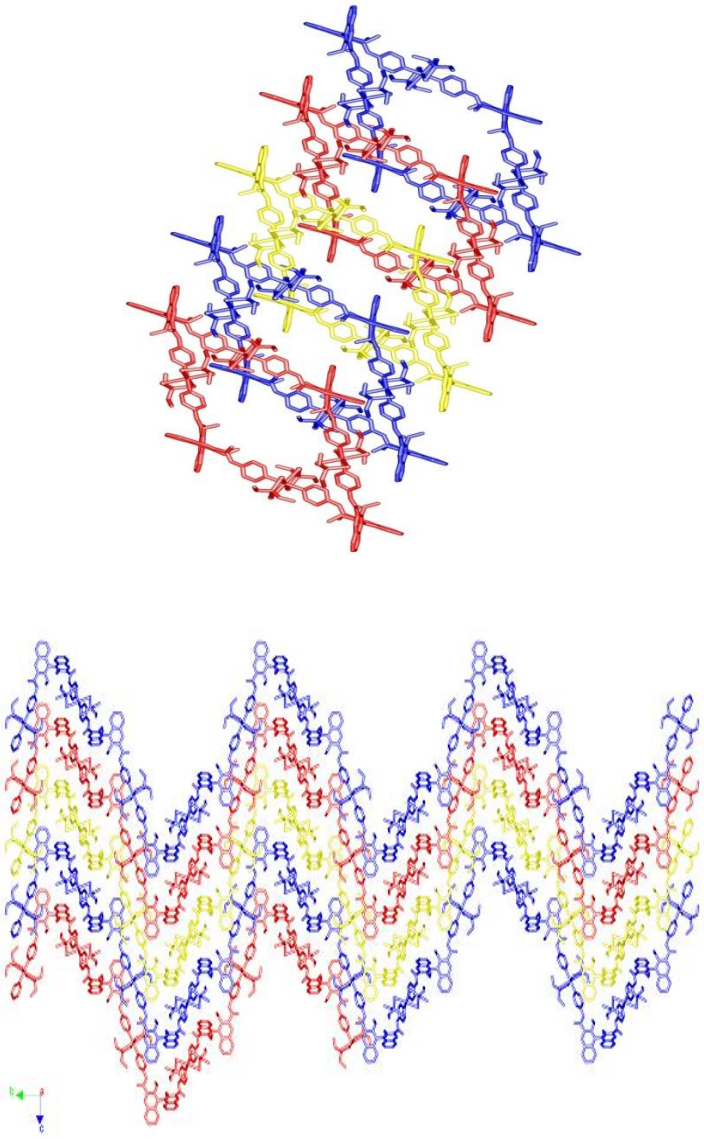

Figure 2.25 Packing Views of intertwining Helices of **(D1·L3)**$_\infty$ along *b* (left) and *a* (right) axes. H atoms have been omitted and the spirals have been pointed out by using different colors for clarity.

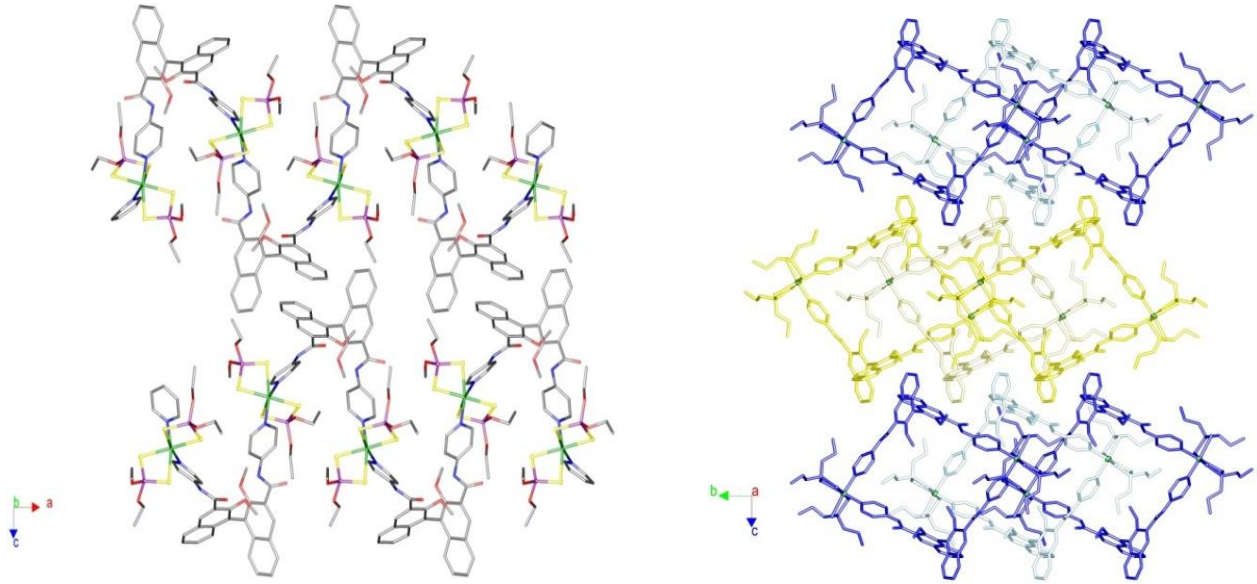

Figure 2.26 View of the Helices of **(D2·L3)**$_\infty$ running along the −100 (top) and 100 (bottom) directions; right: Packing View along the *a* axis showing alternating planes formed by intertwining spirals running along the −100 (yellow) and 100 (blue) directions. H atoms have been omitted for clarity.

It is interesting to note that, different from what was previously observed for **(D1·L3)**$_\infty$ the crystal packing of **(D2·L3)**$_\infty$ does not involve the P atom substituents given that spirals intertwine through H bonds involving the amido groups, the MeO substituents and the pyridine rings of the binaphthyl ligands and the S1 atom coordinated to the metal ion. The planes formed by differently oriented helices pack on each other leaving small empty spaces of about 120 Å3, comprising 2.6% of the cell volume.

2.3.2.2 2,5-bis(4-pyridyl)-4-thia-1,3-thiazolidine (L4) and 2,5-bis(3-pyridyl)-4-thia-1,3-thiazolidine (L5)

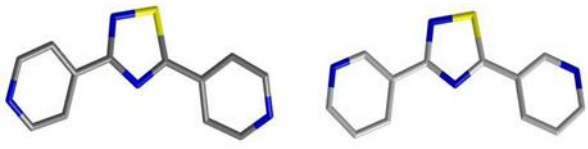

L4 **L5**

The bis-functional ligands 2,5-bis(4-pyridyl)-4-thia-1,3-thiazolidine (**L4**) and 2,5-bis(3-pyridyl)-4-thia-1,3-thiazolidine (**L5**) were firstly isolated by Meltzer et al. in 1955,[56] but their complexing ability towards metal ions, or as Lewis donors, has not ever been investigated to date. They have been prepared following the synthetic method described in Scheme 3.5 and following the

procedure described in § 3.3.4. They differ for the position of the N-donor atoms in the pyridinic rings. The free rotation of the pyridinic rings allows the spacer to adopt different conformations but keeping a certain rigidity tied to the presence of the three aromatic rings that constitute the molecule. The pyridyl rings in **L4** and **L5** feature different geometry and separation lengths (9.95 and 9.60 Å, respectively). Moreover, due to the different position of the nitrogen atoms in **L5** and to the different rotational conformations allowed to the pyridyl rings, several orientations of the binding sites can be expected. In the case of **L5**, two planar isomers, cissoid and transoid, are possible, differing in energy by less than 1 kcal mol^{-1} and showing similar metric parameters.[57] Ligands **L4** and **L5** have been reacted under solvothermal conditions with nickel dithiophosphato and dithiophosphonato Ni^{II} complexes $[((MeO)_2PS_2)_2Ni]$ (**D1**), $[((EtO)_2PS_2)_2Ni]$ (**D2**), $[((MeO\text{-}C_6H_4)(MeO))PS_2)_2Ni]$ (**D3**), and $[((MeO\text{-}C_6H_4)(EtO))PS_2)_2Ni]$ (**D4**). The reactions afforded solid and crystalline compounds, which have been isolated and fully characterized as described in paragraphs 3.4.12-3.4.20. Due to topology reasons, the two nitrogen atoms cannot bind to the same atom Ni^{II}, therefore **L4** and **L5** are expected to bridge two dithiophosphato or dithiophosphonato units acting as a rigid spacers. Single crystals suitable for X-ray diffraction were obtained for all compounds with the only exception of (**D4**·**L5**), and structural analysis was performed on the resulting compounds confirming a polymeric nature in the cases of $(\mathbf{D1}\cdot\mathbf{L4})_\infty$, $(\mathbf{D2}\cdot\mathbf{L4})_\infty$, $(\mathbf{D3}\cdot\mathbf{L4})_\infty$, $(\mathbf{D3}\cdot\mathbf{L5})_\infty$, and $(\mathbf{D4}\cdot\mathbf{L5})_\infty$. A dimeric nature for compounds $(\mathbf{D1}\cdot\mathbf{L5})_2$ and $(\mathbf{D2}\cdot\mathbf{L5})_2$ was found instead. Crystallographic data and selected bond lengths and angles for $(\mathbf{D1}\cdot\mathbf{L4})_\infty$-$(\mathbf{D3}\cdot\mathbf{L4})_\infty$; and for $(\mathbf{D1}\cdot\mathbf{L5})_2$-$(\mathbf{D2}\cdot\mathbf{L5})_2$ and $(\mathbf{D3}\cdot\mathbf{L5})_\infty$-$(\mathbf{D4}\cdot\mathbf{L5})_\infty$ are reported in Tables 2.10, 2.11 and 2.12, 2.13, respectively. As exemplified in Fig. 2.9, and 2.10 all compounds show the nickel ion lying in a distorted octahedral environment with the equatorial positions occupied by two dithiophosphoric units acting as isobidentate ligands with almost equivalent Ni-S and P-S bonds, featuring the P-substituents in the original *trans* configuration. The pyridine units of **L4** and **L5** are axially coordinated to the Ni^{II} ion of two adjacent dithiophosphoric units, thus forming the above mentioned polymeric chains and the two dimers. The coordination of a neutral donor reduces the net positive charge on the central Ni^{II} ion leading to a lengthening of the Ni-S bond lengths and a consequent decrease in the S-Ni-S angle with respect to the corresponding Ni^{II} square planar complex. At the same time increases the negative charge on the sulfur atoms with a consequent opening of the S-P-S angle. The polymeric structures obtained by using the ligand **L4** are neutral parallel chains running in undulated lines with Ni-Ni distances of 13.70, 14.15, and 13.97 Å for $(\mathbf{D1}\cdot\mathbf{L4})_\infty$, $(\mathbf{D2}\cdot\mathbf{L4})_\infty$, and $(\mathbf{D3}\cdot\mathbf{L4})_\infty$, respectively, Fig. 2.9. The orientation of the nitrogen atoms para-positioned in the outwards pyridyl rings of **L4** self-govern the geometry of the resulting supramolecular aggregates, leading to coordination polymers with the same primary motif independently from the nature of the dithiophosphorous complex used. The polymeric chains

interact by weak hydrogen bonds especially of the C-H···S type, involving the pyridine rings and the coordinated sulfur atoms, and pack in 2D layers as shown in the Fig. 2.10.

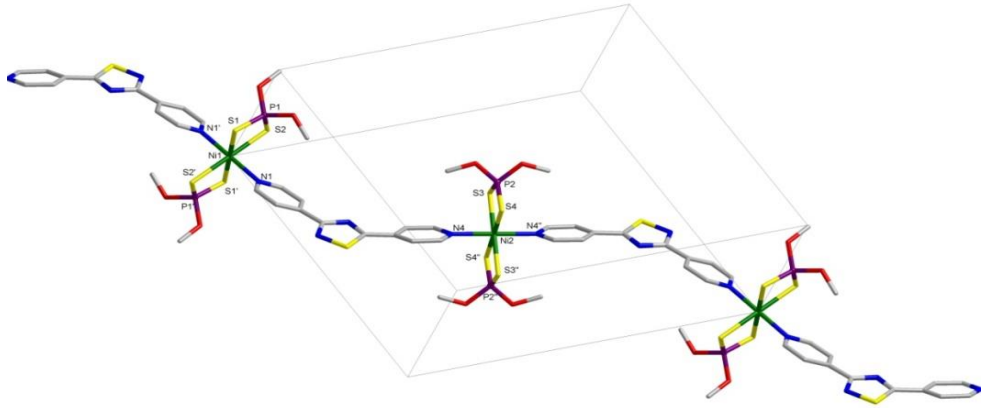

(D1·L4)$_\infty$

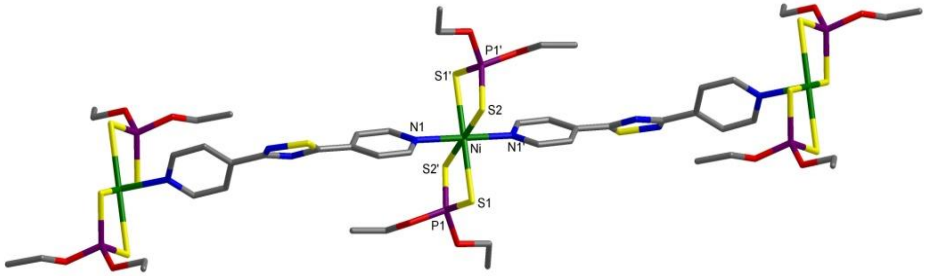

(D2·L4)$_\infty$

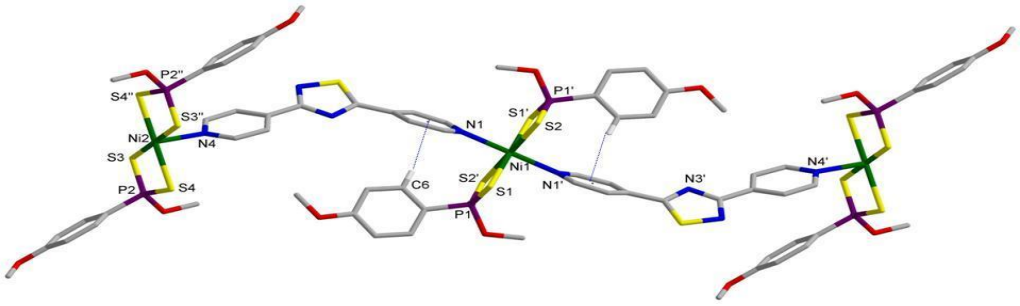

(D3·L4)$_\infty$

Figure 2.27 Polymeric Chains of Compounds **(D1·L4)**$_\infty$ and **(D2·L4)**$_\infty$ **(D3·L4)**$_\infty$. For clarity, only non-carbon atoms have been labeled and hydrogen atoms omitted.

Table 2.11 Summary of Basic Crystal Data for **(D1·L4)**$_\infty$, **(D1·L4)**$_\infty$ and **(D2·L4)**$_\infty$

Empirical Formula	$C_{16}H_{20}N_4NiO_4P_2S_5$ **(D1·L4)**$_\infty$	$C_{20}H_{28}N_4NiO_4P_2S_5$ **(D2·L4)**$_\infty$	$C_{28}H_{28}N_4NiO_4P_2S_5$ **(D3·L4)**$_\infty$
Formula weight (g mol^{-1})	613.34	669.41	765.52

Temperature (K)	120(2)	120(2)	120(2)
Crystal system	Monoclinic	Orthorhombic	Triclinic
Space group	P2(1)/c (no. 14)	Pbcn (no. 60)	P-1 (no. 2)
a, b, c (Å)	16.542(3) 7.489(2) 20.642(6)	11.6939(8) 15.2594(14) 15.9310(13)	9.7075(2) 10.6736(2) 17.4582(2)
α, β, γ (°)	90; 94.29(2); 90	90; 90; 90	73.230; 87.086(1); 72.131
Volume (Å^3)	2550.0(11)	2842.8(4)	1647.02(4)
Z	4	4	2
Calculated density (g cm^{-3})	1.598	1.564	1.544
Reflections collected/Unique	32091/5840/0.0707	21763/3263/0.0403	36271/7555/0.047
Wavelength	λ =71075	λ =71075	λ =71075
Final R indexes [I>=2σ (I)]	R_1 = 0.0492, wR_2 = 0.1031	R_1 = 0.0331, wR_2 = 0.0817	R_1 = 0.0361, wR_2 = 0.0798

Table 2.12 Selected Bond Lengths (Å) and Angles (°) for (**D1·L4**)$_\infty$, (**D2·L4**)$_\infty$, and (**D3·L4**)$_\infty$

Atoms	$C_{16}H_{20}N_4NiO_4P_2S_5$(**D1·L4**)$_\infty$	$C_{20}H_{28}N_4NiO_4P_2S_5$(**D2·L4**)$_\infty$	$C_{28}H_{28}N_4NiO_4P_2S_5$(**D3·L4**)$_\infty$
Ni-S1	2.5148(12)	2.4847(6)	2.4468(5)
Ni-S2	2.4628(11)	2.4683(5)	2.4818(5)
Ni-N1	2.095(3)	2.1042(16)	2.1322(16)
Ni2-N4	2.100(3)	2.1326(17)	-
S1-P1	1.9700(15)	1.9694(8)	2.0010(7)
S2-P1	1.9821(15)	1.9884(7)	1.9951(7)
P2-S3	1.9807(15)	-	1.9994(7)
P2-S4	1.9771(15)	-	1.9914(8)
S1-Ni-S2	81.89(4)	97.99(2)	97.16(2)
S1-P1-S2	111.27(7)	110.39(3)	109.36(3)
S1-Ni-N1	91.02(8)	89.72(5)	90.84(4)
S2-Ni-N1	89.58(9)	90.39(5)	82.84(2)
N4-Ni2-S3	88.96(9)	-	90.94(5)
N4-Ni2-S4	90.67(8)	-	90.73(5)
S3-Ni2-S4	82.19(4)	-	82.27(2)
S3-Ni2-S4	110.63(6)	-	110.03(3)

It is interesting to note that in (**D3·L4**)$_\infty$, the presence and orientation of the aromatic rings bound the phosphorus atoms influence the final architecture of the polymers by the formation of C-H···π or π-π intramolecular interactions (**D3·L4**)$_\infty$, $(C_6H_5)\cdots(C_5H_4N)_{centroid}$: 2.61 Å, leading to the formation of cavities of about 61 Å^3.

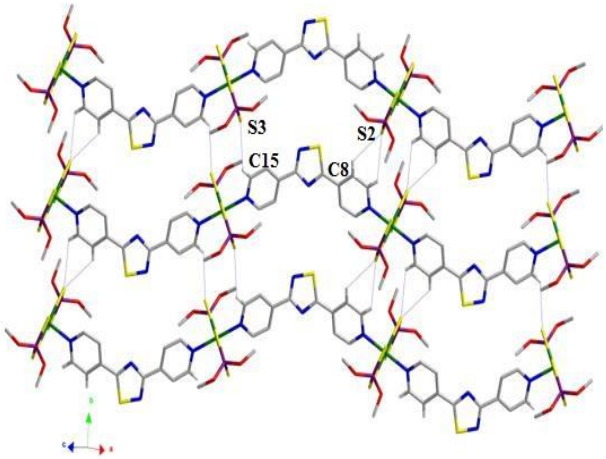

$(\mathbf{D1{\cdot}L4})_{\infty}$

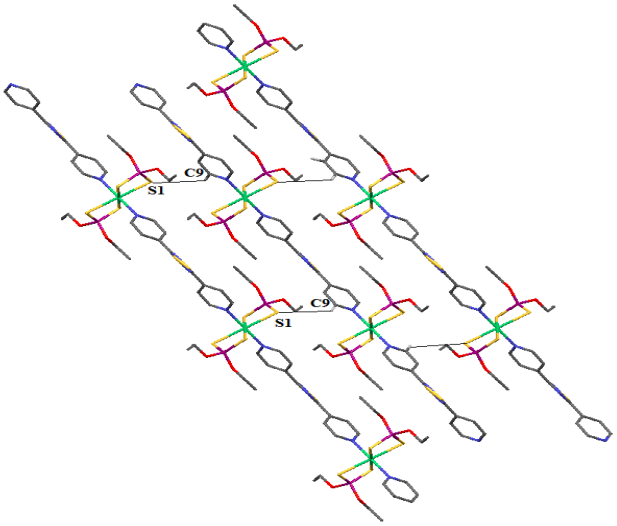

$(\mathbf{D2{\cdot}L4})_{\infty}$

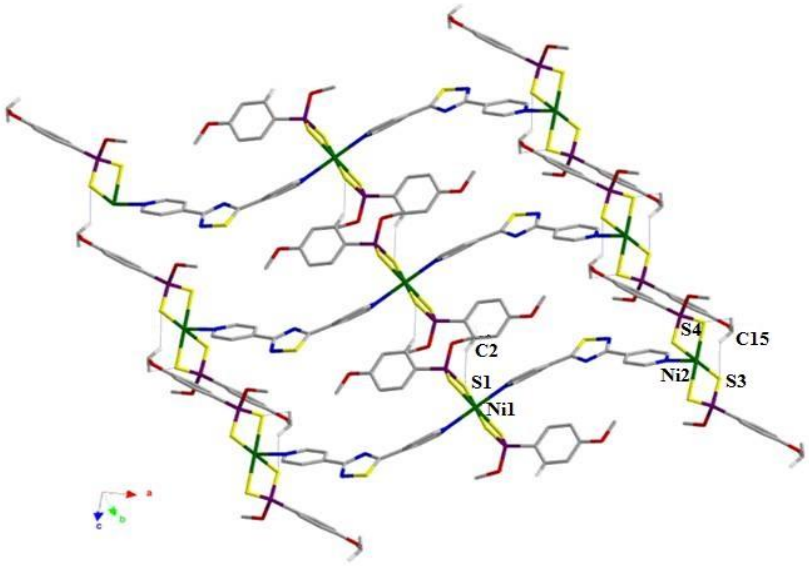

$(\mathbf{D3{\cdot}L4})_{\infty}$

Figure 2.28 Crystal Packing Views of Compounds $(\mathbf{D1{\cdot}L4})_{\infty}$, $(\mathbf{D2{\cdot}L4})_{\infty}$, and $(\mathbf{D3{\cdot}L4})_{\infty}$, evidencing the following H-bonds interactions: $(\mathbf{D1{\cdot}L4})_{\infty}$: C2–H2···S1 3.04; C15–H15···S3 2.85; C8–H8···S2 2.89 Å; $(D2{\cdot}L4)_{\infty}$: C9–H9···S1 2.90; C15–H15···S3 2.91 Å; $(\mathbf{D3{\cdot}L4})_{\infty}$: C2–H2···S1 2.73 Å. Hydrogen atoms not involved in the showed interactions have been omitted for clarity reasons.

The use of **L5** as spacer turns out to lead to less predictable final products if compared with the results obtained by using **L4.** The reactions of **L5** with the four dithiophosphorous nickel complexes under solvothermal conditions afforded crystalline compounds recognized by means of single crystal X-ray diffraction as the dimers $(\mathbf{D1{\cdot}L5})_2$, $(\mathbf{D2{\cdot}L5})_2$ and the coordination polymers $(\mathbf{D3{\cdot}L5})_{\infty}$, and $(\mathbf{D4{\cdot}L5})_{\infty}$, Fig. 2.11.

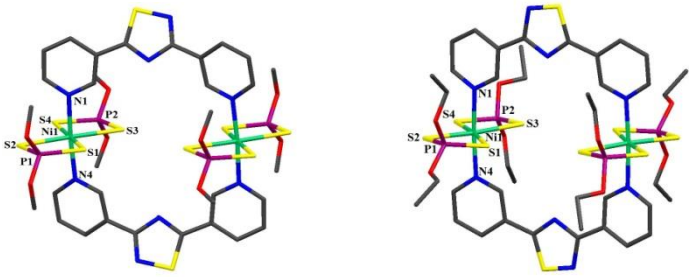

(D1·L5)$_2$ **(D2·L5)**$_2$

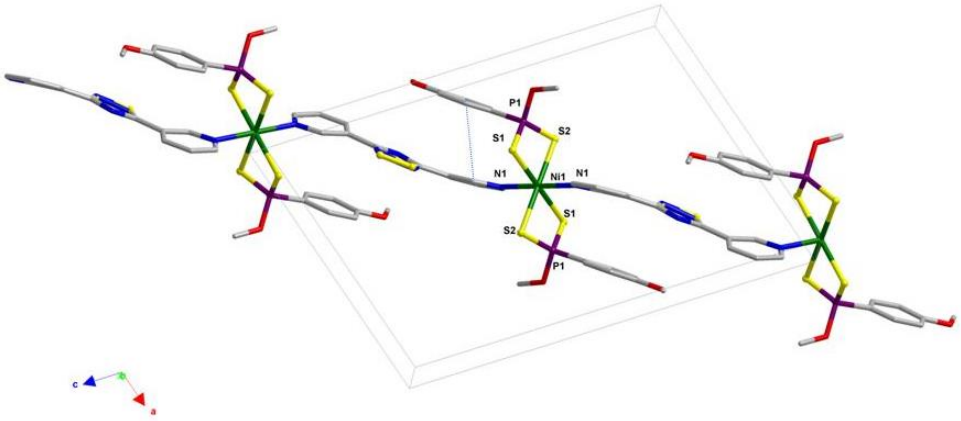

(D3·L5)$_\infty$

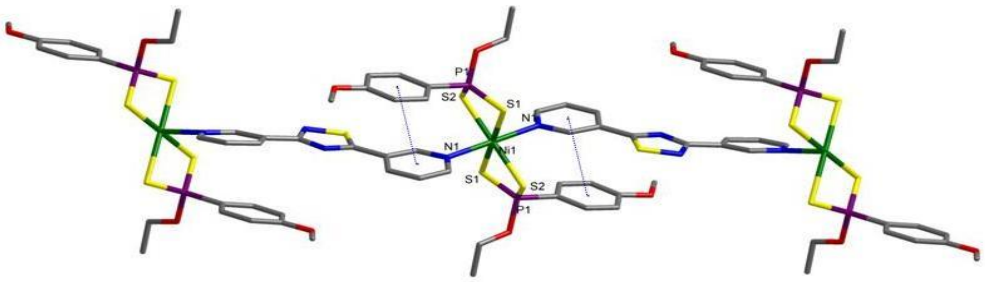

(D4·L5)$_\infty$

Figure 2.29 Dimeric Units **(D1·L5)**$_2$ and **(D2·L5)**$_2$ and Polymeric Chains **(D3·L4)**$_\infty$ and **(D4·L4)**$_\infty$. For clarity, only non-carbon atoms have been labeled and hydrogen atoms omitted.

Notwithstanding the similarities with the results obtained with **L4**, the use of **L5** as a linker leads to different constructs. In fact **L5** can exist either as a transoid or cissoids isomer, and in this last case can show a convergent or a divergent conformation depending on the orientation of N-atoms meta-positioned in the pyridyl rings that can point inwards or outwards with respect to the ligand bite angle. The different constructs experimentally found exemplify the different conformations of the

ligand: $(\mathbf{D1{\cdot}L5})_2$ and $(\mathbf{D2{\cdot}L5})_2$ feature **L5** in a cissoids convergent conformation, whilst polymers $(\mathbf{D3{\cdot}L4})_\infty$ and $(\mathbf{D4{\cdot}L4})_\infty$ feature **L5** in a cissoids divergent conformation.

Table 2.13 Summary of Basic Crystal Data for $(\mathbf{D1{\cdot}L5})_2$, $(\mathbf{D2{\cdot}L5})_2$, $(\mathbf{D3{\cdot}L4})_\infty$, and $(\mathbf{D4{\cdot}L4})_\infty$

Empirical Formula	$C_{32}H_{28}N_4$ Ni O_4 P_2 S_4 $(\mathbf{D1{\cdot}L5})_2$	$C_{40}H_{56}N_8Ni_2O_8P_4S_{10}$ $(\mathbf{D2{\cdot}L5})_2$	$C_{28}H_{28}N_4NiO_4P_2S_5$ $(\mathbf{D3{\cdot}L5})_\infty$	$C_{30.}H_{32.}N_4Ni_2O_4P_2S_5$ $(\mathbf{D4{\cdot}L5})_\infty$
Formula weight (g mol^{-1})	1226.68	1338.89	765.81	793.58
Temperature (K)	120 (2)	120(2)	120(2)	120 (2)
Crystal system	Monoclinic	Triclinic	Monoclinic	Monoclinic
Space group	P21/n (No.14)	*P-1* (no. 2)	*P2/n(No.13)*	*P2/n(No.13)*
a, b, c (Å)	14.0311(13); 14.9236(13); 12.8460(5)	11.728(2) 14.354(3) 18.657(4)	12.8213(3); 7.2342(2); 19.1246(6)	12.8337 (2); 7.2101 (1); 20.3035(3)
α, β, γ (°)	90; 113.786(5); 90	104.40(3);103.02(3); 101.92(3)	90; 106.1860(10); 90	90; 101.8880(10);90
Volume (Å^3)	2461.4(3)	2862.9(13)	1703.53(7)	1838.43 (5)
Z	4	2	2	2
Calculated density (g cm^{-3})	1.655	1.553	1.493	1.434
Reflections collected/Unique	19049/5601	25481/2921	19777/3900	24334/4211
Wavelength	λ =71075	λ =71075	λ =71075	λ =71075
Final R indexes [I>=2σ (I)]	R_1 = 0.0641, wR_2 = 0.1917	R_1 = 1277, wR_2 = 0.2445	R_1 = 0.0372, wR_2 = 0.0778	R_1 = 0.0330, wR_2 = 0.0863

Table 2. 14 Selected Bond Lengths (Å) and Angles (°) for $(\mathbf{D1{\cdot}L5})_2$, $(\mathbf{D2{\cdot}L5})_2$, $(\mathbf{D3{\cdot}L4})_\infty$, and $(\mathbf{D4{\cdot}L4})_\infty$

Atoms	$C_{32}H_{28}N_4\,Ni\,O_4\,P_2\,S_4$	$C_{40}H_{56}N_8Ni_2O_8P_4S_{10}$	$C_{28}H_{28}N_4NiO_4P_2S_5$	$C_{30.}H_{32.}N_4Ni_2O_4P_2S_5$
Ni-S1	2.5255(18)	2.480(3)	2.4915(6)	2.4772(5)
Ni-S2	2.4800(18)	2.469(2)	2.4871(6)	2.4886(5)
Ni-S3	2.4891(18)	2.495(2)	-	-
Ni-S4	2.4601(18)	2.501(3)	-	-
Ni-N1	2.093(5)	2.109(5)	2.160(2)	2.1582(14)
Ni-N4	2.4601(18)	2.111(5)		-
S1-P1	1.971(2)	1.970(4)	1.9974(8)	1.9962(7)
S2-P1	1.983(2)	1.970(4)	-	1.9986(7)
S3-P2	1.979(2)	1.981(3)	-	-
S4-P2	1.987(2)	1.967(4)	-	-
S1-Ni-S2	81.67(6)	82.86(8)	81.86(2)	97.82 (2)
S1-P1-S2	111.75(10)	112.4(2)	109.71(4)	109.58(3)
S1-Ni-N1	90.66(15)	88.6(2)	88.91(5)	88.86(4)
S2-Ni-N1	88.99(15)	89.02(18)	90.52(5)	88.76 (4)

The polymeric structures of $(\mathbf{D3{\cdot}L5})_\infty$ and $(\mathbf{D4{\cdot}L5})_\infty$, consist of undulated chains where the pyridine rings are axially coordinated to the Ni^{II} ion of two adjacent dithiophosphoric units. It is interesting to note that in $(\mathbf{D3{\cdot}L5})_\infty$ the nickel atoms lay in the corner of the unit cell and the presence of aromatic rings to the phosphorous atom disposed parallel (7.48°),influencing the final architecture of the polymers by the formation of π-π stacking interactions $(C_5H_4N)\cdots(C_6H_5\text{-}OCH_3)_{centroid}$ 3.72 Å that influence the final network. The coordination polymers pack in parallel chains interacting through the substituents at the phosphorus atoms to yield the 3D networks shown in Fig. 2.12. Instead as already mentioned the reaction with dithiophosphato complexes yields the dimers. $(\mathbf{D1{\cdot}L5})_2$ and $(\mathbf{D1{\cdot}L5})_2$ In this case probably, due to the small size of the substituents to the phosphorous atoms, a convergent coordination is preferred, leading to the formation of a hexagonal dimers. They interact towards S···H-C and N···H-C in $(\mathbf{D1{\cdot}L5})_2$, S···H-C and π-π stacking interactions $(C_2N_2S)\cdots(C_2N_2S)_{centroid}$ 3.43 Å in $(\mathbf{D2{\cdot}L5})_2$, creating bidimensional grids that present square openings of about 8 x 8 Å. Fig. 2.11

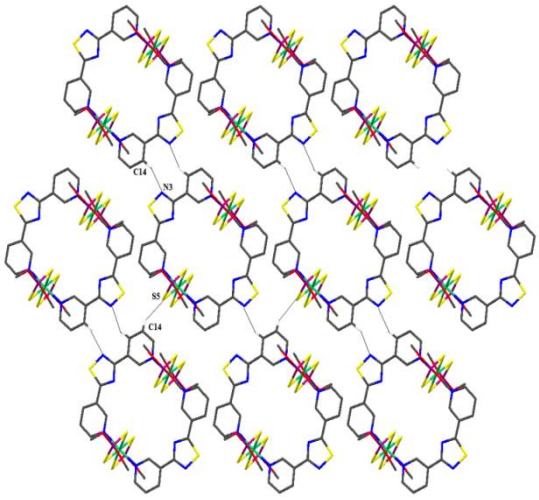

(**D1·L5**)$_2$

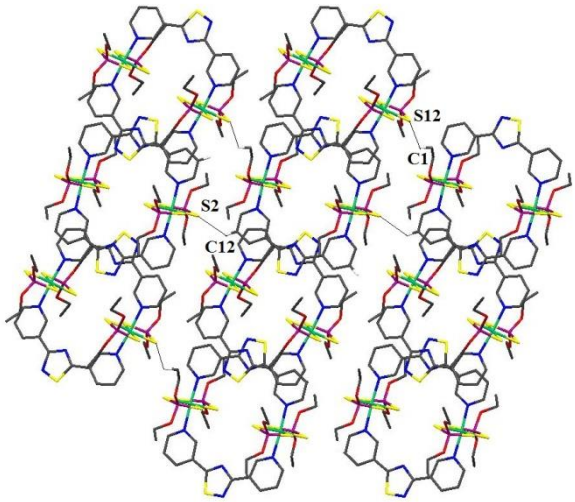

(**D1·L5**)$_2$

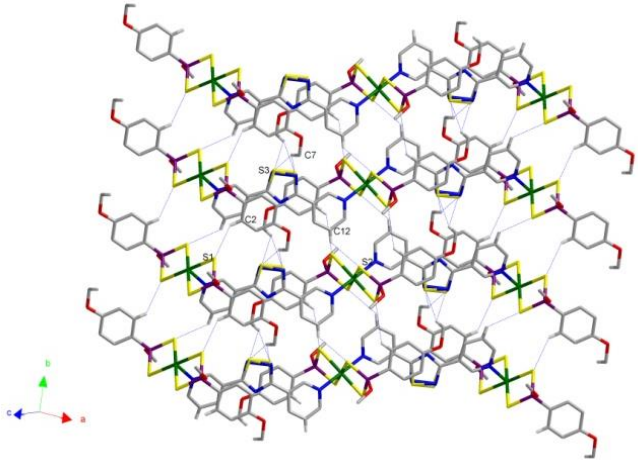

(**D3·L5**)$_\infty$

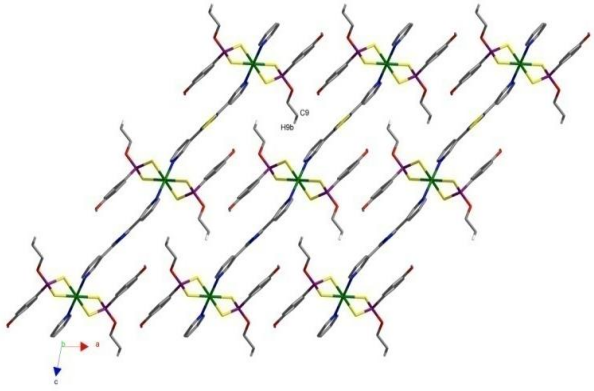

(**D4·L5**)$_\infty$

Figure 2.30 Crystal Packing Views of (**D1·L5**)$_2$, (**D3·L5**)$_\infty$ and (**D4·L5**)$_\infty$ showing the main interactions: (**D1·L5**)$_2$: C15-H1···S3 2.9 Å, C14-H14····N3 2.7 Å; C1-H1a···S12 2.99 Å C12-H12a····S2 2.88 Å (**D2·L5**)$_2$, C7-H7···S3 2.87Å. , C12-H12···S2 2.80 Å (**D3·L5**)$_\infty$: For clarity, only non-carbon atoms have been labeled and hydrogen atoms omitted.

2.3.3.Polypidiridin Ligands

2.3.3.1 1,3,5-tris-(3-pyridyl-ethynyl)-benzene (L6)

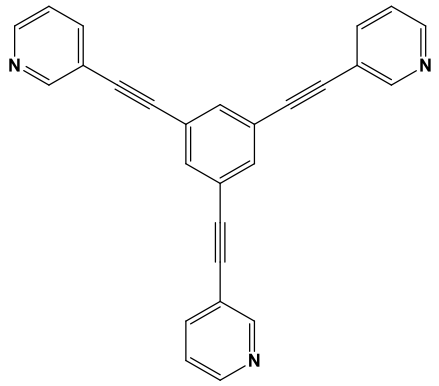

Ligand **L6** is a rigid multidentate spacer prepared following the synthetic method described in Scheme 3.6 and the procedure described in detail in § 3.3.5. Ligand **L6** has been reacted under solvothermal conditions in a 1:1 molar ratio with the nickel dithiophosphato and dithiophosphonato Ni^{II} complexes $[((MeO)_2PS_2)_2Ni]$ (**D1**), $[((EtO)_2PS_2)_2Ni]$ (**D2**), $[((MeO\text{-}C_6H_4)(MeO))PS_2)_2Ni]$ (**D3**), and $[((MeO\text{-}C_6H_4)(EtO))PS_2)_2Ni]$ (**D4**), using pure chloroform or a mixture of chloroform and the pertinent alcohol as solvent. The reactions afforded solid compounds, which have been isolated and fully characterized as described in § 3.4.20-3.4.24. Single crystals suitable for X-ray diffraction were obtained only from the reactions with **D2**, and, unexpectedly, crystal characterization performed on the compound revealed a dimeric nature corresponding to the formulation $(\mathbf{D2}\cdot\mathbf{L6})_2$. Crystallographic data and selected bond lengths and angles for $(\mathbf{D2}\cdot\mathbf{L6})_2$ are reported in Tables 2.14 and 2.15, respectively. As exemplified in Fig. 2.13, the compound $(\mathbf{D2}\cdot\mathbf{L6})_2$ shows the nickel ion lying in a distorted octahedral environment with the equatorial positions occupied by two dithiophosphato units acting as isobidentate ligands with almost equivalent Ni-S and P-S bonds. Only two of the three pyridyl units of **L6** interact with the metal ions and are axially coordinated to the Ni^{II} ion bridging two adjacent dithiophosphato units forming hexagonal dimers. The convergent coordination is probably preferred due to the small size of the substituents to phosphorus atoms. The coordination of the pyridyl neutral donors reduces the net positive charge on the central Ni^{II} ion leading to a lengthening of the Ni-S bond lengths and a consequent decrease in the S-Ni-S angle with respect to the corresponding Ni^{II} square planar complex. At the same time increases the negative charge on the atoms of sulfur with a consequent opening of the S-P-S angle.

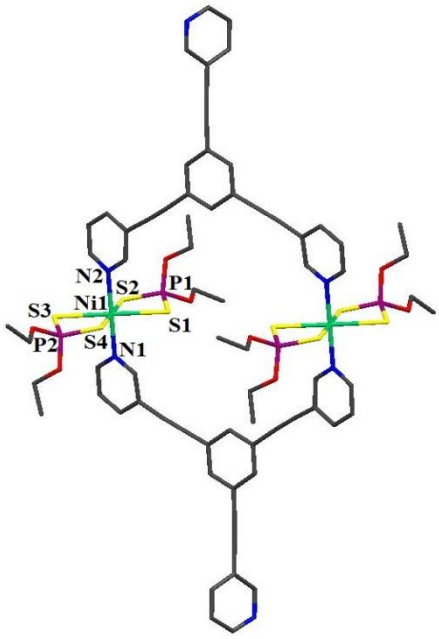

Figure 2.31 Dimer Structure of Compound (**D2·L6**)$_2$. Hydrogen atoms are omitted for clarity reason.

Table 2. 15 Summary of Basic Crystal Data for (**D2·L6**)$_2$

Empirical Formula	$C_{35}H_{36}N_3NiO_4P_2S_4$ (**D2·L6**)$_2$
Formula weight (g mol^{-1})	875.62
Temperature (K)	100
Crystal system	Triclinic
Space group	P -1
a, b, c (Å)	9.2130(5);15.0313(11);15.3960(11)
α, β, γ (°)	73.451(6);75.604(6);86.980(7)
Volume (Å^3)	1979.2(2)
Z	2
Calculated density (g cm^{-3})	1.458
Reflections collected/Unique	35815/25.242
Wavelength	λ =0.71075
Final R indexes [I>=2σ (I)]	R_1 =0.0603 wR_2 = 0.1704

Table 2. 16 Selected Bond Lengths (Å) and Angles (°) for (**D2·L6**)

Atoms	$C_{35}H_{36}N_3NiO_4P_2S_4$ $(\mathbf{D2{\cdot}L6})_2$
Ni-S1	2.5033(11)
Ni-S2	2.5267(12)
Ni-S3	2.5259(16)
Ni-S4	2.4936(15)
Ni-N1	2.111(4)
Ni-N2	2.104(4)
S1-P1	1.9827(19
S2-P1	1.9839(19)
S3-P2	1.979(2)
S4-P2	1.976(2)
S1-Ni-S2	82.37(4)
S1-Ni-S3	178.77(5)
S3-Ni-S2	98.77(5)
S4-Ni-S1	96.53(5)
S4-Ni-S2	178.86(5)
S4-Ni-S3	82.29(5)
S1-Ni-N1	90.31(13)
S2-Ni-N1	89.92(12)
S3-Ni-N1	89.37(13)
S4-Ni-N1	90.51(12)
S1-Ni-N2	91.33(13)
S2-Ni-N2	90.36(12)
S3-Ni-N2	88.99(13)
S4-Ni-N2	89.24(12)
S1-P1-S2	112.63(6)
S3-P2-S4	113.22(9)
N1-Ni-N2	178.35(17)

The dimers mainly interact through the C21-H21···S6' hydrogen bond involving one of the coordinated sulfur atoms and a hydrogen of one coordinated pyridine unit thus creating bi-dimensional grids that present square openings of about 10 x10 $Å^2$. (C21-H21···S6': H···S 2.845(2) Å, C···S 3.689(5) Å, C-H···S 152° (' -x, 2-y, 1-z;). (Fig.2.14)

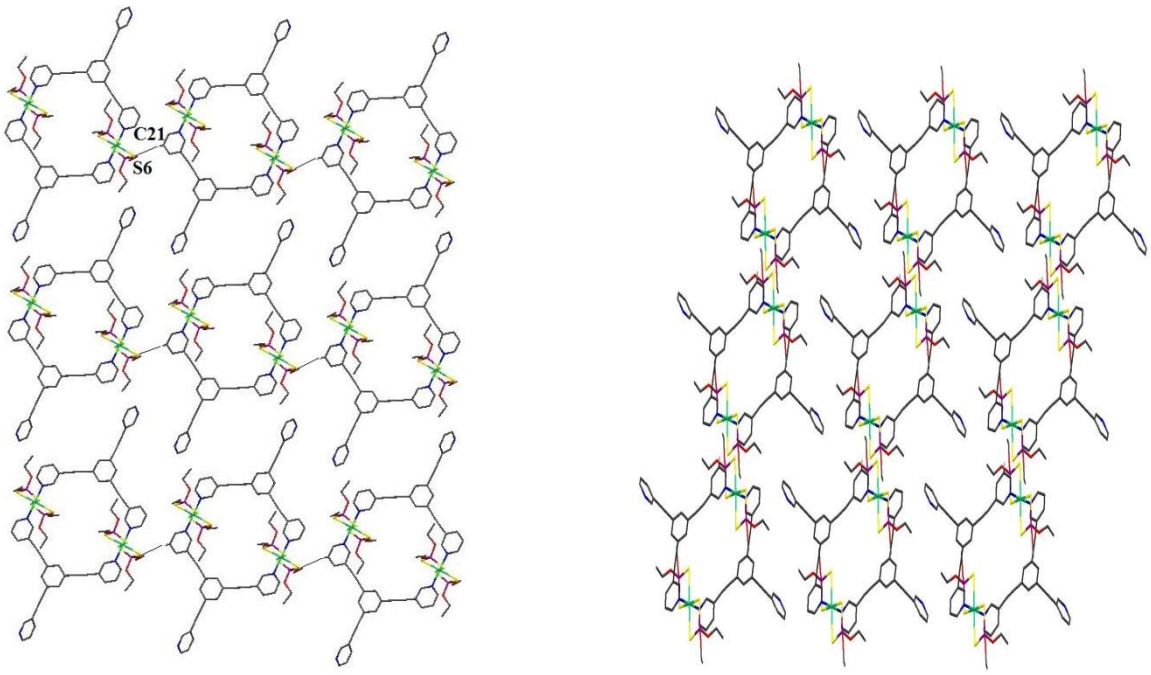

Figure 2.32 Crystal Packing Views of (**D2·L6**)$_2$. For clarity, only non-carbon atoms have been labeled and Hydrogen atoms are omitted for clarity reason.

2.3.3.2 1,3,5-benzene-tri(N-(3-Pyridyl))-carboxamide (L7)

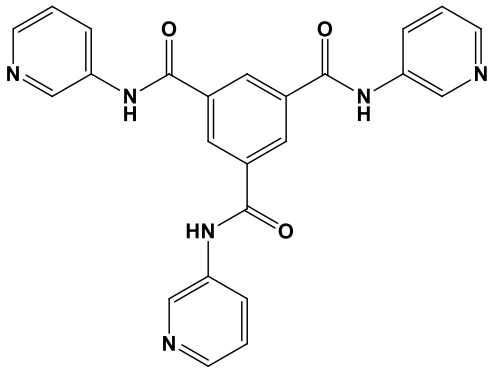

Ligand **L7** has been prepared following the synthetic method described in Scheme 3.7 and the procedure described in § 3.3.6. Ligand **L7** has been reacted under solvothermal conditions in a 1:1 molar ratio with the nickel dithiophosphato and dithiophosphonato Ni^{II} complexes [((MeO)$_2$PS$_2$)$_2$Ni] (**D1**), [((EtO)$_2$PS$_2$)$_2$Ni] (**D2**), [((MeO-C$_6$H$_4$)(MeO))PS$_2$)$_2$Ni] (**D3**), and [((MeO-C$_6$H$_4$)(EtO))PS$_2$)$_2$Ni] (**D4**), using pure chloroform or a mixture of chloroform and the pertinent

alcohol as solvent. The reactions afforded solid compounds, which have been isolated and fully characterized as described in § **3.4.24-3.4.29**. Single crystals suitable for X-ray diffraction were obtained only from the reactions with **D2**, and **D3** and, unexpectedly, crystal characterization performed on the compounds revealed the formation of the simple monomeric complexes [**D2**(**L7**)$_2$] and [**D3**(**L7**)$_2$]. Crystallographic data and selected bond lengths and angles for [**D2**(**L7**)$_2$] and [**D3**(**L7**)$_2$] are reported in Tables 2.16 and 2.17, respectively. As exemplified in Fig. 2.14, the two octahedral complexes show the nickel ion lying in a distorted octahedral environment with the equatorial positions occupied by two dithiophosphoric units acting as isobidentate ligands with almost equivalent Ni-S and P-S bonds, with **D3** featuring the P-substituents in the original *trans* configuration. Two ligands **L7** acting as a monodentate donors, with only one pyridine unit axially coordinated to the Ni^{II} ion, complete the metal coordination sphere thus leading to the octahedral complexes [**D2**(**L7**)$_2$] and [**D3**(**L7**)$_2$]. The coordination of a neutral donor reduces the net positive charge on the central Ni^{II} ion leading to a lengthening of the Ni-S bond lengths and a consequent decrease in the S-Ni-S angle with respect to the corresponding Ni^{II} square planar complex. At the same time increases the negative charge on the sulfur atoms with a consequent opening of the S-P-S angle.

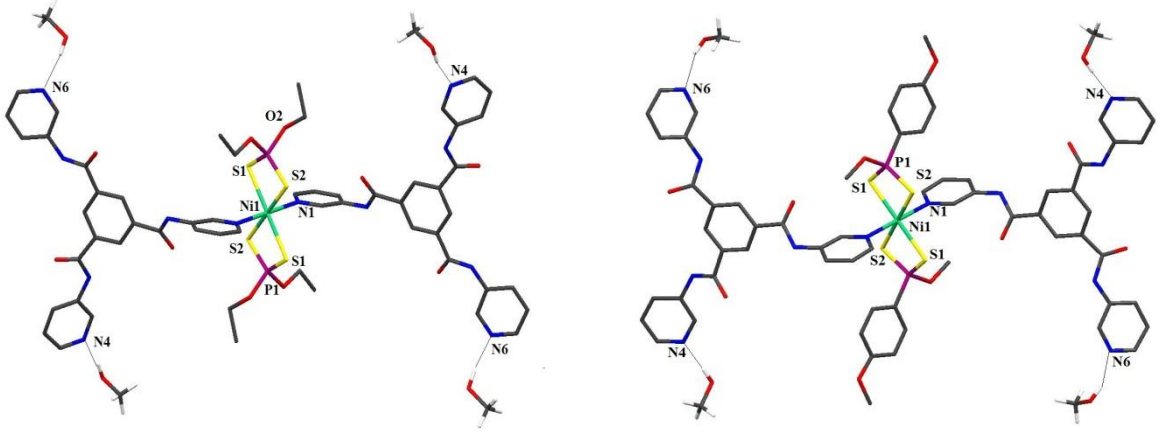

Figure 2.33 Octahedral Complexes [**D2(L7)$_2$**] and [**D3(L7)$_2$**]. For clarity, only non-carbon atoms have been labeled and hydrogen atoms omitted.

The four nitrogen atoms of the uncoordinated pyridine rings interact with methanol molecules (reaction solvent present in structure) through the very strong hydrogen bonds: [**D2(L7)$_2$**]: O7-H7A···N4': H···N 1.91 Å, O···N 2.733(3) Å, O-H···N 166°; O6-H6A···N6": H···N 2.00 Å, O···N 2.827(4) Å, O-H···N 169° (' -1+x, y, z; " 1+x, y, 1+z). [**D3(L7)$_2$**]: O45-H45···N4': H···N 1.91 Å, O···N 2.734(6) Å, O-H···N 176°; O46-H46···N6": H···N 1.95 Å, O···N 2.755(6) Å, O-H···N 160° ' -1+x, y, z; " 2-x, 2-y, 1-z).

The formation of these bonds can in our opinion explain the unexploited formation of coordination polymers.

Table 2.17 Summary of Basic Crystal Data for [**D2**(**L7**)$_2$] and [**D3**(**L7**)$_2$]

Empirical Formula	$C_{56}H_{56}N_{12}NiO_{10}P_2S_4$, $4(CH_3OH)$ [**D2**(**L7**)$_2$]	$C_{64}H_{56}N_{12}NiO_{10}P_2S_4$, $4(CH_3OH)$, $CHCl_3$ [**D3**(**L7**)$_2$]
Formula weight (g mol^{-1})	1434.18	1649
Temperature (K)	100 (2)	170 (2)
Crystal system	Triclinic	Triclinic
Space group	P-1	P-1
a, b, c (Å)	7.9460(17); 12.496(3); 18.259 4)	8.496(8); 12.951(12); 18.174 (17)
α, β, γ (°)	100.073(4);99.976(3);95.183 (3)	96.409(8);101.161(13);100.163 (13)
Volume (Å^3)	1744.(7)	1909(3)
Z	1	1
Calculated density (g cm^{-3})	1.365	1.435
Reflections collected/Unique	23297/8008	15133/8512
Wavelength	λ =71075	λ =71075
Final R indexes [I>=2σ (I)]	R_1 = 0.0653 wR_2 =0.1766	R_1 =0.1188 wR_2 = 0.2139

Table 2.18 Selected Bond Lengths (Å) and Angles (°) for [**D2**(**L7**)$_2$]and [**D3**(**L7**)$_2$]

Atoms	$C_{56}H_{56}N_{12}NiO_{10}P_2S_4 \cdot 4(CH_3OH)$ [**D2**(**L7**)$_2$]	$C_{64}H_{56}N_{12}NiO_{10}P_2S_4$, $4(CH_3OH)$, $CHCl_3$ [**D3**(**L7**)$_2$]
Ni-S1	2.493(2)	2.493(2)
Ni-S2	2.489(2)	2.489(2)
Ni-N1	2.147(4)	2.147(4)
S1-P1	1.998(2)	1.998(2)
S2-P1	1.995(2)	1.993(3)
P1-S2	1.971 (11)	1.995(2)
S1-Ni-S2	81.835(12)	97.82(8)
S1-P1-S2	109.99(2)	108.62(16)
S1-Ni-N1	90.03(4)	87.9(2)
S2-Ni-N1	90.36(3))	90.9(3)
N1-Ni-N1	180.00(12)	180.0

The crystal packing of both [**D2**(**L7**)$_2$] and [**D2**(**L7**)$_2$] is mainly built up through H-bondings involving the methanol molecules and the amido groups of the ligands: [**D2(L7)$_2$**]: N2-H2···O4': H···O 2.1 Å, O···N 2.933(3) Å, N-H···O 157°; N3-H3···O6": H···O 2.01(5) Å, O···N 2.882(3)Å, O-H···N 170°; N5-H5···O7"': H···O 2.0 Å, O···N 2.847(3) Å, O-H···N 162° (' 1+x, 1+y, z; "1-x, 1-y, 1-z; "' -x, 1-y, -z); **[D3**(**L7**)$_2$**]**: N5-H5···O45': H···O 1.95(5) Å, O···N 2.859(6) Å, N-H···O 176°; N3-H3···O46": H···O 2.12(5) Å, O···N 2.877(6) Å, O-H···N 171° (' 1-x, 2-y, 1-z; " -1+x, 1+y, z). Weak hydrogen bonds, especially of the C-H···S type that involve the dithiophosphoric units and pyridine hydrogens along with π-π intramolecular interactions involving the benzene rings with intercentroid distances of 3.95, and 3.91 Å for **[D2**(**L7**)$_2$**]** and **[D3**(**L7**)$_2$**]**, respectively, contribute to the formation of the bidimensional networks showed in Fig. 2.17 characterized by small cavities occupied by solvent molecules.

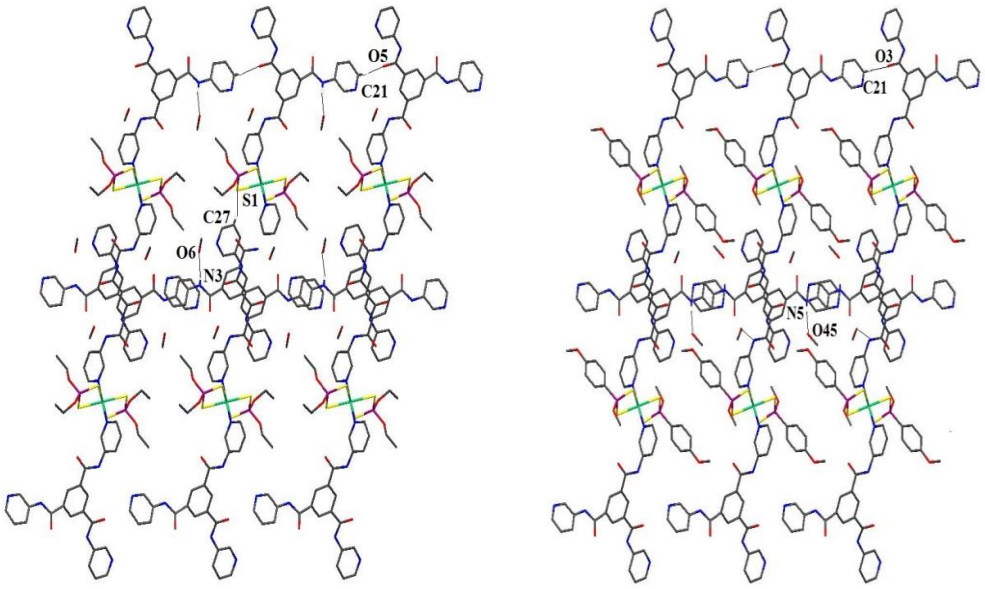

[**D2**(**L7**)$_2$] [**D3**(**L7**)$_2$]

Figure 2.34 Crystal Packing Views of Compounds [**D2(L7)$_2$**] and [**D3(L7)$_2$**] along axis *a* evidencing some weak H-bonds: C21–H21···O5 2.23 Å; C27–H27···S1 2.98 Å for [**D2(L7)$_2$**]; C21–H21···O3 2.24 Å for [**D3(L7)$_2$**]. Hydrogen atoms not involved in the showed interactions have been omitted for clarity reasons.

2.3.3.1 1,3,5-benzene-tri-(N-(4-Pyridyl))-carboxamide (L8).

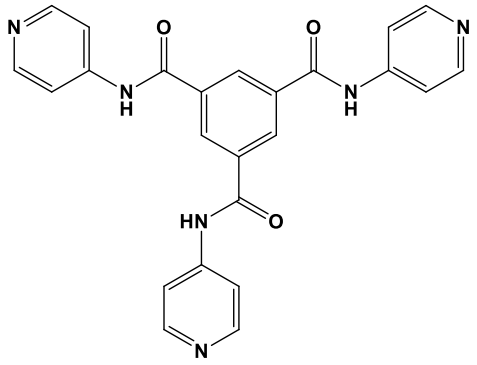

Ligand **L8** differs from the previous ligand **L7** for the position of the pyridine nitrogen atom. It has been prepared following the synthetic method described in Scheme 3.7 and the procedure described in § 3.3.6. Ligand **L8** has been reacted under solvothermal conditions in a 1:1 molar ratio with the nickel dithiophosphato and dithiophosphonato Ni^{II} complexes $[((MeO)_2PS_2)_2Ni]$ (**D1**), $[((EtO)_2PS_2)_2Ni]$ (**D2**), and $[((MeO\text{-}C_6H_4)(EtO))PS_2)_2Ni]$ (**D4**), using pure chloroform or a mixture of chloroform and the pertinent alcohol as solvent. The reactions afforded solid compounds, which have been isolated and fully characterized as described in § 3.4.29-3.4.31**.** Single crystals suitable for X-ray diffraction were obtained only from the reactions with **D4**, crystal characterization performed on the compound revealed the formation of the coordination polymer $(\mathbf{D4}\cdot\mathbf{L8})_\infty$. Crystallographic data and selected bond lengths and angles for $(\mathbf{D4}\cdot\mathbf{L8})_\infty$, are reported in Tables 2.18 and 2.19, respectively. As exemplified in Fig.2.16, $(\mathbf{D4}\cdot\mathbf{L8})_\infty$ show the nickel ion lying in a distorted octahedral environment with the equatorial positions occupied by two dithiophosphoric units acting as isobidentate ligands with almost equivalent Ni-S and P-S bonds, featuring the P-substituents in a *cis* configuration. Only two of the three pyridine units of **L8** are axially coordinated to the Ni^{II} ion and bridge of two adjacent dithiophosphonato units, thus forming polymeric chains. The non coordinated pyridyl ring features a protonated nitrogen atom that confers an overall positive charge counterbalanced by the presence of a dithiophosphonato anion. The coordination of a neutral donor reduces the net positive charge on the central Ni^{II} ion leading to a lengthening of the Ni-S bond lengths and a consequent decrease in the S-Ni-S angle with respect to the corresponding Ni^{II} square planar complex. At the same time increases the negative charge on the sulfur atoms with a consequent opening of the S-P-S angle. The $(\mathbf{D4}\cdot\mathbf{L8})_\infty$ present a zig-zag primary structure characterized by the endless repetition of metal centers and **L8** molecules with Ni···Ni distances of 15.60 Å (Fig. 2.17).

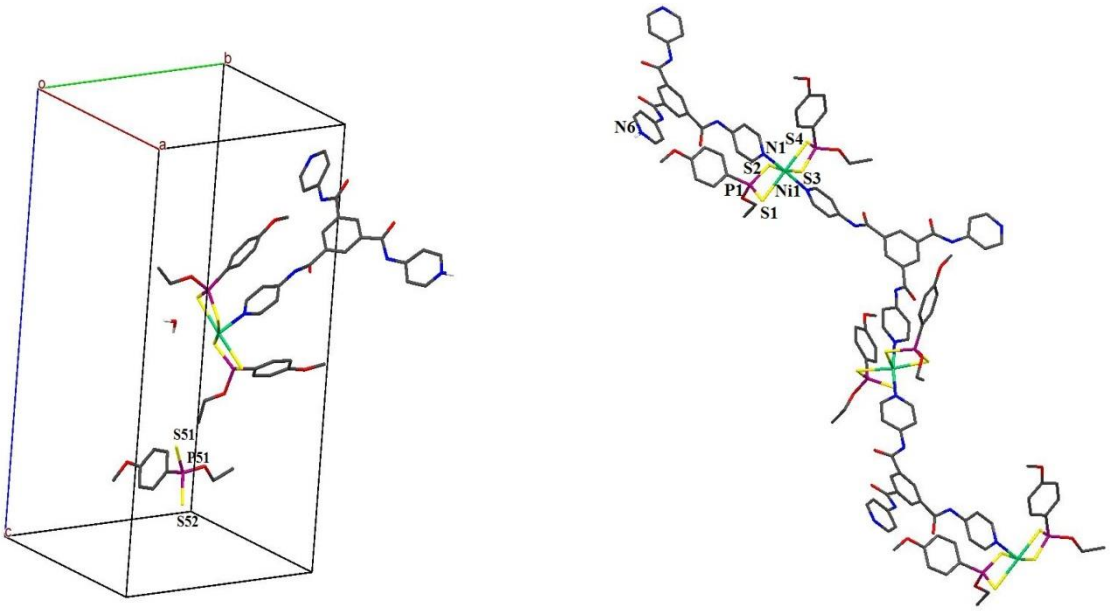

Figure 2.35 Unit Cell and Zig-Zag Polymeric Chain of Compounds $(\mathbf{D4{\cdot}L8})_{\infty}$. For clarity, only non-carbon atoms have been labeled and hydrogen atoms omitted

Table 2. 19 Summary of Basic Crystal Data for $(\mathbf{D4{\cdot}L8})_{\infty}$

Empirical Formula	$C_{42}H_{43}N_6Ni\ O_{10}P_2S_4$, $(C_9H_{12}O_2PS_2)^{-}\cdot\ H_2O$ $(\mathbf{D4{\cdot}L8})_{\infty}$
Formula weight	1258
Temperature (K)	100 (2)
Crystal system	Monoclinic
Space group	$P2_1/n$
a, b, c (Å)	14.329(4); 14.873(4); 27.117(7)
α, β, γ (°)	90; 92.22(5); 90
Volume (Å^3)	5755
Z	4
Calculated density (g cm^{-3})	1.447
Reflections collected/Unique	40176/10159
Wavelength	λ =71075
Final R indexes [I>=2σ (I)]	R_1 = 0.1119 wR_2 =0.1624

Table 2.20 Selected Bond Lenghts (Å) and Angles (°) for $(\mathbf{D4{\cdot}L8})_{\infty}$

Atoms	$C_{42}H_{43}N_6Ni\ O_{10}\ P_2\ S_4\ (C_9H_{12}O_2PS_2)\cdot\ H_2O$ $(\mathbf{D4{\cdot}L8})_{\infty}$
Ni-S1	2.5068(16)
Ni-S2	2.5464(15)
Ni-S3	2.5056(15)
Ni-S4	2.5492(16)
Ni-N1	2.084(4)
Ni-N2	2.101(4)
S1-P1	1.9989(19)
S2-P1	1.984(2)
S51-P51	1.995(2)
S52-P52	1.993(2)
S3-P2	1.987(2)
S4-P2	2.0092(19)
S1-Ni-S2	81.06(5)
S1-Ni-S3	91.80(5)
S3-Ni-S2	171.51(5)
S4-Ni-S1	171.08(5)
S4-Ni-S2	107.19(5)
S4-Ni-S3	80.24(5)
S1-Ni-N1	92.03(12)
S2-Ni-N1	86.12(12)
S3-Ni-N1	89.58(12)
S4-Ni-N1	91.94(12)
S1-Ni-N2	171.88(16)
S2-Ni-N2	91.81(12)
S3-Ni-N2	87.42(12)
S4-Ni-N2	97.45(12)
S1-P1-S2	111.07(9)
S3-P2-S4	109.20(8)
N1-Ni-N2	171.88(16)

Compound $(\mathbf{D4{\cdot}L8})_{\infty}$ packs in parallel chains running along the 101 direction mainly interacting through hydrogen bonds involving the water molecules (Fig. 2.18).

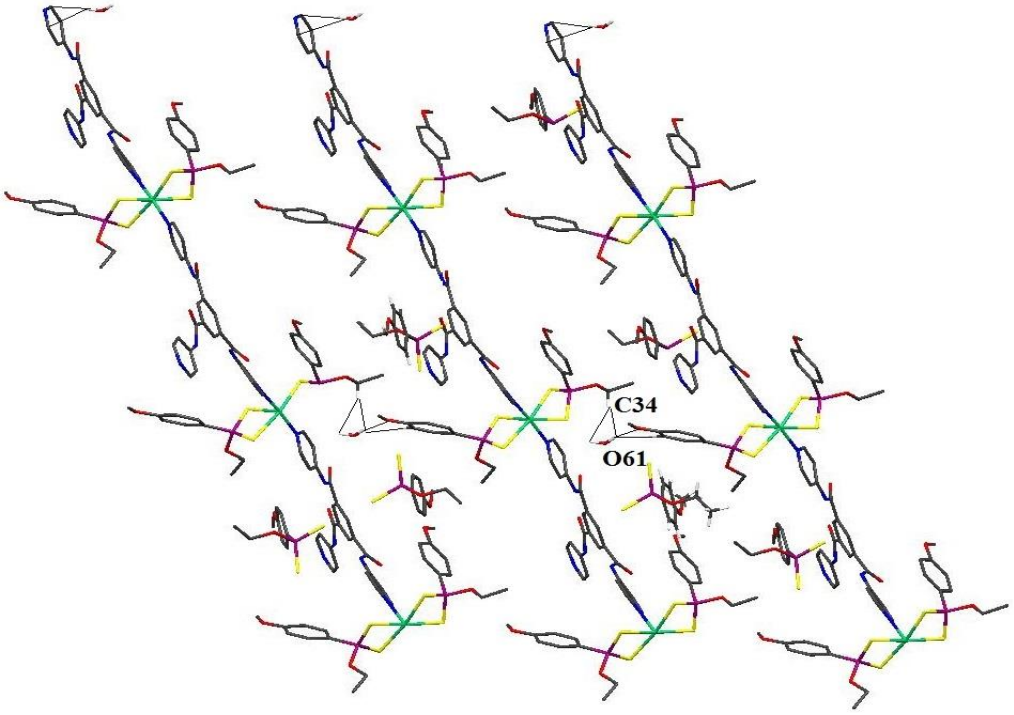

Figure 2.36 Crystal Packing View of Compounds $(\mathbf{D4{\cdot}L8})_{\infty}$ along axis b. The main interaction involving water co-crystallized molecules are showed.(C34-H34···O61 2.46 Å).Hydrogen atoms not involved in the showed interactions have been omitted for clarity reasons.

2.3.3.1 1,3,5-Benzenetricarboxylic acid-1,3-bis-4-pyridyl ester (L9b)

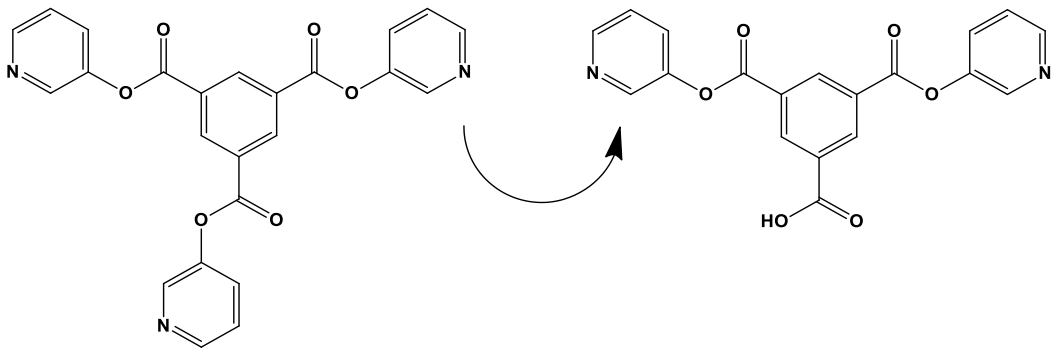

(L9) **(L9b)**

Ligand **L9b** has been obtained in a failed attempt to prepare **L9** following the synthetic method described in Scheme 3.8. The synthetic procedure is described in § 3.3.7. In fact, unexpectedly, the reaction yielded the hydrolyzed form of the bis-pyridyl ester. Since the carboxylic group is capable to form coordination bonds with the metal center of the nickel dithiophosphoric unit, we proceed by reacting **L9b** under solvothermal conditions in a 1:1 molar ratio with the nickel dithiophosphato and

dithiophosphonato Ni^{II} complexes $[((MeO)_2PS_2)_2Ni]$ (**D1**), $[((EtO)_2PS_2)_2Ni]$ (**D2**), $[((MeO\text{-}C_6H_4)(MeO))PS_2)_2Ni]$ (**D3**), and $[((MeO\text{-}C_6H_4)(EtO))PS_2)_2Ni]$ (**D4**), using pure chloroform or a mixture of chloroform and the pertinent alcohol as solvent. The reactions afforded solid compounds, which have been isolated and fully characterized as described in § 3.4.32-3.4.35. Single crystals suitable for X-ray diffraction were obtained only from the reaction with **D2**, crystal characterization performed on the compound revealed the formation of the unexpected 3D coordination network corresponding to the formulation $[2\mathbf{D2}\cdot 2\mathbf{L9b}\cdot Ni(EtOH)_2]_\infty$. Crystallographic data and selected bond lengths and angles for $[2\mathbf{D2}\cdot 2\mathbf{L9b}\cdot Ni(EtOH)_2]_\infty$ are reported in Tables 2.20 and 2.21 respectively.

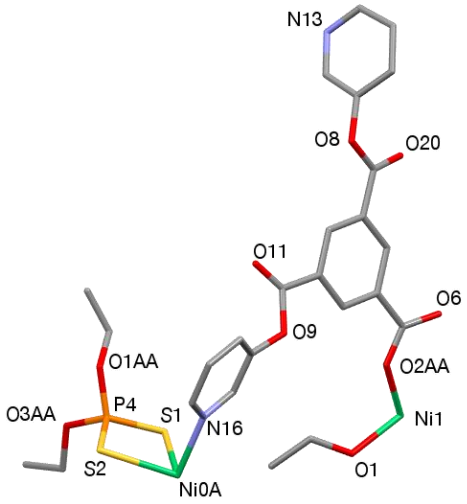

Figure 2.37 Asymmetric Unit with the Numbering Scheme Compounds $[2\mathbf{D2}\cdot 2\mathbf{L9b}\cdot Ni(EtOH)_2]_\infty$.For clarity, hydrogen atoms omitted.

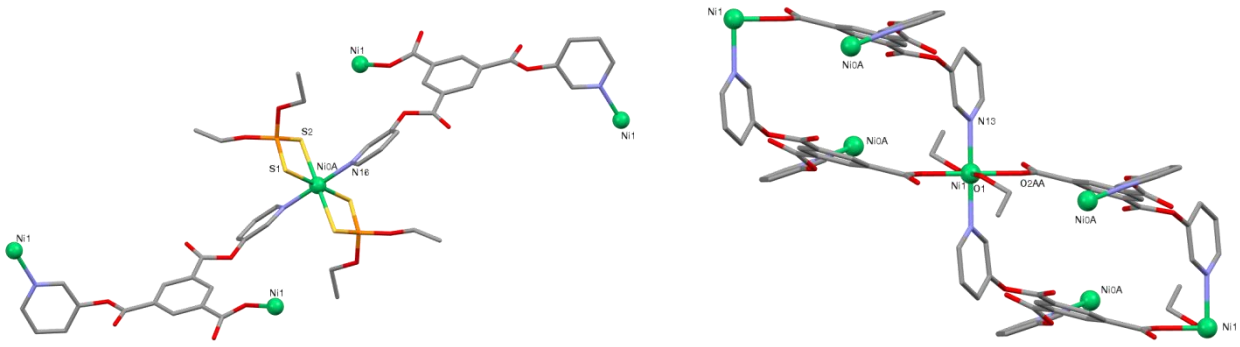

Figure 2.38 Views of $[2\mathbf{D2}\cdot 2\mathbf{L9b}\cdot Ni(EtOH)_2]_\infty$ two fragments evidencing the two different coordination environment of Ni0A (left) and Ni1 (right).

As can be seen in Fig. 2.18, the complex network $[2\mathbf{D2}\cdot 2\mathbf{L9b}\cdot Ni(EtOH)_2]_\infty$ contains two nickel ions (Ni0A and Ni1) featuring very different coordination environments. One of them (Ni0A) can be

easily recognized as belonging to the dithiophosphato **D2** reagent, and show the typical configuration with the nickel ion lying in a distorted octahedral environment with the equatorial positions occupied by two dithiophosphato units acting as isobidentate ligands with almost equivalent Ni-S and P-S bonds, and two pyridine units coming from different L9b ligands axially coordinated to the Ni^{II} ion through the nitrogen N16 atom (Figure 2.22 bottom left). The other one (Ni1) probably comes from impurities of $NiCl_2$ coming from the synthesis of **D2** and feature a distorted octahedral coordination geometry with four oxygen atoms in the equatorial plane: two coming from the O2AA oxygen of the carboxylate groups of two different L9b ligands and the other two belonging to two ethanol molecules (Fig. 2.22 bottom right). This means that each L9b ligand is coordinated to three different nickel ions: nitrogen N16 is bound to Ni0A, nitrogen N13 to Ni1 and the oxygen atom O2AA of the carboxylic group to another N1 ion. The resulting structure can be described as a tridimensional grid network formed by the alternation of polymeric parallel chains of type (**D2**·**L9b**)$_\infty$ containing **D2** units bridged by **L9b** ligands and chains of the type (**Ni(EtOH)$_2$**·**L9b**)$_\infty$, formed by Ni1 nickel ions axially bridged by **L9b** connected through the coordination bonds between the carboxylate **L9b** substituents and Ni1 ions. The result is the tridimensional grid with rectangular holes of about 13x7 $Å^2$ occupied by additional ethanol molecules.

Table 2.21 Summary of Basic Crystal Data for [2**D2**·2**L9b**·Ni(EtOH)$_2$]$_\infty$

Empirical Formula	$C_{27}H_{33}N_2NiO_{10}PS_2$ [2**D2**·2**L9b**·Ni(EtOH)$_2$]$_\infty$
Formula weight (g mol^{-1})	666.59
Temperature (K)	293(2)
Crystal system	Triclinic
Space group	P-1
a, b, c (Å)	9.4529(7);11.2927(8);16.2264(11)
α, β, γ (°)	103.090(7); 102.147(7); 102.147(7)
Volume (Å^3)	1567.6(2)
Z	2
Calculated density (g cm^{-3})	1.482
Reflections collected/Unique	7233/27468
Wavelength	λ =0.71073
Final R indexes [I>=2σ (I)]	R_1 = 0.1381 wR_2 =0.4138

Table 2.22 Selected Bond Lenghts (Å) and Angles (°) for [2**D2**·2**L9b**·Ni(EtOH)$_2$]$_\infty$

Atoms	$C_{27}H_{0.50}N_2NiO_{10}PS_2$ [2**D2**·2**L9b**·Ni(EtOH)$_2$]$_\infty$
Ni0A-S1	2.478(2)
Ni0A-S2	2.489(2)
Ni0A-N16	2.115(3)
Ni1-O1	2.066(5)
Ni-O2AA	2.028(6)
Ni-N13	2.110(7)
S1-P4	1.977(3)
S2-P4	1.976(4)
S1-N0A-S2	82.03(7)
S1-P4-S2	111.07(14)
S1-Ni0A-N16	88.88(19)
S2-Ni0A-N16	90.78(18)
N16-Ni0A-N16	180.00
O1-Ni1-O2AA	89.3(2)
O1-Ni1-N13	88.4(2)
O2AA -Ni1 -N13	90.9(3)
N13 -Ni1-N13	180.00

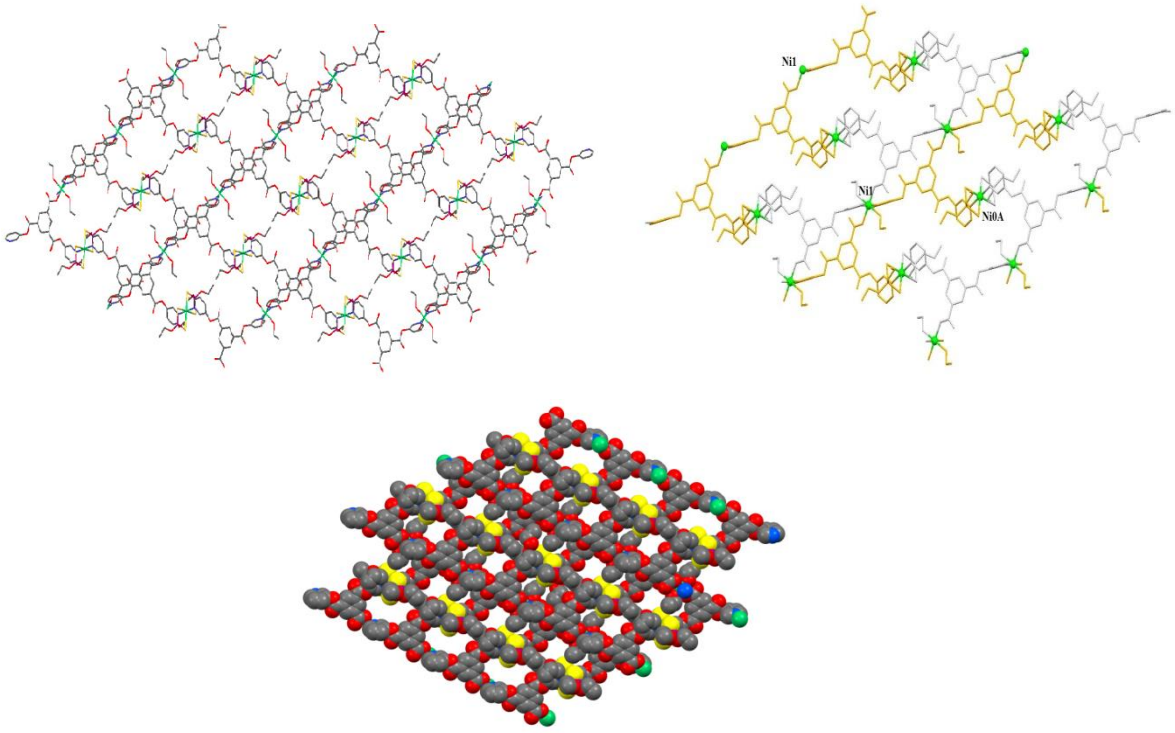

Figure 2.39 Crystal Packing Views along b axis and Space Filled Representation evidencing the cavities of [2**D2**·2**L9b**·Ni(EtOH)$_2$]$_\infty$

2.4 Spectroscopic Characterizations

The synthesized compounds have been characterized by means of different spectroscopic techniques. In particular, on the synthesized building blocks, both on the phosphorodithioato Ni^{II} complexes **D1**-**D4** and on the ligands **L1**-**L10**, ^{1}H-NMR and Infrared Spectroscopic characterizations were performed in order to verify the identity of the compounds and to check for their pureness before using them for the synthesis of the coordination polymers. UV-Visible and fluorescence spectra were recorded for the ligands, and the relevant data reported. Singularly, for ligand **L1** UV-vis spectroscopic determinations of the formation constants of the octahedral adducts between **L1** and the **D1**-**D4** square-planar complexes were performed due to a certain solubility of the reagents and of the intermediate adducts formed that allowed to accomplish the measurements before the precipitation of the insoluble polymer. Microcrystalline compounds were also analyzed by X-Ray powder diffraction and, when available, the data were compared with the powder spectra **calculated from the single crystal X-Ray diffraction data.**

2.4.1 NMR studies

NMR measurements were mainly performed in order to confirm the nature and pureness of the synthesized ligands **L1**-**L10**, whilst the nickel complexes **D1**-**D4** were usually obtained as crystals and characterized by means of melting point and IR spectra comparison with literature data.[45] In contrast, NMR measurements on the synthesized coordination polymers were not performed due to the paramagnetic nature of the central ion in the resulting octahedral environment. NMR measurements on the ligands were performed solubilizing the samples in suitable deuterated solvents such as $CDCl_3$ and DMSO-*d6* in standard 5 mm NMR tubes and recording the spectra at 25°C on either a Varian INOVAX-400 or Varian INOVAX-500 spectrometer. The spectra were then analyzed and compared with literature data, when available. Following is the detailed analysis of the data relative to the new ligand (*R*)-2,2′-dimethoxy-1,1′-binaphthyl-3,3′-bis(4-pyridyl-amido) **L3**, synthesized as described in § 3.3.3 in collaboration with the University of Pavia (Italy), specifically designed in order to introduce chirality and impart a helicoidal shape to the resultant coordination polymers. Fig. 2.24 shows the ^{1}H NMR ($CDCl_3$) spectrum of **L3**. . The eight signals were assigned to the protons $H_{1\text{-}11}$ (see **L3** formula scheme in the inset of Fig. 2.24) as follows: δ = 10.19 (s) (2H, H_7, NHCO); δ = 9.03 (s) (2H, H_1, binaphthyl); δ = 8.60 (d) (4H, $H_{9,10}$, J = 5.7, β-pyridine); δ = 8.14 (d) (2H, H_2, J = 8.1, binaphthyl); δ = 8.03 (d) δ = 7.70 (d) (4H, $H_{8,11}$, J = 5.7, β-pyridine), δ =7.58 (t) (2H, H_3, J = 6.6, binaphthyl); δ =7.42 (t),(2H, H_4, J = 6.6, binaphthyl) , 7.19 (d) (2H, H_5, J = 8.7, binaphthyl); δ =3.46 (s) (6H, H_6,OCH3).

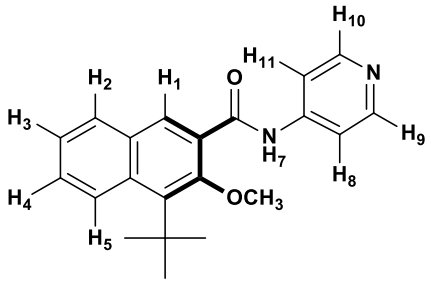

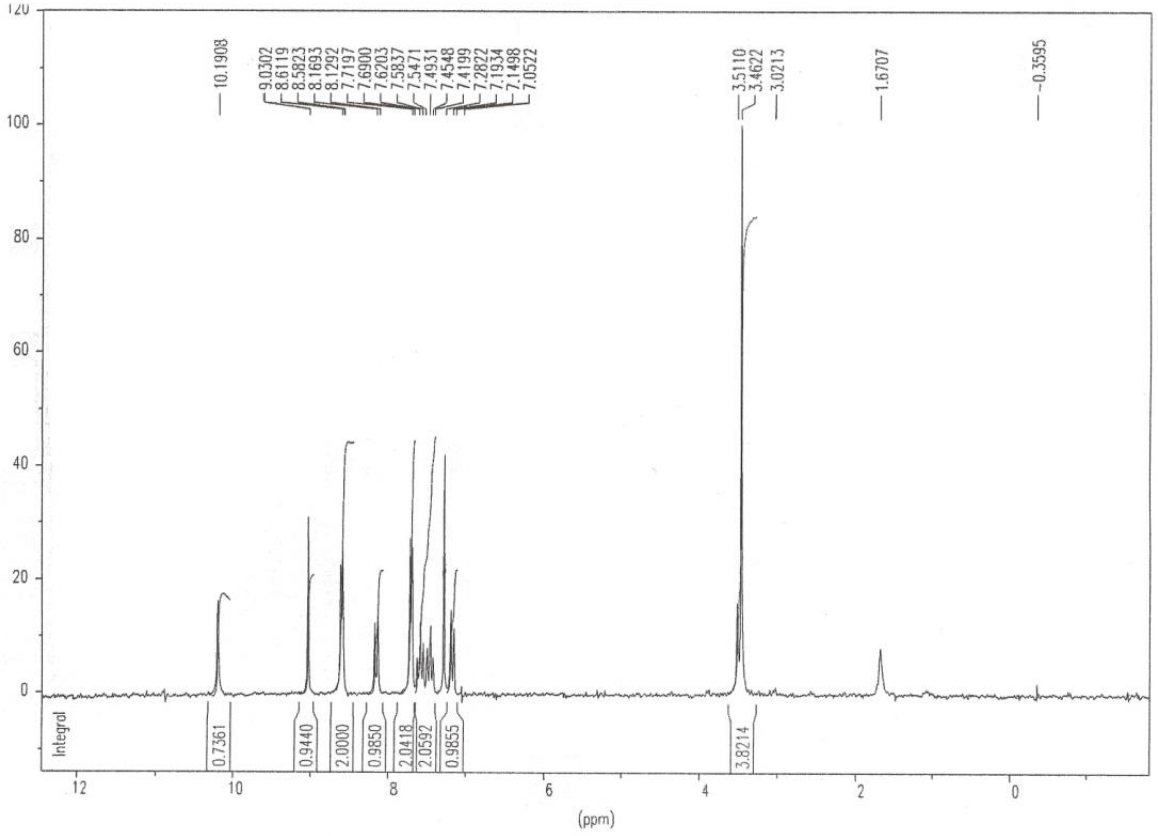

Figure 2. 40 ^{1}H NMR (CDCl3) Chemical Shift and Integration Peaks of **L3**

As far as the other ligands are concerned, the recorder data were analyzed as exemplified for the case here presented of ligand 1,3,5-benzene-tri-(N-(4-Pyridyl))-carboxamide (**L8).** Fig. 2.25 shows the ^{1}H NMR (DMSO-d6) spectrum of **L8** along with main peaks magnification. The four signals were assigned to the protons H_1-H_{18} (see **L8** formula scheme in the inset of Figure 2.25) as follows: δ = 11.10 (s) (3H: H_9, H_4, H_{14}); δ = 8.79 (s) (3H: H_1, H_2, H_3); δ = 8.57 (d) (6H: H_6-H_7, H_{11}-H_{12}, H_{16}-H_{17}); δ = 7.90 (d) (6H: H_5-H_8, H_{10}-H_{13}, H_{15}-H_{18}). The recorded spectrum was compared with literature data,[58] thus confirming the nature of the synthesized compound. Small differences, such as the strong visible sharp peak at 3.33 ppm and the signals at 2.08 ppm were attributed to the washing

water used in the experimental synthetic procedure (see experimental § 3.3.6) and to solvent impurities (acetone), respectively.

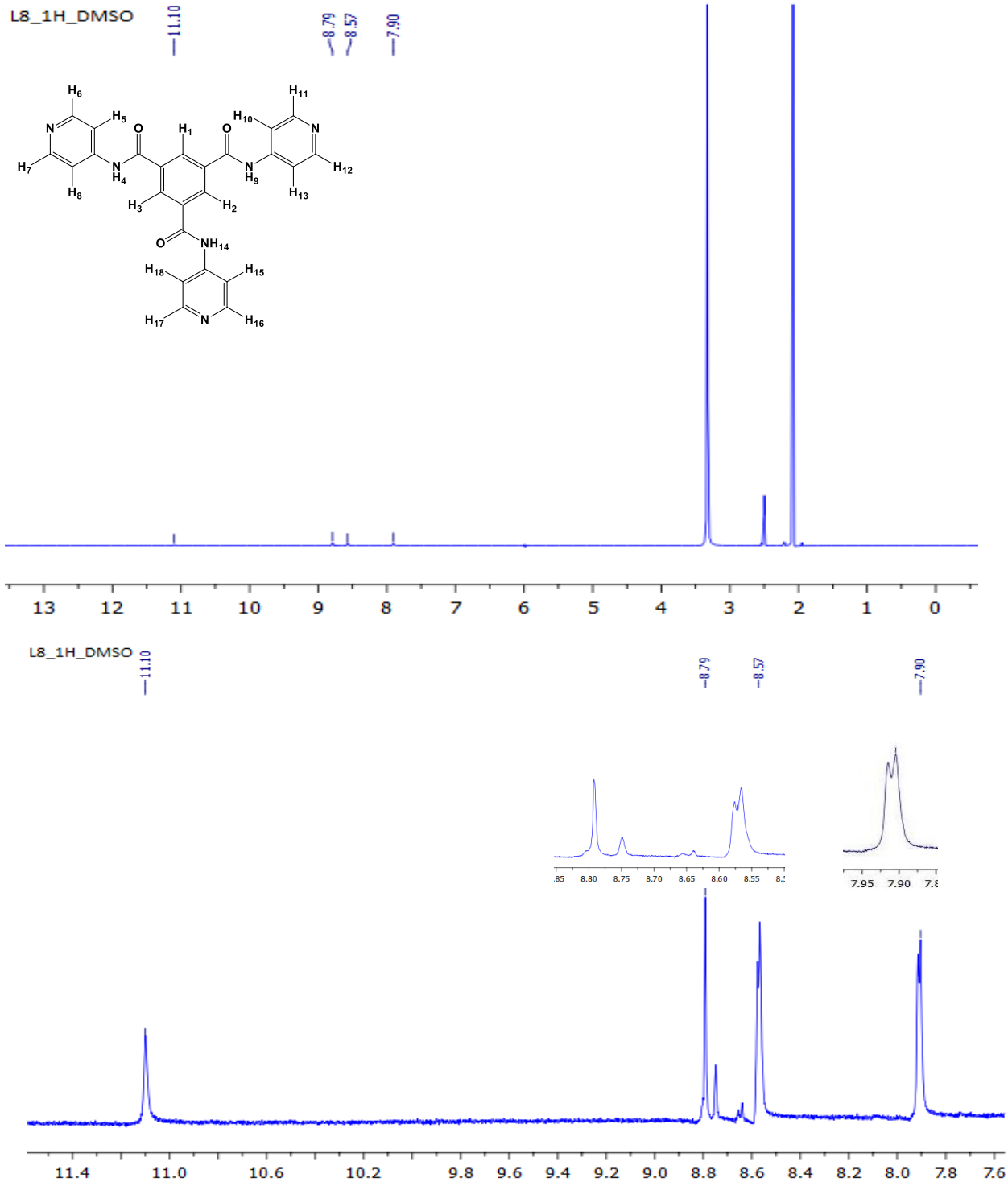

Figure 2.41 [1]H NMR DMSO(*d6*) Spectrum of 1,3,5-benzene-tri-(N-(4-Pyridyl))-carboxamide (**L8**) on the top and magnification of main peaks on the bottom.

The results recorded for ligands **L1-L10** are summarized in Table 2.22, along with the solvent used, and the pertinent literature references used for comparison.

Table 2. 23 ^{1}H Chemical Shifts of Ligands used

References	Ligands	Solvents	Chemical Shifts (**δ**) ppm
66	**L1**	$CDCl_3$	δ = 8.77 (d), δ = 8.61 (dd), δ = 7.82 (dt), δ = 7.30 (t)
59	**L2**	$CDCl_3$	δ = 8.5 (d), δ = 7.6 (d), δ = 7.45(s)
70	**L3**	$CDCl_3$	δ = 10.19 (s) (2H, $H_{7,}$ NHCO); δ = 9.03 (s) (2H, H_1, binaphthyl); δ = 8.60 (d) (4H, $H_{9,10}$**,** J = 5.7, β-pyridine); δ = 8.14 (d) (2H, H_2, J = 8.1, binaphthyl); δ = 8.03 (d) δ = 7.70 (d) (4H, $H_{8,11}$, J = 5.7, β-pyridine), δ =7.58 (t) (2H, H_3, J = 6.6, binaphthyl); δ =7.42 (t),(2H, H_4, J = 6.6, binaphthyl) , 7.19 (d) (2H, H_5, J = 8.7, binaphthyl); δ =3.46 (s) (6H, H_6OCH3).
60	**L4**	$CDCl_3$	δ = 8.63(t), δ = 7.51 (m)
60	**L5**	$CDCl_3$	δ = 8.64(d), δ = 8.54 (m), δ = 7.86 (tt) δ = 7.37 (q)
61	**L6**	$CDCl_3$	δ = 8.79 (d), δ = 8.56 (dd), δ = 7.90 (dt), δ = 7.69 (s), δ = 7.28 (t)
62	**L7**	DMSO	δ = 10.91 (s), δ =8.98 (s), δ = 8.78 (d), δ = 8.36 (dd), δ = 8.22 (dt), δ = 7.42(t)
68	**L8**	DMSO	δ = 11.10 (s), δ =8.79 (s), δ = 8.57 (d), δ = 7.91 (d).
63	**L9b**	DMSO	δ = 9.05 (s), δ = 8.93 (dd), δ = 8.65 (d), δ = 8.55 (dd)
68	**L10**	DMSO	δ = 8.79 (d), δ = 8.75 (d), δ = 8.60 (s), δ = 7.51 (d).

It is interesting to note that the comparison of the ^{1}H-NMR data recorded for the theorical compound 1,3,5-benzenetricarboxylic-acid-1,3,5-tris-4-pyridyl-ester (**L9**) revealed differences with literature values which have been ascribed to the formation of the hydrolyzed form of the bis-pyridinyl ester **L9b**.

2.4.1 Infrared Spectroscopic Techniques

Infrared measurements were recorded on the sample compounds dispersed in anhydrous KBr pellets in the 500-4000 cm^{-1} range (see experimental §3.1). The IR spectra of **L1-L10** ligands and **D1-D4** complexes were mainly recorded in order to detect the main functional bands and obtain confirmation of their identity. In the case of the octahedral adducts obtained by reacting the molecular building blocks, the measurement were mainly performed to check for the simultaneous presence of the peaks assigned to the ligands and those related to the Ni^{II} complexes, since no information on their coordination polymers nature can be obtained from this techniques. The spectra relative to the square planar complexes **D1**-**D4** are reported in Fig. 2.26 and compared with the vibrational assignments in the literature.[64] The presence of the aromatic metoxyphenyl ring in **D3** and **D4** implies many vibrational peaks related in particular to aromatic C=C stretching in the 1600-1475 cm^{-1} range. It is interesting to note the sharp peaks at 958 and 941 and cm^{-1} for **D2** and **D4** spectra, respectively which are assigned to a vibrational mode of the ethoxy substituent and are therefore absent in the spectra of complexes **D1** and **D3**. The presence of this strong peak found in the reaction products between **D2** and **D4** and the pyridyl ligands along with the change of color from purple to greenish confirms the formation of the relative octahedral adduct.

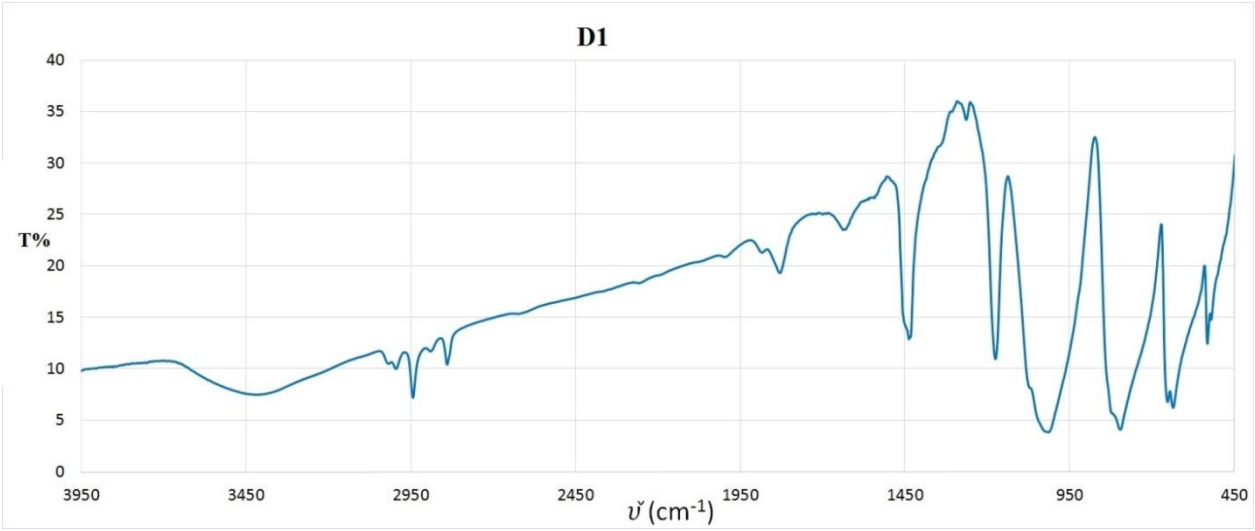

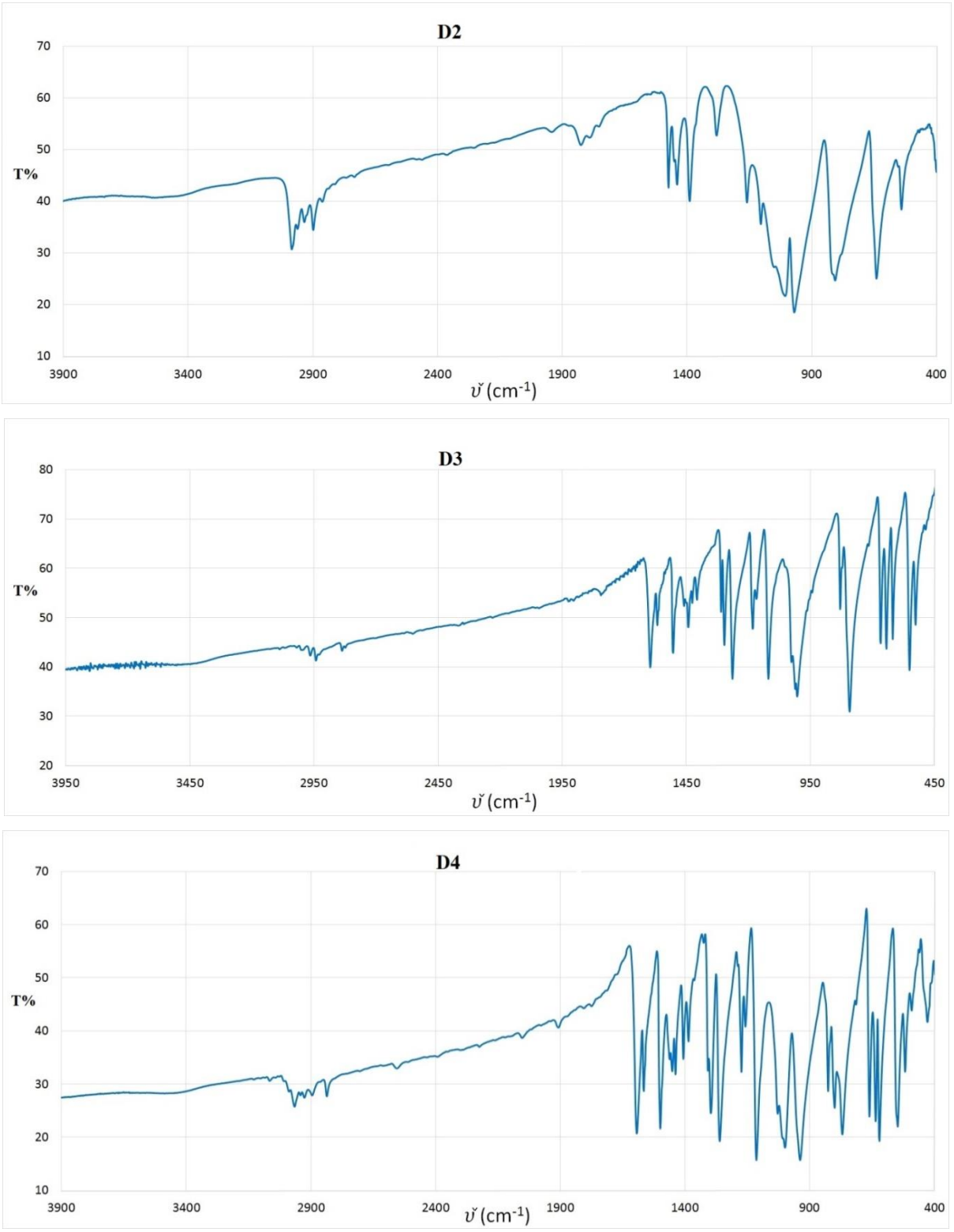

Figure 2.42 Infrared Spectra of [Nidtf(OMe)](**D1**), [Nidtf(OEt)](**D2**), [Nidtp(OMe)](**D3**),[Nidtp(OEt)](**D4**).

As an example, the comparison between the IR-spectra of the (**D2·L9b**) and (**D4·L9b**) adducts obtained by reacting ligand **L9b** and complexes **D2** and **D4**, and the spectra of the corresponding reagents is reported in Fig.2.26. The ligand spectrum (Fig. 2.26 a) shows a strong peak at 1764 cm^{-1} and the C-O stretching at 1207 cm^{-1} characteristic for the presence of a carboxylic group. In the

spectra of the adducts, the presence of both **L9b** and either **D3** or **D4** can be recognized by the corresponding peaks. In particular, a magnification of the three compared spectra shows the presence in 964 cm^{-1} and 944 cm^{-1} of the characteristic -OEt vibration in (**D2·L9b**) and (**D4·L9b**), respectively (Fig. 2.26 d).

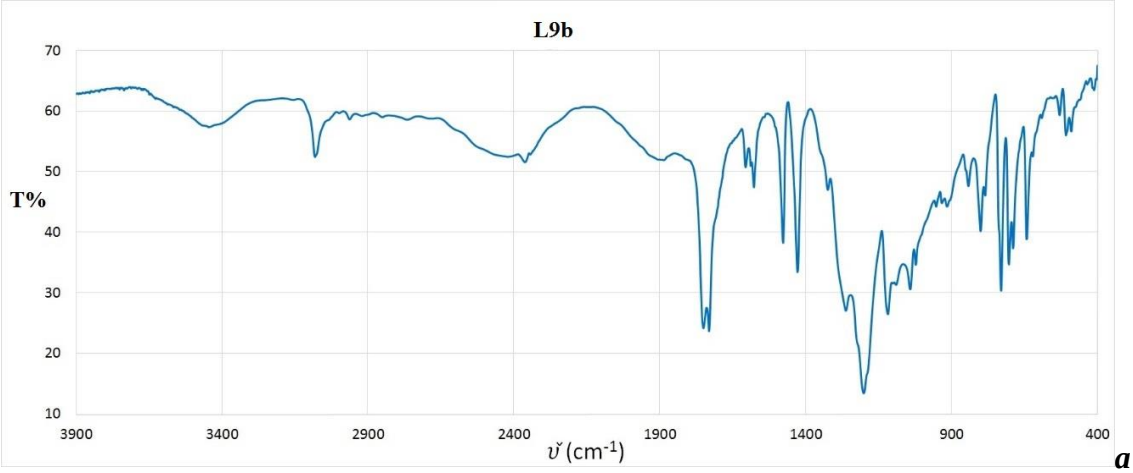

a

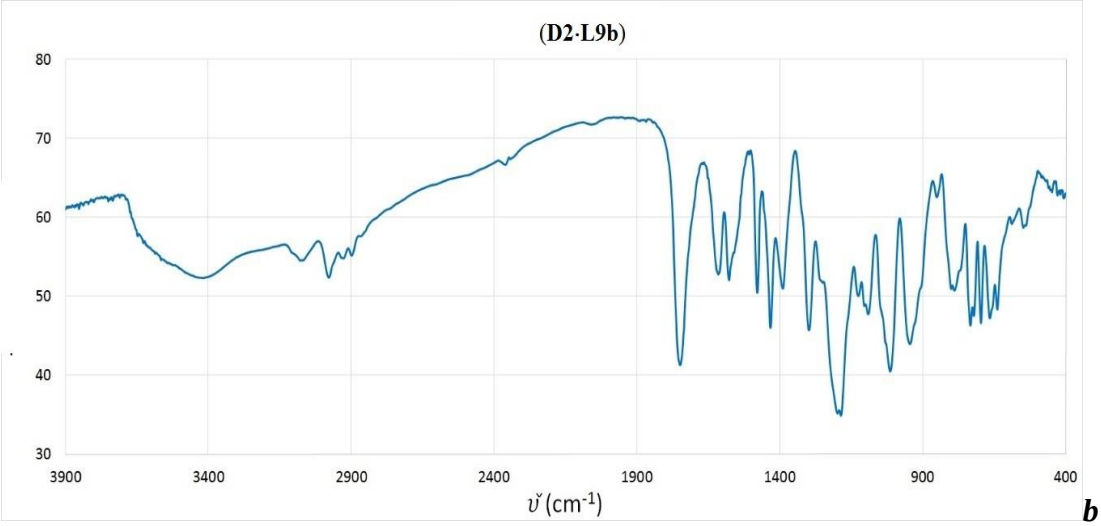

b

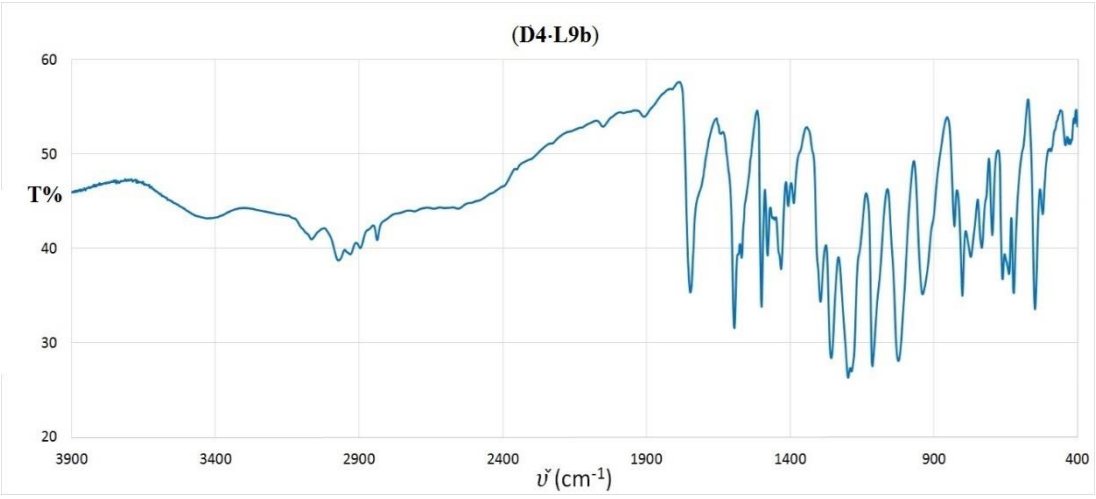

c

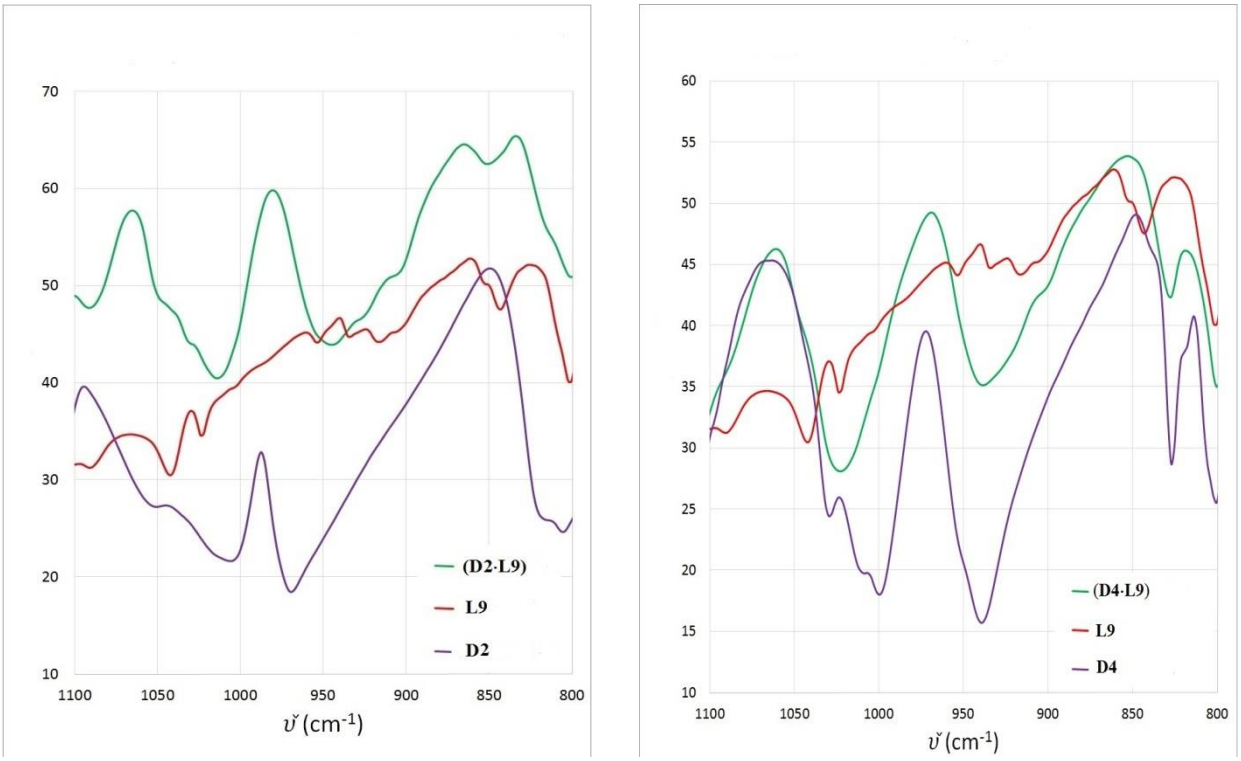

Figure 2.43 IR Spectra of **L9b** (a), (**D2**·**L9b**) (b), (**D4**·**L9b**) (c), and magnification of the IR-spectra comparison between the adducts (green) and the corresponding reagents **L9b** (red), and complexes (**D2**, **D4**, purple) (d).

2.4.2 Molecular Fluorescence Studies

Molecular fluorescence studies have been performed on the prepared ligands **L1**-**L10**. Notwithstanding the measurements have been carried out on all the ligands, only in the case of ligands **L1**, **L9** and **L10** a reliable fluorescence emission were detected. Preliminary UV measurements performed on a $1.63 \cdot 10^{-6}$ M solution of **L1** in $CHCl_3$ revealed absorption peaks at 247, 292, 310, and 330 nm. Therefore, molecular fluorescence measurements on a $1.14 \cdot 10^{-6}$ M solution in $CHCl_3$ of **L1** in the range 240-440 nm were performed with excitation lengths varying between 220 and 345 nm performing scans at regular intervals (5 nm) and slit = 5x5. Fig. 2.28 shows the 2D (a) and 3D (b) representation of the fluorescence emission spectra recorded at different excitation wavelengths. As can be seen, **L1** shows emission peaks at 357 nm and 369 nm with a maximum intensity for λ_{ex} = 263 nm.

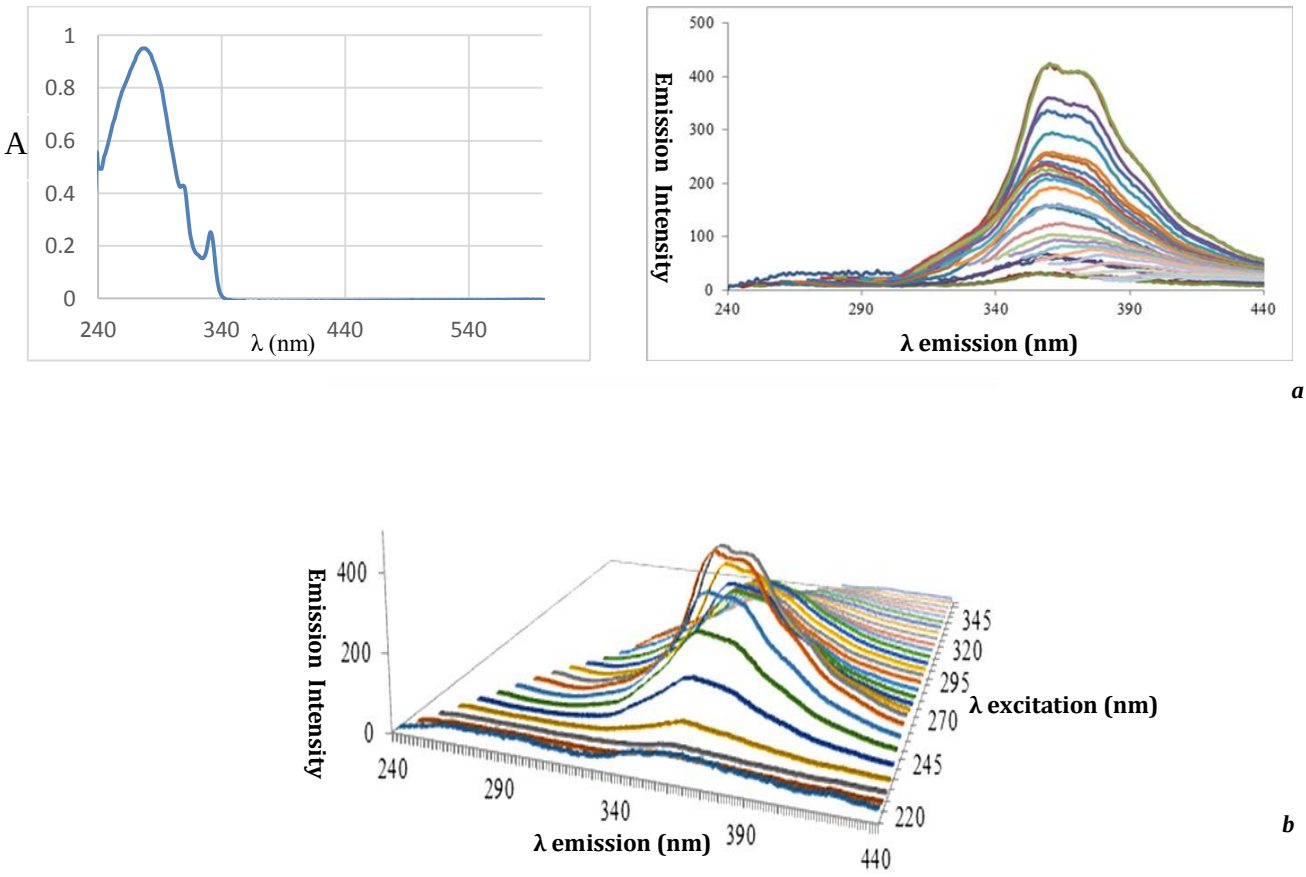

Figure 2.44 UV-Absorption and 2D (a) and 3D (b) Representation of the Emission spectra of **L1** at different Excitation Wavelengths.

Preliminary UV measurements performed on a $1 \cdot 10^{-4}$ M solutions of **L9** and **L10** in EtOH show similar absorption spectra profiles for the two ligands with absorption peaks at 192, 194, and 198 nm for **L9** and at 194, 198, and 203 nm for **L10**. Therefore, molecular fluorescence measurements on a $1.56 \cdot 10^{-4}$ M solution in EtOH of **L9** in the range 260-420 nm were performed with excitation lengths varying between 220 and 300 nm performing scans at regular intervals (5 nm) and slit = 5x5. Fig. 2.29 shows the 2D (a) and 3D (b) representation of the fluorescence emission spectra recorded at different excitation wavelengths. As can be seen, **L9** shows an emission peak at 311 nm with a maximum intensity for λ_{ex} = 275 nm.

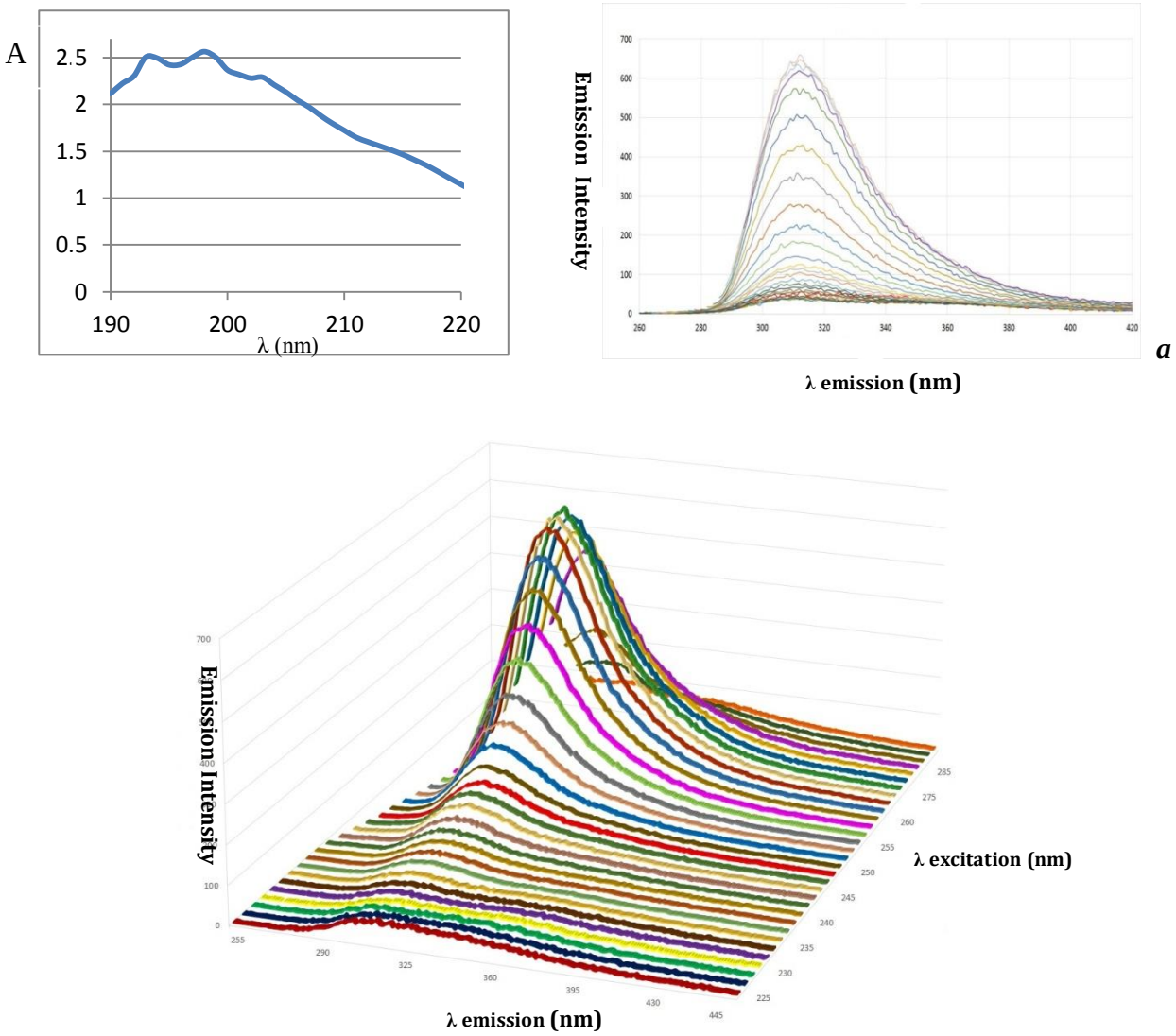

Figure 2.45 UV-Absorption and 2D (a) and 3D (b) Representation of the Emission Spectra of **L9** at different Excitation Wavelengths.

Molecular fluorescence measurements on a $1.45 \cdot 10^{-6}$ M solution in EtOH of **L10** in the range 280-440 nm were performed with excitation lengths varying between 220 and 260 nm, performing scans at regular intervals (5 nm) and slit = 5x5. Figure 2.30 shows the 2D (a) and 3D (b) representation of the fluorescence emission spectra recorded at different excitation wavelengths. As can be seen, **L10** shows an emission peak at 347 nm with a maximum intensity for λ_{ex} = 240 nm.

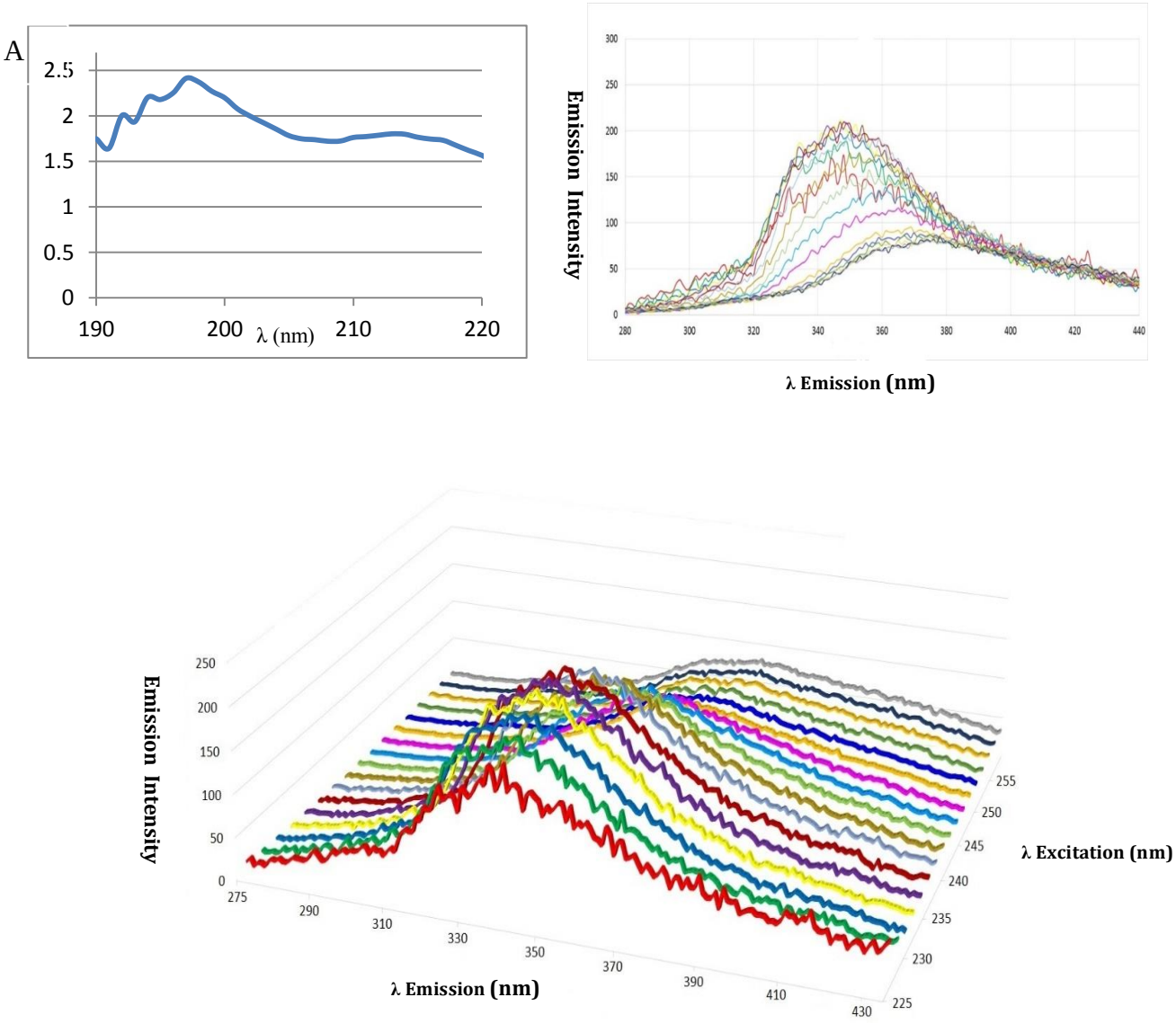

Figure 2.46 UV-Absorption and Emission Spectrum of **L10** (a) and 3D View of **L10** Emission Spectrum varying Excitation Wavelengths (b).

2.4.3 Spectrophotometric Titrations

In order to further investigate the reactivity of Ni^{II} phosphonodithioato complexes toward the ligands synthesized, solution equilibria studies have been performed. Unfortunately, in most of the cases the reaction between the ligands and the Ni^{II} complexes, leaded to the immediate precipitation of the product with the exception of ligand **L1**. As a consequence, for ligand **L1** UV-vis spectroscopic determinations of the formation constants of the octahedral adducts between **L1** and the **D1-D4** square-planar complexes were performed. Solutions of the square planar complexes **D1-D4** solutions were prepared in $CHCl_3$ and the spectra recorded with an UV spectrophotometer Thermo Nicolet Evolution (190-1100 nm) in a range of 400-800 nm. Then known amounts of a solution of **L1** in the same solvent were added and the spectra recorded after each addition. The set of spectra

recorded for each titration has been analyzed using the program SPECFIT[65] which first calculates both the concentration profiles and the spectra of all the absorbing species by Evolving Factor Analysis (EFA) without any model assumption and then performs a least-squares optimization based on an equilibrium model. A good agreement between the spectra and the distribution curves calculated by the model and experimental ones confirm the validity of the proposed model.

2.4.3.1 Titration of D1 with L1

The Fig. 2.31 reports the UV-visible spectra recorded during the titration of a $9.81 \cdot 10^{-3}$ M of **D1** solution in $CHCl_3$ with increasing amounts of a $2.49 \cdot 10^{-2}$ M **L1** solution in $CHCl_3$ using an Eppendorf electronic automatic dispenser (5-100µL). The starting volume of the solution, the **L1** added amounts, the final concentrations calculated for the reagents and their molar ratios are reported in Table 2.23. The data were analyzed by "Factor Analysis" and the corresponding eigenvalues, collected in Table 2.24, reveal that only two species are present in solution. In our opinion, the two species are the square planar complex **D1** and a **D1**·**L1**$_2$ adduct formed through the addition of two **L1** ligands to the central Ni^{II} ion. The coordination of the second pyridyl group of the ligand to another **D1** moiety leads to the formation of the insoluble coordination polymer that precipitates from the solution as a green powder. The data were than fitted by the program following the proposed 1:2 model and the equilibrium formation constant for the equilibrium:

$$D1 + 2L1 \leftrightarrows D1L1_2$$

corresponding to the octahedral adduct formation was calculated with a least squares method, obtaining the value: $\log \beta_{eq} = 4.63 \pm 0.04$. In Fig. 2.32 the calculated distribution curves for the two absorbing species **D1** and **D1L1**$_2$ involved in the equilibrium are reported, and Fig. 2.33 shows the plot of the absorbance values relative to the **D1L1**$_2$ adduct as a function of the molar ratio [**L1**] / [**D1**].

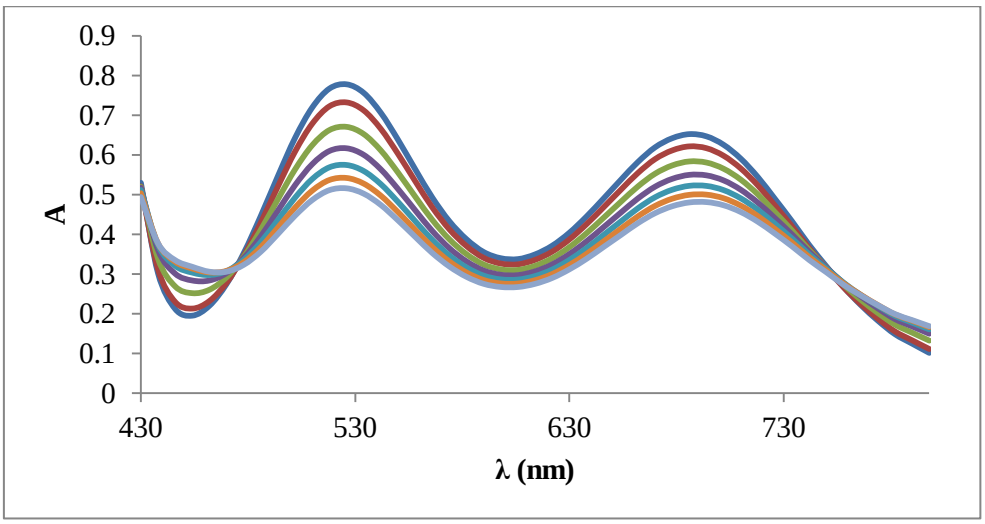

Figure 2.47 UV-Visible Spectra collected during the Titration of **D1** with **L1** corrected considering the Dilution Factor.

Table 2.24 Experimental Data for the Titration of **D1** with **L1**

Solution	Addition/μL (± 0.2 %)	V_{tot}/mL	[L1]/10^{-3} M	[D1]/10^{-3} M	[L1]/[D1]
1	-	1.50	0	9.81	0
2	100	1.60	1.61	8.55	0.19
3	100	1.70	3.12	6.50	0.48
4	100	1.80	4.53	4.74	0.96
5	100	1.90	5.86	3.50	1.68
6	100	2.00	7.12	2.65	2.69
7	100	2.10	8.31	2.07	4.02

Table 2.25 Factor Analysis Eigenvalues and Parameters for the set of Data Collected for **D1** and **L1**

Nº	Eigenvalue	Squaresum	Sigma(abs)
1	$5.986 \cdot 10^{1}$	0.268	$2.860 \cdot 10^{-2}$
2	0.252	$1.590 \cdot 10^{-2}$	$6.973 \cdot 10^{-3}$
3	$1.580 \cdot 10^{-2}$	$1.054 \cdot 10^{-4}$	$5.686 \cdot 10^{-4}$
4	$5.109 \cdot 10^{-5}$	$5.429 \cdot 10^{-5}$	$4.087 \cdot 10^{-4}$

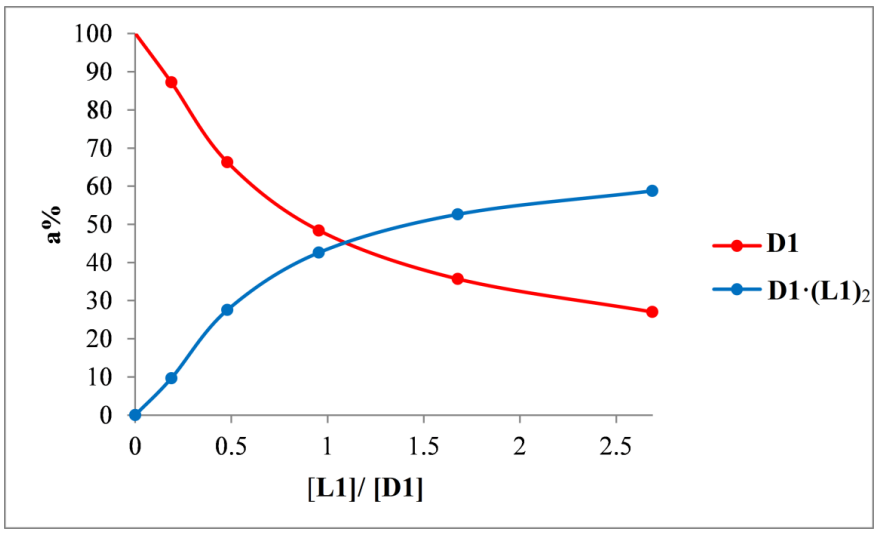

Figure 2.48 Distribution Curves: Percentage Fractions of **D1** and **D1L1**$_2$ as a function of the Molar Ratio [**L1**]/[**D1**].

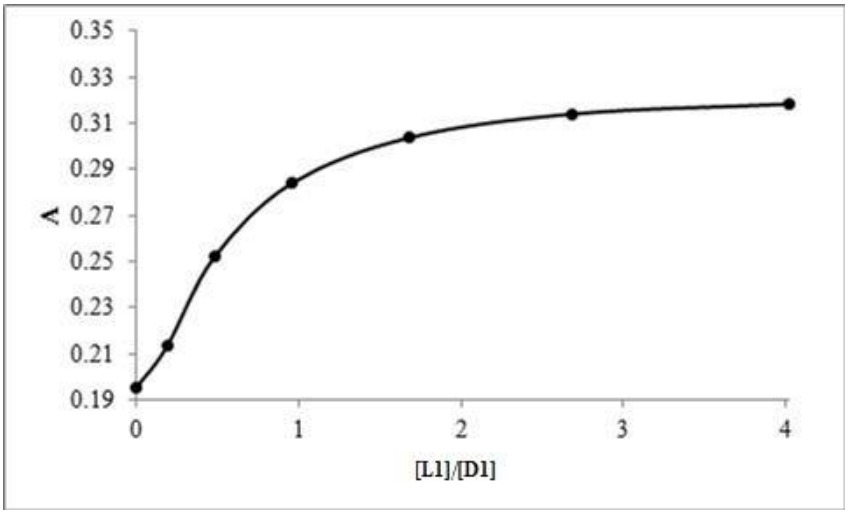

Figure 2.49 Plot of Absorbance Values at 454 nm as a Function of the Molar Ratio [**L1**] / [**D1**].

2.4.3.2 Titration of D2 with L1

The titration of **D2** with **L1** has been performed with a procedure analogous to that just described for **D1**. The Fig. 2.34 reports the UV-visible spectra spectra recorded during the titration of a $9.41 \cdot 10^{-3}$ M solution of **D2** in $CHCl_3$ with increasing amounts of a $2.49 \cdot 10^{-2}$ M solution of **L1** in the same solvent. The titration data are summarized in Table 2.24. The Factor Analysis on the recorded data provided the eigenvalues collected in Table 2.25, confirming in this case also that only two species are present in solution, recognizable as the square planar complex **D2** and the octahedral **D2L1**$_2$ adduct. The data were than fitted by the program following the proposed 1:2 model and the equilibrium formation constant for the equilibrium:

$$D2 + 2L1 \leftrightarrows D2L1_2$$

was calculated with a least squares method, obtaining the value: $\log \beta_{eq} = 4.16 \pm 0.01$.

In Fig. 2.35 the calculated distribution curves for the two absorbing species **D2** and **D2L1**$_2$ involved in the equilibrium are reported, and Figure 2.36 shows the plot of the absorbance values relative to the **D2L1**$_2$ adduct as a function of the molar ratio [**L1**] / [**D2**].

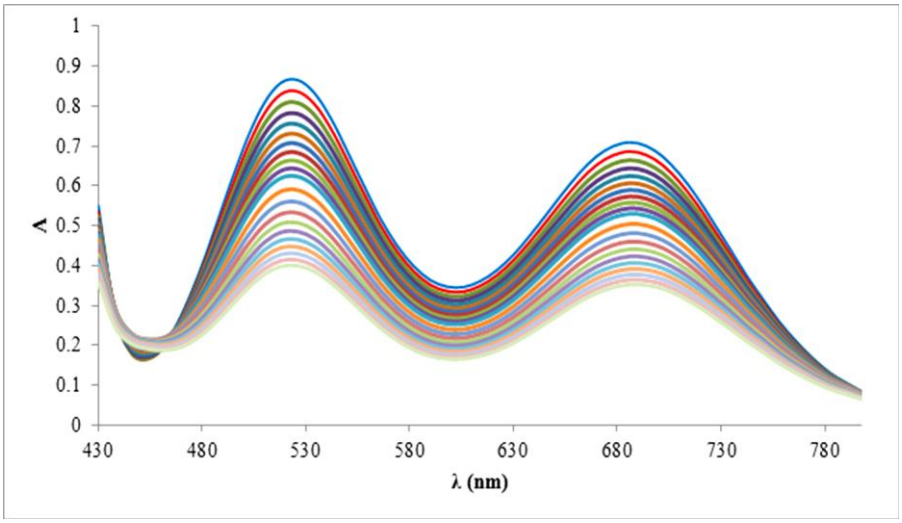

Figure 2.50 UV-Visible Spectra collected during the Titration of **D2** with **L1** corrected considering the Dilution Factor.

Table 2. 26 Experimental Data for the Titration of **D2** with **L1**.

Solution	Addition /µL (± 0.2 %)	V_{tot}/mL	[L1]/10^{-3} M	[D2]/10^{-3} M	[L1]/[D2]
1	-	1.50	0	9.41	0
2	50	1.55	0.80	9.03	0.17
3	50	1.60	1.56	8.53	0.27
4	50	1.65	2.27	7.97	0.37
5	50	1.70	2.93	7.40	0.48
6	50	1.75	3.56	6.83	0.61
7	50	1.80	4.15	6.29	0.75
8	50	1.85	4.72	5.79	0.91
9	50	1.90	5.25	5.33	1.08
10	50	1.95	5.75	4.91	1.27
11	50	2.00	6.23	4.54	1.57
12	100	2.10	7.12	3.90	2.04
13	100	2.20	7.93	3.38	2.57
14	100	2.30	8.67	2.96	3.16
15	100	2.40	9.35	2.61	3.81
16	100	2.50	9.97	2.33	4.52
17	100	2.60	10.54	2.10	5.29
18	100	2.70	11.08	1.90	6.10

19	100	2.80	11.57	1.73	6.96
20	100	2.90	12.03	1.58	7.86

Table 2.27 Factor Analysis Eigenvalues and Parameters for the set of Data collected for **D2** and **L1**

Nº	**Eigenvalue**	**Squaresum**	**Sigma(abs)**
1	$1.524 \cdot 10^{2}$	0.333	$1.838 \cdot 10^{-2}$
2	0.333	$4.209 \cdot 10^{-4}$	$6.537 \cdot 10^{-4}$
3	$1.197 \cdot 10^{-4}$	$3.012 \cdot 10^{-4}$	$5.533 \cdot 10^{-4}$
4	$9.976 \cdot 10^{-5}$	$2.014 \cdot 10^{-4}$	$4.527 \cdot 10^{-4}$

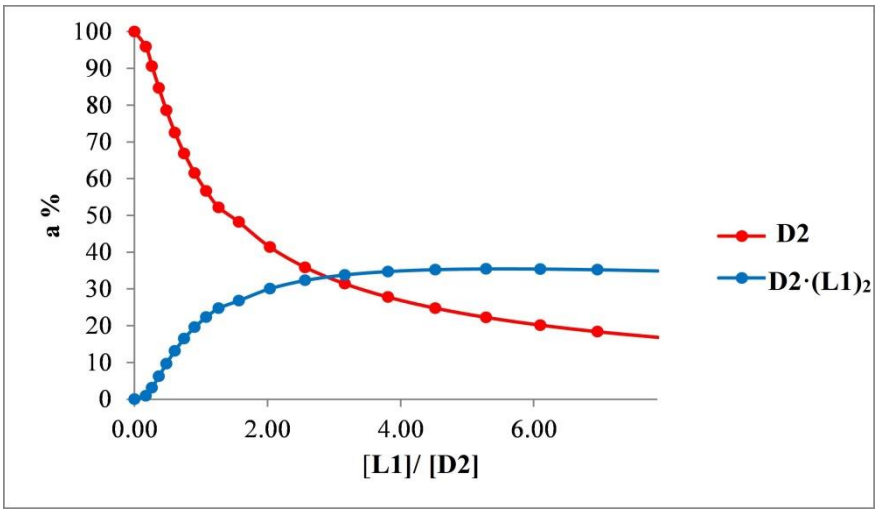

Figure 2.51 Distribution Curves: Percentage Fractions of **D2** and **D2L1**$_2$ as a Function of the Molar Ratio [**L1**]/[**D2**].

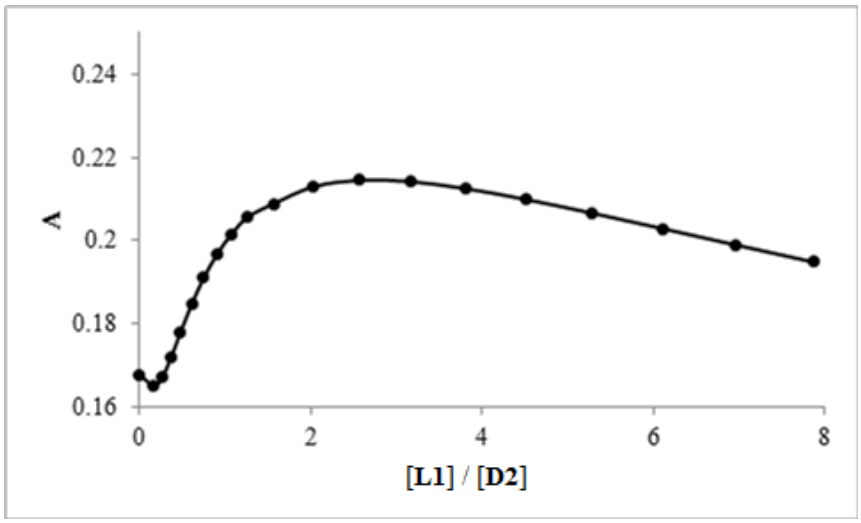

Figure 2.52 Plot of Absorbance Values at 454 nm as a Function of the Molar Ratio [**L1**] / [**D2**].

2.4.3.2 Titration of D3 with L1

Following the same procedure above described, a $9.33 \cdot 10^{-3}$ M solution of **D3** in $CHCl_3$ was titred by adding increasing amounts of a $2.49 \cdot 10^{-2}$ M solution of **L1** in the same solvent. In Fig. 2.37 the UV-visible spectra recorded during the titration are reported, and the titration data are summarized in Table 2.27. The Factor Analysis on the recorded data provided the eigenvalues collected in Table 2.28, confirming the presence in solution of the two species **D3** and **D3L1**$_2$ adduct. The data were than fitted by the program following the proposed 1:2 model and the equilibrium formation constant for the equilibrium:

$$D3 + 2L1 \leftrightarrows D3L1_2$$

was calculated with a least squares method, obtaining the value: $\log \beta_{eq} = 4.52 \pm 0.02$.

In Fig. 2.38 the calculated distribution curves for the species **D3** and **D3L1**$_2$ involved in the equilibrium are reported, and Fig. 2.39 shows the plot of the absorbance values relative to the **D3L1**$_2$ adduct as a function of the molar ratio [**L1**] / [**D3**].

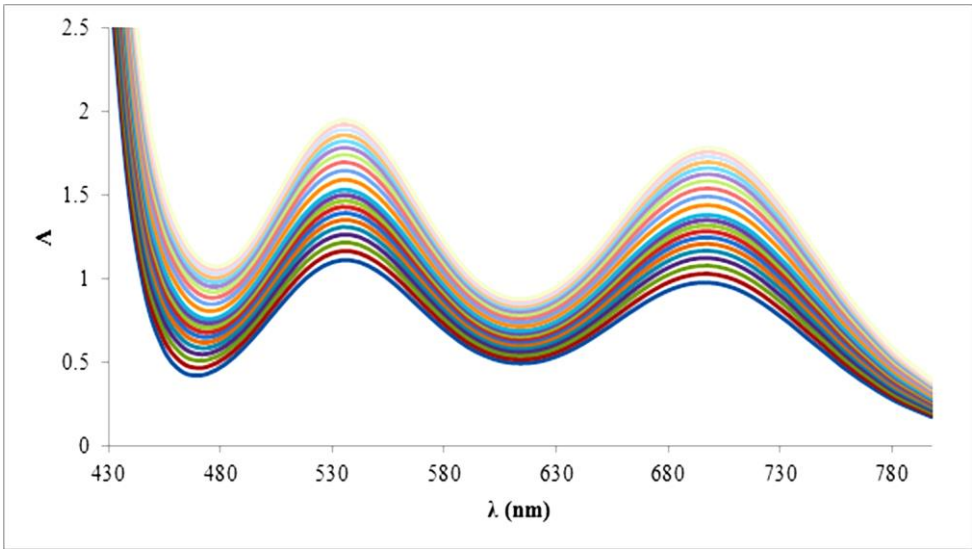

Figure 2.53 UV-Visible Spectra collected during the Titration of **D3** with **L1**, corrected considering the Dilution Factor.

Table 2.28 Experimental Data for the Titration of **D3** with **L1**

Solution	Addition /µL (± 0.2 %)	V_{tot}/mL	[L1]/10^{-3} M	[D3]/10^{-3} M	[L1]/[D3]
1	-	1.5	0	9.33	0
2	50	1.55	0.80	8.84	0.09
3	50	1.6	1.56	8.10	0.19
4	50	1.65	2.27	7.25	0.31
5	50	1.7	2.93	6.41	0.46
6	50	1.75	3.56	5.64	0.63
7	50	1.8	4.15	4.95	0.84

8	50	1.85	4.72	4.36	1.08
9	50	1.9	5.25	3.86	1.36
10	50	1.95	5.75	3.43	1.68
11	50	2	6.23	3.06	2.03
12	100	2.1	7.12	2.49	2.86
13	100	2.2	7.93	2.07	3.84
14	100	2.3	8.67	1.75	4.96
15	100	2.4	9.35	1.50	6.23
16	100	2.5	9.97	1.31	7.63
17	100	2.6	10.54	1.15	9.16
18	100	2.7	11.08	1.03	10.80
19	100	2.8	11.57	0.92	12.56
20	100	2.9	12.03	0.83	14.42

Table 2.29 Factor Analysis Eigenvalues and Parameters for the set of Data collected for **D3** and **L1**

N⁰	**Eigenvalue**	**Squaresum**	**Sigma(abs)**
1	$4.336 \cdot 10^{2}$	0.543	$2.360 \cdot 10^{-2}$
2	0.543	$5.949 \cdot 10^{-3}$	$2.458 \cdot 10^{-3}$
3	$5.088 \cdot 10^{-3}$	$8.619 \cdot 10^{-4}$	$9.359 \cdot 10^{-4}$
4	$5.319 \cdot 10^{-4}$	$3.300 \cdot 10^{-4}$	$5.794 \cdot 10^{-4}$

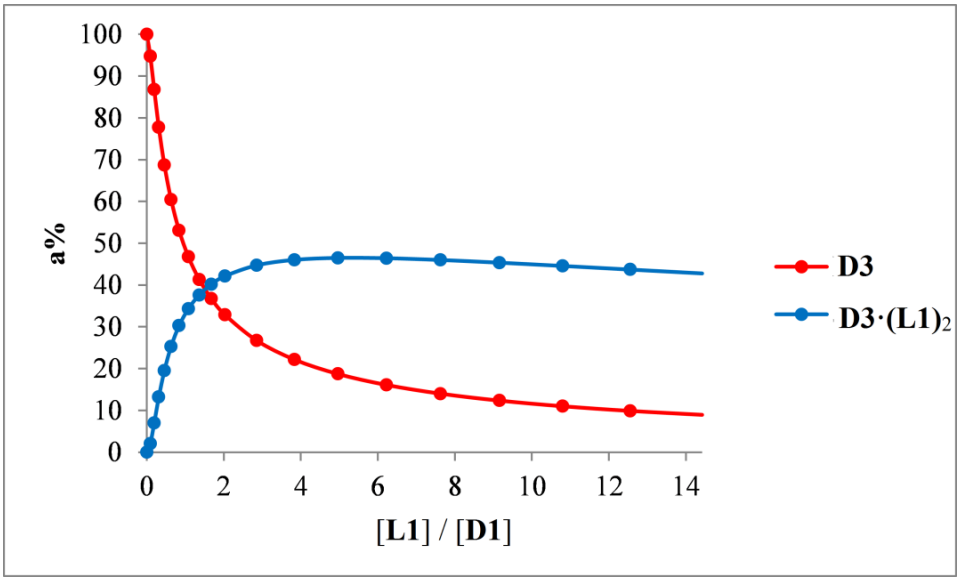

Figure 2.54 Distribution curves: Percentage Fractions of **D3** and **D3L1**$_2$ as a Function of the Molar Ratio [**L1**]/[**D3**].

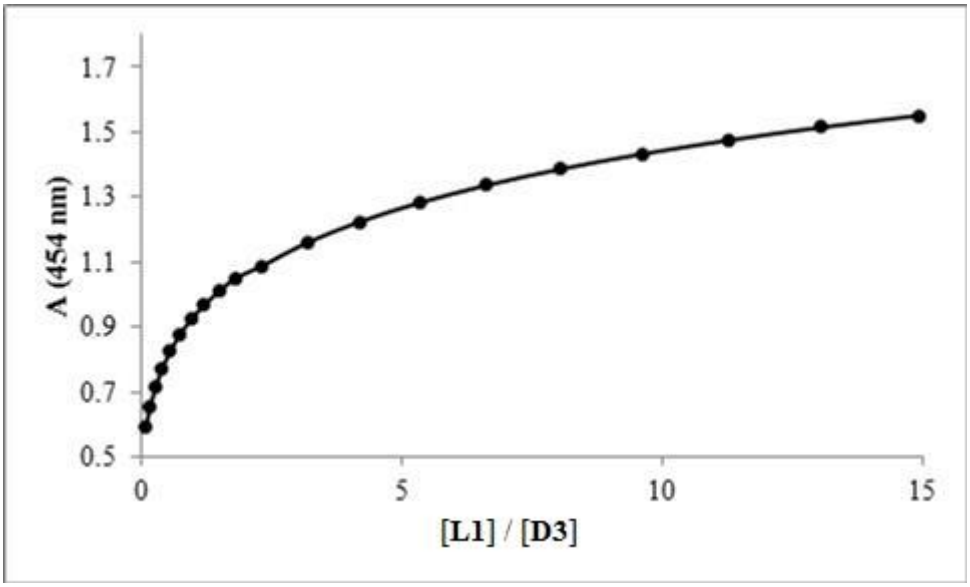

Figure 2.55 Plot of Absorbance Values at 454 nm as a Function of the Molar Ratio [**L1**] / [**D3**].

Unfortunately, it was not possible to calculate the formation constant relative to the adduct between **D4** and **L1** due to incipient precipitation of the final product. The calculated formation constants have been compared with those previously reported for the adduct formation between **D3** and pyridine (Py) and *o*-, *m*-, *p*-aminopyridine (*o*-, *m*-, *p*-NH_2Py),[50] showing very similar values especially if compared with the para-substituted aminopyridine (Table 2.29).

Table 2.30 Comparison between the Rxperimental Constant Values and those present in Literature.

Adducts	**logβ_{eq}**
D1L1$_2$	4.63 ± 0.04
D2L1$_2$	4.16 ± 0.01
D3L1$_2$	4.52 ± 0.02
D3(Py)$_2$	3.20 ± 0.02
D3(*o*-NH$_2$Py)$_2$	1.88 ± 0.02
D3(*m*-NH$_2$Py)$_2$	3.46 ± 0.01
D3(*p*-NH$_2$Py)$_2$	4.71 ± 0.01

3 Experimental

Most of the experimental work of the PhD was employed on the organic synthesis of the building blocks followed by the preparation of the coordination polymers. Most of the synthesis were performed in oven dried glassware under a positive pressure of nitrogen. Starting materials and solvents were purchased from commercial sources and when necessary the solvents have been distilled according to standard literature techniques.

- Melting point measurements were carried in capillaries, using electro thermal melting point apparatus (0-250° Celsius range).
- Elemental analysis were performed with an EA1108 CHNS-O Fisons instrument.
- ^{1}H-NMR (400-MHz) and ^{13}C-NMR (100-MHz, 126-MHz) were recorded at 25 °C on a Varian INOVAX-400 spectrometer and Varian INOVAX-500 spectrometer. Chemical shifts for ^{1}H-NMR and ^{13}CNMR are reported in parts per million (ppm), calibrated to the residual solvent peak set, with coupling constants J reported in Hertz (Hz). The following abbreviations are used for spin multiplicity: s singlet, d = doublet, t = triplet, m =multiplet.
- Infrared (IR) spectra were recorded on a Thermo Nicolet 5700 FTXIR spectrophotometer using KBr pellets and it's reported in wavenumbers (cm^{-1}).
- FT-Raman spectra (resolution of 4 cm^{-1}) were recorded using a Bruker RFS100 FT-Raman spectrometer, fitted with an In-Ga-As detector (room temperature) operating with a Nd:YAG laser (excitation wavelength 1063 nm) with a 180ºC scattering geometry. The excitation power was modulated between 50 and 800 mW depending on the characteristics of the substance.
- Fluorescence spectra were determined on a Varian Cary Eclypse spectrofluorimeter, with a xenon lamp 60-75 kw power, (190-900 nm) wavelength range.
- Single crystal diffraction data has been record at the EPSRC UK National Crystallography service at the University of Southampton (U.K) using a Bruker-Nonius Kappa CCD area detector situated at the window of a rotating anode (graphite Mo-K_α radiation, λ = 0.71073Å). The structures were solved by direct methods procedure in SHELXL-97, and refined by full- matrix least squares on F^2 using SHELXL-97 and Olex 2.Anisotropic displacement parameters were assigned to all non-hydrogen atoms. Hydrogen atoms are included in the refinement but thermal parameters and geometry were constrained to ride on the atom to which they are bonded.

3.2 Synthesis and Characterization of Dithiophosphato Complexes

3.2.1 bis(O-methyldithiophosphato)Ni(II)(D1)

A mixture of $NiCl_2 \cdot 6H_2O$ (0.235 g, 1.0 mmol) and P_2S_5 (0.222 g, 0.5 mmol) in methyl alcohol (50 mL) was refluxed for 1 hour, and the solvent was then removed under reduced pressure to give a purple solid (0.7423, 1.99 mmol, 43 % yield). The purple solid was then recrystallized with a 1:1 mixture of CH_2Cl_2 and MeOH. **D1** was obtained as purple crystals, suitable for X-ray analysis. M.p.: 121-124 ºC. Elemental analysis found (Calc. for $C_4H_{12}O_4P_2S_4Ni$; formula mass = 373.0 uma): C, 13.00 (12.88); H, 3.19 (3.24); S, 34.00 (34.88). FT-IR (KBr, 2000-50 cm^{-1}): 1832 vw, 1444 s, 1173 vw, 1117 s, 796 vs, 654 vs, 532 m, 469 m, 433 m, 396 m 353 m, 351 m, 333 w, 326 w, 325 vw, 302 w, 279 w, 246 w, 225 vw, 179 w, 151 m, 120 vw, 107 w, 74 w cm^{-1}. FT-Raman (3500-50 cm^{-1}, 50 mW, solid state, relative intensities between parentheses related to the highest peak taken equal to 10.0): 3022 (0.5), 2944 (3.0), 2841 (1.2), 1438 (0.6), 1067 (0.2), 819 (0.7), 635 (7.3), 522 (10.0), 471 (1.1), 395 (1.3), 341 (1.7), 312 (6.1), 248 (5.3), 216 (5.8), 124 (6.5) cm^{-1}.

3.2.2 bis(O-ethyldithiophosphato)Ni(II)(D2)

A mixture of $NiCl_2 \cdot 6H_2O$ (1.1971 g, 5.4 mmol) and P_2S_5 (0.2220 g, 0.5 mmol) in EtOH (50 mL) was refluxed for 1 hour, and the solvent was then removed under reduced pressure to give a purple solid (0.3731 g, 2.19 mmol, 48.2 % yield). The purple solid was then recrystallized with a 1:1 mixture of CH_2Cl_2 and EtOH. **D2** was obtained as purple crystals, suitable for X-ray analysis. M.p.: 105 ºC (m). Elemental analysis found (Calc. for $C_8H_{20}O_4P_2S_4Ni$; formula mass = 429.1 uma): C, 22.28 (22.39); H, 4.88 (4.70); S, 29.29 (29.88). FT-IR (KBr, 2000-50 cm^{-1}): 1822 w, 1690 vw, 1659 vw, 1641 vw, 1549 w, 1529 w, 1473 mw, 1451 m, 1440 m 1389 s, 1282 s, 1159 mw, 1103 mw, 1049 w, 1004 m, 951 ms, 822 s, 806 s, 642 vw, 542 m, 434 w, 418 vs, 392 s, 357 vs, 325 m, 309 m, 280 m, 266 vw, 248 s, 226 s, 205 s, 186 m, 166 m, 150 mw, 121 m, 90 m, 73 s, 54 w cm^{-1}. FT-Raman (3000-50 cm^{-1}, 50 mW, solid state, relative intensities between parentheses related to the highest peak taken equal to 10.0): 2979 (0.3), 2962 (2.8), 2936 (4.1), 2923 (3.5), 2897 (1.6), 2864 (1.0), 2720 (0.3), 2472 (0.5), 2452 (1.1), 1388 (0.6), 1104 (1.5), 1053 (0.8), 1005 (0.4), 824 (2.0), 781 (1.1), 635 (3.4), 547 (9.6), 402 (1.9), 345 (2.2), 332 (4.4), 304 (4.7), 242 (3.3), 159 (6.3), 95 (10.0) cm^{-1}.

3.2.3 trans-bis[O-methyl-(4-methoxyphenyl)dithiophosphonato]Ni(II)(D3)

A mixture of $NiCl_2 \cdot 6H_2O$ (0.4788 g, 2.0 mmol) and LR (0.8904 g, 2.2 mmol) in MeOH (100 mL) was refluxed for 1 hour, and the solvent was then removed under reduced pressure to give a purple solid (0.9432 g, 1.9 mmol, 91 % yield). The purple solid was then recrystallized with a 1:1 mixture of CH_2Cl_2 and CH_3OH. **D3** was obtained as purple crystals, suitable for X-ray analysis. M.p.: 184

°C (m). Elemental analysis found (Calc. for $C_{16}H_{20}O_4P_2S_4Ni$; formula mass = 523.9 uma): C, 37.1 (36.6); H, 3.9 (3.8); S, 24.3 (24.4). FT-IR (KBr, 3500-100 cm^{-1}): 3075 vw, 2997 w, 2972 w, 2941 mw, 2837 vw, 1907 vw, 1597 vs, 1567 mw, 1500 s, 1465 mw, 1440 m 1426 w, 1407 mw, 1348 w, 1332 vw, 1307 ms, 1294 s, 1269 vs, 1177 s, 1165 m, 1118 vs, 1029 ms, 1011 vs, 1003 vs, 836 m, 820 vw, 808 mw, 789 vs, 667 s, 640 s, 622 ms, 550 s, 524 m, 491 vw, 435 m, 375 m, 351 m, 297 mw, 277 w, 256 vw, 252 vw, 202 w, 165 w, 148 vw, 130 w, 122 w, 100 vw, 88 vw, 73 vw, 53 vw cm^{-1}. FT-Raman (3500-50 cm^{-1}, 50 mW, solid state, relative intensities between parentheses related to the highest peak taken equal to 10.0): 3074 (3.8), 2998 (2.1), 2943 (3.8), 2838 (1.4), 1590 (6.3), 1566 (1.2), 1259 (1.2), 1118 (7.2), 1002 (1.2), 801 (2.8), 667 (2.6), 639 (3.3), 553 (9.1), 491 (1.2), 440 (1.3), 314 (6.1), 296 (1.7), 238 (2.6), 102 (9.7), 84 (10.0) cm^{-1}.

3.2.4 trans-bis[O-ethyl-(4-methoxyphenyl)dithiophosphonato]Ni(II)(D4)

A mixture of $NiCl_2 \cdot 6H_2O$ (0.4755 g, 2.0 mmol) and LR (0.8917 g, 2.2 mmol) in EtOH (100 mL) was refluxed for 1 hour, and the solvent was then removed under reduced pressure to give a purple solid (0.7015 g, 1.3 mmol, 63 % yield). The purple solid was then recrystallized with a 1:1 mixture of CH_2Cl_2 and EtOH. **D4** was obtained as purple crystals, suitable for X-ray analysis. M.p: 133 °C (m). Elemental analysis found (Calc. for $C_{18}H_{24}O_4P_2S_4Ni$; formula mass = 553.3 uma): C, 39.4 (39.1); H, 4.4 (4.4); S, 23.9 (23.2). FT-IR (KBr, 3500-100 cm^{-1}): 2969 mw, 2928 w, 2838 mw, 2559 vw, 2055 vw, 1912 vw, 1776 vw, 1594 vs, 1566 ms, 1500 s, 1461 m, 1452 m, 1438 m, 1408 m, 1386 m, 1308 s, 1298 vs, 1262 vs, 1175 ms, 1159 m, 1115 vs, 1030 s, 1001 vs, 942 vs, 826 ms, 801 s, 772 s, 661 s, 638 s, 623 s, 493 m, 445 m, 428 m, 389 w, 359 ms, 346 s, 320 m, 294 m, 286 m, 272 mw, 262 w, 251 vw, 238 mw, 219 vw, 199 q, 183 w, 163 mw, 125 mw, 116 mw, 72 ms cm^{-1}. FT-Raman (3500-50 cm^{-1}, 50 mW, solid state, relative intensities between parentheses related to the highest peak taken equal to 10.0): 3068 (2.4), 2968 (1.9), 2922 (2.3), 1593 (5.3), 1566 (0.8), 1306 (1.0), 1294 (1.0), 1245 (0.8), 1178 (1.8), 1114 (7.8), 802 (2.3), 663 (2.3), 634 (2.3), 616 (2.3), 555 (5.1), 310 (2.3), 277 (1.9), 234 (1.3), 112 (8.9), 80 (10.0) cm^{-1}.

3.3 Synthesis and Characterization of the Polypyridyl Ligands.

3.3.1 1,4-di-3-pyridyl-1,3-butadiyne(L1)

The ligand 1,4-di-3-pyridyl-1,3-butadiyne (**L1**) was synthesized by a different way from the literature methods[66] thus optimizing yield and reaction time by using small quantity of bis (triphenylphosphine) palladium (II) dichloride catalyst. A mixture of 3-ethynylpyridine (0.996 g, 9.65

mmol), copper iodide (0.056 g, 0.30 mmol), bis (triphenylphosphine) palladium(II) dichloride (0.133 g 0.19 mmol) and diethylamine (50 mL) was stirred at reflux temperature for 5 hours.The mixture was then filtered under reduced pressure, washed with brine (20 mL) and extracted with ethyl acetate (3x15 mL) dried with Na_2SO_4 and the solvent evaporated under reduced pressure. The crystallization of the yellow solid from dichloromethane-ethanol yielded **L1** as a light yellow crystals (0.603 g, 2,95 mmol, 61 % yield). M.p 148 °C.

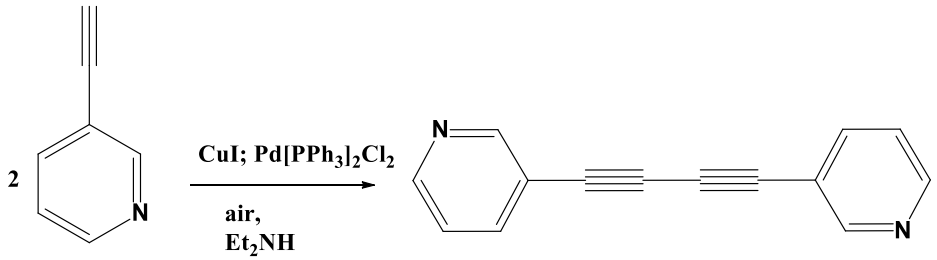

Scheme 3.1 1,4-di-3-pyridyl-1,3-butadiyne (**L1**) Synthetic Procedure.

Spectral data: ^{1}H NMR (500 MHz $CDCl_3$ 298 K) δ = 8.77 (d, 2H,), δ = 8.61 (dd), δ = 7.82 (dt), δ = 7.30 (t). FT-IR (KBr, 4000-400cm^{-1}) $\tilde{\nu}$ = 2128 (w), 1577 (m), 1473 (m), 1412 (s), 1188 (m), 1022 (s), 802 (s), 698 (s), 627 (m), 513 (w). Fluorescence ($CHCl_3$; λex = λ_{ex} = 263 nm.; slit = 5x5): λem = 357 nm and 369 nm, M = $1.14 \cdot 10^{-6}$.

The catalyst bis (triphenylphosphine) palladium (II)dicloride [$PdCl_2(PPh_3)_2$] was synthesized through following synthetic method. A solution of triphenylphosphine (1.0 g, 8.1 mmol) in 10 mL of warm EtOH has been add to a solution of $(NH_4)_2PdCl_4$ (0.6 g 1.9·mmol) in 10 mL of warm H_2O and 10 mL of warm EtOH and stirred for 15 minutes. The yellow solid has been isolated by filtration, recrystallized in toluene and dried under vacuum. M.p.: >230°C. FT-IR (KBr, 4000-400cm^{-1}): 3420 w, 3048 w, 2360 w, 1480 m, 1435 s, 1330 w, 1309 w, 1186 w, 1159 w, 1098 s, 1027 m, 998 m, 745 m, 708 m, 692 s, 521 s, 500 s, 455 w, 440 w cm^{-1}. FT-Raman (500-50 cm^{-1}, 50 mW, solid state, relative intensities between parentheses related to the highest peak taken equal to 10.0): 304 (5.7), 277 (0.9), 254 (1.2), 226 (1.1), 201 (1.9), 151 (3.3), 89 (10.0) cm^{-1}.

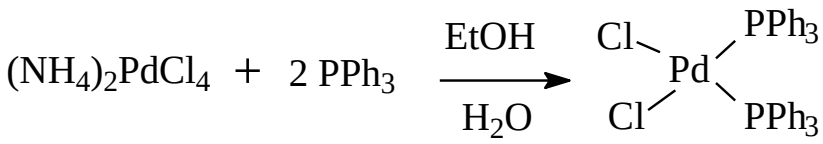

Scheme 3.2 bis(triphenylphosphine)palladium(II)dicloride [$PdCl_2(PPh_3)_2$] Synthetic Procedure.

3.3.2 1,4-bis(4-pyridylethynyl)benzene(L2)

A mixture of 1,4-diiodobenzene (1.79 g, 2.4 mmol), 4-ethynylpyridine hydrochloride (1.53 g, 11.0 mmol), copper iodide (0.05 g, 0.25 mmol) and bis(triphenylphosphine)palladium(II) dichloride (0.18 g, 0.25 mmol) and freshly distilled diethylamine (50 mL) was degassed and stirred under nitrogen at 80 °C for 7 hours and stirred at room temperature for 2 days. The mixture was then filtered under reduced pressure, extracted with $CHCl_3$ and washed with water (3x50 mL). The combined organic extracts were dried (Na_2SO_4) and the solvent evaporated under reduced pressure. The residue was purified by chromatography on alumina using diethyl ether as eluent to yield **L2** (0.46 g, 1.6 mmol, 62 % yield) as pale yellow solid. M.p.: 155-156 °C (m).

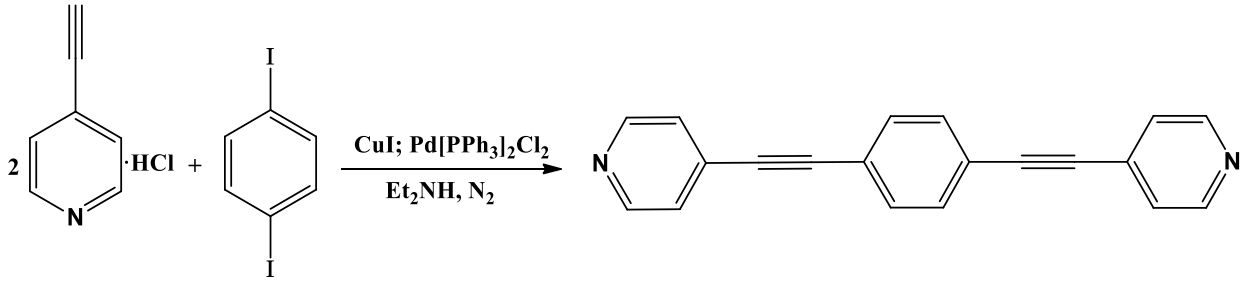

Scheme 3.3 1,4-bis(4-pyridylethynyl)benzene (**L2**) Synthetic Procedure.

Spectral data: ^{1}H NMR (500 MHz $CDCl_3$ 298 K) δ = 8.5 (d), δ = 7.6 (d), δ = 7.45(s). FT-IR (KBr, 4000-400 cm-1): 3340 m, 2217 m, 1653 m, 1590 s, 1577 m, 1559 m, 1540 m, 1522 m, 1507 m, 1490 m, 1261 m, 1210 w, 1098 m, 1067 m, 1008 m, 991 m, 841 m, 821 s, 804 s, 714 w, 668 w, 626 m, 535 m, 521 m, 470 m, 443 w, 419 w cm-1. FT-Raman (500-50 cm^{-1},25 mW, solid state, relative intensities between parentheses related to the highest peak taken equal to 10.0): 168 (7.1), 154 (9.0), 117 (10.0) cm^{-1}.

3.3.3 2,2'-dimetoxy-1,1' -binaphtyl-3,3'-bis(4pyridyl-amido)(R)(L3)

The ligand (*R*)-**L3** was synthesized and characterized in collaboration with Prof. Pasini group in University of Pavia (Italy). The spacer is synthesized in two steps from optically-pure (*R*)-2,2'-dimethoxy-1,1'-binaphthyl-3,3'-dicarboxylic acid under nonracemizing conditions. The precursor could be obtained in enantiopure form after a published four step procedure[67] (including an enanti-

oresolution step) from commercially available 2-naphthol. The dicarboxylic acid was subsequently activated as the acid chloride, and then amidation in the presence of 4-dimethylamino pyridine (excess), and triethylamine as the non nucleophilic acid scavenger, afforded the title compound (*R*)-**L3** in 30% yields after purification by column chromatography.

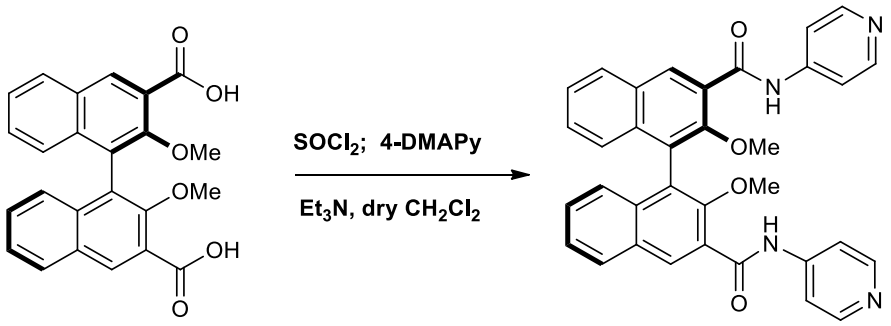

DMAPy: 4-dimethylaminopyridine

Scheme 3.4 2,2'-dimetoxy-1,1' -binaphtyl-3,3'-bis(4pyridyl-amido)(R) (**L3**) Synthetic Procedure.

Spectral data: ^{1}H NMR (200 MHz, $CDCl_3$): δ =10.19 (s, 2H, NHCO), 9.03 (s, 2H, Binaphthyl-H4), 8.60 (d, 4H, J=5.7, α-pyridine), 8.14 (d, 2H, J=8.1, Binaphthyl), 7.70 (d, 4H, J=5.7, β-pyridine), 7.58 (t, 2H, J=6.6, Binaphthyl), 7.42 (t, 2H, J=6.6, Binaphthyl), 7.19 (d, 2H, J=8.7, Binaphthyl), 3.46 (s, 6H, OCH_3).

3.3.4 2,5-bis (4-pyridyl)-4-thia-1,3-thiazolidine (L4) and 2,5-bis (3-pyridyl)-4-thia-1,3-thiazolidine (L5)

Ligands 2,5-bis(4-pyridyl)-4-thia-1,3-thiazolidine (**L4**) and 2,5-bis(3-pyridyl)-4-thia-1,3-thiazolidine (**L5**) were synthesized according to literature methods.[56] To a solution of thioisonicotinamide (for **L4**) or thionicotinamide (for **L5**) (2.00 g, 14.4 mmol) in 20 mL of warm absolute ethanol, was added a solution of iodine (5.55 g, 22 mmol) in 50 mL of absolute ethanol. The reaction is maintained itself just under reflux temperature for one hour. The mixture was filtered to remove the remaining insoluble sulphur and it was then left to stand at room temperature overnight, during which time a large mass of dark needles had deposited. The solid filtrate was chilled in an ice-bath and the precipitated dark needles were removed by filtration and washed with ethanol/hexane 1:1 The dark crystals were suspended in 30 mL of water, the mixture was then made alkaline with 1 mL of 4N sodium hydroxide, and treated with an excess of solid sodium thiosulfate to effect decolourization. The mixture was warmed gently to hasten the reduction of the iodine and then chilled to precipitate the product. Recrystallisation of the product from benzene raised **L4** (0.94 g, 0.004 mmol, 56 %

yield) as a white solid, M.p 110°C or **L5** (0.38 g, 0.002 mmol, 23 % yield) as a pale brown solid, M.p 115°C.

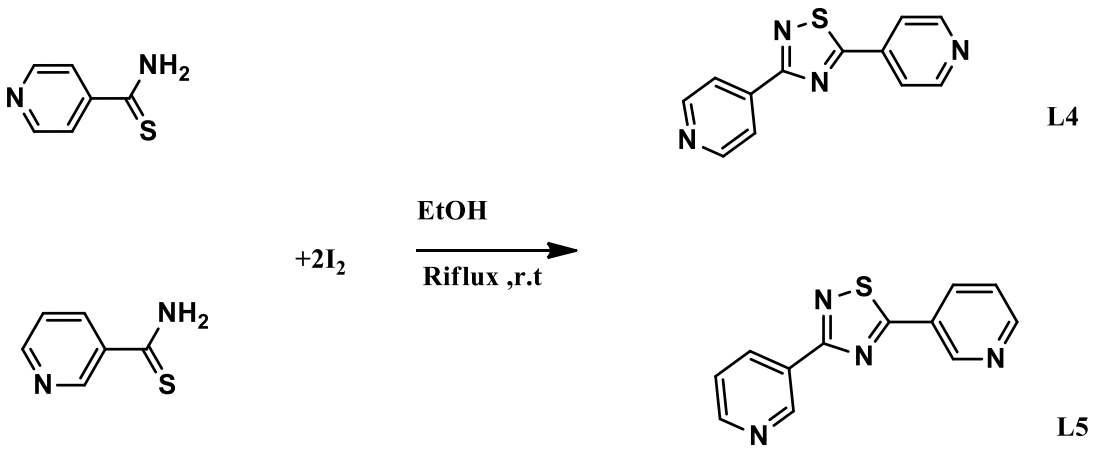

Scheme 3. 5 2,5-bis(4-pyridyl)-4-thia-1,3-thiazolidine(**L4**) and 2,5-bis(3-pyridyl)-4-thia-1,3-thiazolidine (**L5**), Synthetic Procedure.

Spectral data **L4**.^{1}H NMR (500 MHz CDCl3 298 K) δ = 8.63(t), δ = 7.51 (m). FT-IR (KBr, 4000-350 cm–1): 3448 (w), 1589 (m), 1575 (m), 1497 (w), 1478 (s), 1400 (s), 1338 (m), 1297 (m), 1238 vw, 1127 (w), 1047 (vw), 1023 (m), 989 (m), 811 (s), 727 (s), 698 (vs), 617 (w), 493 (vw) cm-1. Fluorescence (CH3CN; λex = 240 nm; slit = 5x5): λem = 416 nm, M = $1.08 \cdot 10^{-4}$.Spectral data **L5**. ^{1}H NMR (500 MHz CDCl3 298 K) δ = 8.64(d), δ = 8.54 (m), δ = 7.86 (tt) δ = 7.37 (q). FT-IR (KBr, 4000-350 cm–1): 3443 (w), 1955 (m), 1600 (s),1466 (w), 1407 (s), 1343 (m), 1291 (m), 1251 (vw), 1127 (w), 1065 (vw), 1007 (m), 990 (m), 842 (s), 834 (s), 676 (vs), 619 (w), 473 (vw) cm^{-1}.

3.3.5 1,3,5 tris (3-pyridylethynyl) benzene (L6)

The ligand 1,3,5 tris (3-pyridylethynyl) benzene **L6** was synthesized through the following synthetic method. A mixture of 1,3,5-tribromobenzene (0.63g, 2.1 mmol), 3-ethynylpyridine (1.03 g, 10 mmol), copper iodide (0.04 g, 0.2 mmol) and bis (triphenylphosphine) palladium (II) dichloride (0.14g, 0.2 mmol) and freshly distilled diethylamine (50 ml) was degassed and stirred under nitrogen at 60 °C for two days. The solvent was removed by reduced pressure and the solid washed with satured acqueous NH_4Cl (60mL) and extracted with ethyl acetate (3x75mL). The combined organic extracts dried on Na_2SO_4 and the solvent evaporated under reduced pressure. Recrystallisation of the residue from ethanol, water (1:1) yielded **L6** (0.49 g, 1,3 mmol 64% yield) M.p 185 °C.

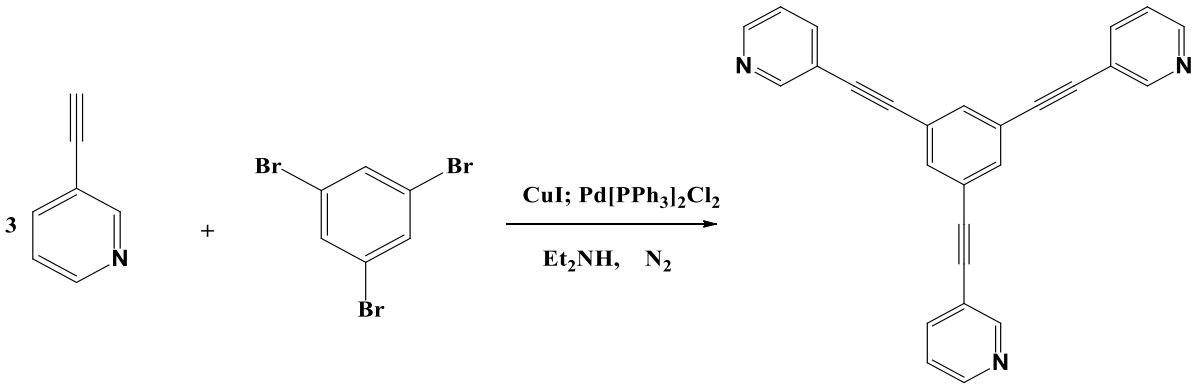

Scheme 3.6 1,3,5 tris (3-pyridylethynyl) benzene Synthetic Procedure.

Spectral data ^{1}H NMR (500 MHz $CDCl_3$ 298 K) δ = 8.79 (d), δ = 8.56 (dd), δ = 7.90 (dt), δ = 7.69 (s), δ = 7.28 (t). FT-IR (KBr, 4000-400cm^{-1}) $\tilde{\nu}$ = 3035 (w), 2212(w), 1635 (m), 1591 (m), 1477 (s), 1022 (s), 874 (s), 803 (s), 700 (s), 677 (m).

3.3.6 N,N',N''-tris (3-pyridin) benzene-1,3,5 tricarboxamide (L7) and N,N',N''-tris(4-pyridin) benzene -1,3,5 tricarboxamide (L8).

Ligands **L7** and **L8** were synthesized according to literature methods.[68] A solution of 1,3,5-benzenetricarbonyl chloride (0.78ml, 3.8 mmol) in THF (10 mL) was added drop wise to the THF solution (25mL) of 3-aminopyridine or 4-aminopyridine (1.128g ,12.1 mmol) and triethylamine (2.6 ml, 19 mmol) at 0 °C under nitrogen atmosphere. The solution was stirred for twenty four hours. THF was distilled off and the yellow precipitate product was washed with water. Recrystal-lisation of the solid from methanol yielded (0.43 g, 1,3 mmol 72% yeld). Mp >230°C for both.

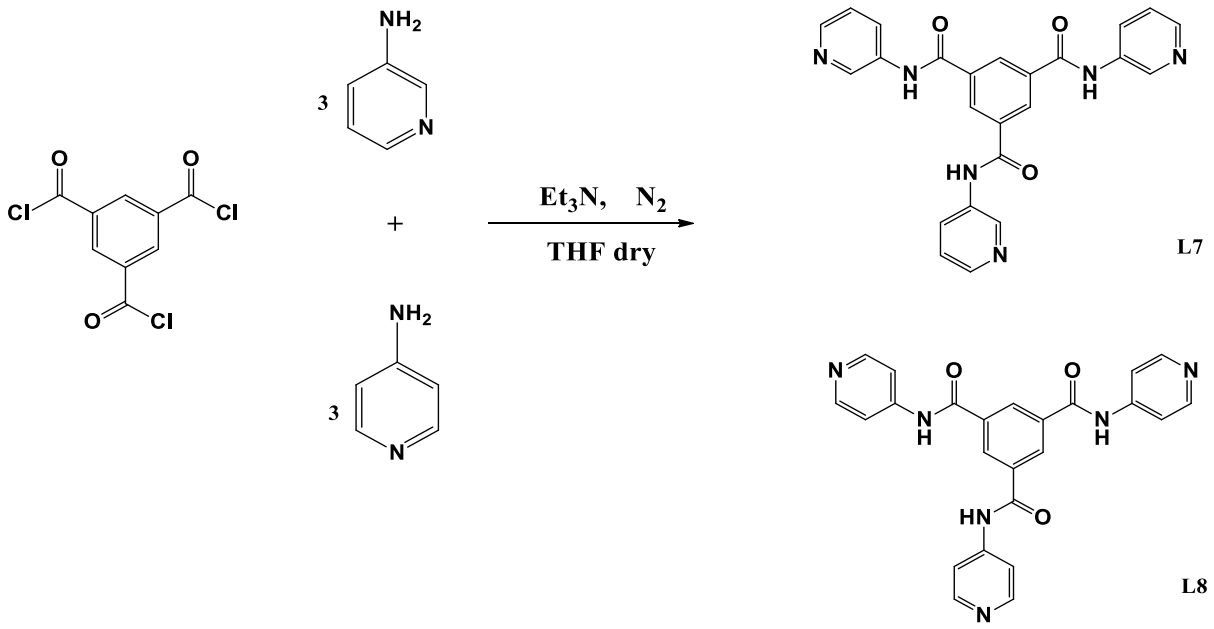

Scheme 3.7 N,N',N''-tris (3-pyridin) benzene-1,3,5 tricarboxamide (**L7**) and N,N',N''-tris(4-pyridin) benzene -1,3,5 tricarboxamide (**L8**) Synthetic Procedure.

Spectral data (**L7**): ^{1}HNMR (500MHz, DMSO *d-6*) δ = 10.91 (s), δ =8.98 (s), δ = 8.78 (d), δ = 8.36 (dd), δ = 8.22 (dt), δ = 7.42(t).^{13}CNMR (500MHz, DMSO *d-6*) δ = 165.58, δ = 144.95, δ = 142.03, δ = 135.55, δ = 134.97 δ = 130.14, δ = 127.48, δ = 123.67. FT-IR (KBr, 4000-400cm^{-1}) $\tilde{v}$ = 3245 (w), 3077 (w), 1685 (s), 1606 (w), 1548 (vs), 1483 (m), 1421 (m), 1237 (m), 1127 (w), 1048 (w) 911 (w), 806(m), 703 (w). Spectral data (**L8**). ^{1}HNMR (500MHz, DMSO *d-6*) δ = 11.10 (s), δ =8.79 (s), δ = 8.56 (d), δ = 7.91 (d). FT-IR (KBr, 4000-400cm^{-1}) $\tilde{v}$ = 3422 (w), 3082 (w), 2116 (w), 1681 (s), 1604 (vs), 1513 (s), 1419 (m), 1332 (m), 1297 (w), 1195 (w) 1085 (w), 830(m), 712 (w), 527 (w).

3.3.7 1,3,5-benzenetricarboxylic acid, 1,3,5-tri-3-pyridinyl ester (L9) and 1,3,5 Benzene-tricarboxylic acid 1,3,5-tri-4-pyridinyl ester (L10).

Ligands **L9** and **L10** were synthesized according to following literature methods.[69] A solution of 1,3,5 benzenetricarbonyl trichloride (0.37 g 1.4 mmol) in 15 mL of dry CH_2Cl_2 was added to a solution of 3-hydroxypyridine (0.40g 4.2 mmol) or 4-hydroxypyridine (0.41 g 4.2 mmol) and triethylamine (0,5 ml 3.40 mmol) in 50 mL of dry CH_2Cl_2. The reaction mixture was heated at reflux for twenty-four hours and the resultant solution washed with brine (10 mL x3). The organic phase was evaporated under reduced pressure and the white solid obtaineed washed with diethyl ether. (0.452g ,1.0 mmol 65% yeld) M.p 170°C for **L9** ; (0.382g 0. 9 mmol 55% yield) M.p 170°C for **L10.**

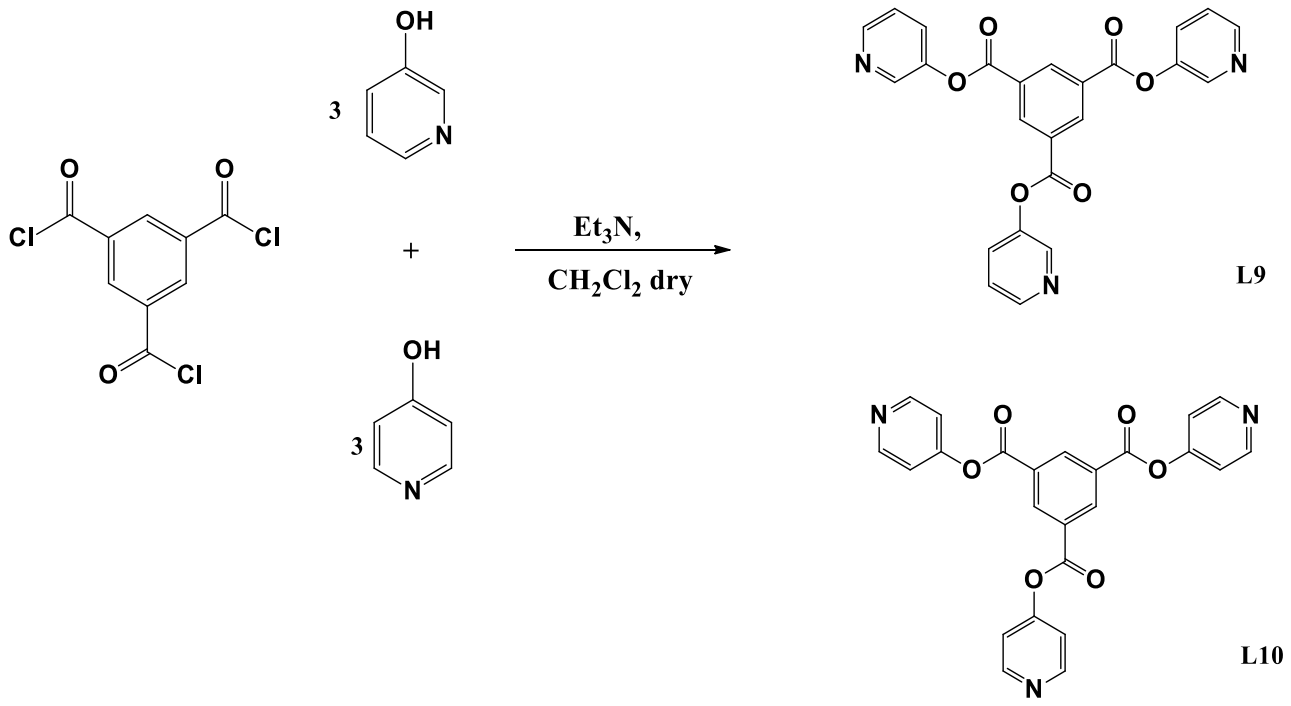

Scheme 3.8 1,3,5-benzenetricarboxylic acid, 1,3,5-tri-3-pyridinyl ester and 1,3,5 benzene-tricarboxylic acid 1,3,5-tri-4-pyridinyl ester Synthetic Procedure.

Spectral data (**L9**): ^{1}H NMR (500 MHz DMSO-*d6* 298 K) δ = 9.05 (s), δ = 8.93 (dd), δ = 8.65 (d), δ = 8.55 (dd). FT-IR (KBr, 4000-400cm^{-1}) $\tilde{\nu}$ = 3418 (w), 2817 (w), 2490 (w), 1764 (s), 1577 (m), 1479 (m), 1353 (m), 1207 (w), 1042 (w), 842 (w), 800 (m), 730 (m), 640 (m). Fluorescence (CH_3OH; λex = λ_{ex}= 275 nm; slit = 5x5): λem = 311 nm, M = $1.0 \cdot 10^{-4}$ shown in the Figure 3.2. Spectral data (**L10)** ^{1}H NMR 500 MHz $CDCl_3$ 298 K) δ = 8.79 (d), δ = 8.75 (d), δ = 8.60 (s), δ = 7.51 (d). FT-IR (KBr, 4000-400cm^{-1}) $\tilde{\nu}$ = 3441 (w), 3078 (w), 1745 (s), 1625 (m), 1506 (m), 1214 (m), 1192 (m), 924 (w), 839 (m), 676 (m). Fluorescence (EtOH; λ_{ex} = 240 nm; slit = 5x5): λ_{em} = 347 nm, M = $1.0 \cdot 10^{-4}$

3.4 Coordination Polymers Synthesis.

All nitrogen ligands donors have been reacted with the four organo-dithiophosphorous metal complexes with classical solvothermal techniques in different molar ratios and using suitable solvents such as chloroform amylene stabilized, methanol and ethanol distilled off. We have obtained for the most part of ligands microcrystalline green solid which were characterized by melting point, FT-IR, while the obtaining of single crystals it was more complicated and opportune crystallization methods described in §2.2 have been necessary to in order to obtain the crystals suitable for the x-ray analysis diffraction X-ray analysis.

3.4.1 $[((MeO)_2PS_2)_2Ni]\cdot$ (1,4 bis (3-pyridyl)butadiyne)]$_\infty$,(**D1**·**L1**)$_\infty$

(29.6 mg, 0.08 mmol) of $[((MeO)_2PS_2)_2Ni]$ (**D1**) and (30.5 mg, 0.15 mmol) of (1,4 bis (3-pyrdyl) butadiyne) (**L1)**, have been reacted at 130 °C in high pressure Aldrich tube in 15 mL of MeOH and 15 mL of $CHCl_3$ (amylene stabilized). After complete dissolving of the reagents, the reaction mixture was transferred in a vial, and slowly cooled at room temperature. After two weeks green needles crystals of (**D1**·**L1**)$_\infty$, suitables for X-ray analysis have been obtained (10 mg, $0.13\cdot10^{-3}$ mmol, 55% yield). M.p > 250°C (m) not detectable. FT-IR (KBr, 4000-400cm^{-1}): 3415 m, 2937 w, 1638 w, 1478 w 1175 w, 1016 s, 798 s, 695 w, 673 w, 659 w.

3.4.2 $[((EtO)_2PS_2)_2Ni\cdot$(1,4 bis (3-pyridyl)butadiyne)]$_\infty$,(**D2**·**L1**)$_\infty$

(56.8 mg, 0.13mmol) of $[((EtO)_2PS_2)_2Ni]$ (**D2**) and (51.0 mg, 0.25 mmol) of (1,4 bis (3-pyridyl)butadiyne) (**L1)** , were reacted at 130 °C in a high pressure Aldrich tube in 15 mL of EtOH and 15 ml of $CHCl_3$ (amylene stabilized). After complete dissolving of the reagents, the reaction mixture was tranferred in a small vial and slowly cooled at room temperature. After two weeks was obtained very few green palette crystals of (**D2**·**L1**)$_\infty$ suitable for X-ray analysis. M.p=170°C. FT-IR (KBr, 4000-400cm^{-1}): 3441 m, 2973 m, 2925 w, 1738 w 1618 w, 1440w, 1384 vw, 1101 m, 1023 s, 801 m 644 m 538 w, cm^{-1}

3.4.3 $[(MeO\text{-}C_6H_4)(MeO)PS2)_2Ni\cdot$(1,4 bis (3-pyridyl)butadiyne)]$_\infty$,(**D3**·**L1**)$_\infty$

(96.0 mg, 0.18 mmol) of $[((MeO)_2PS_2)_2Ni]$ (**D3**) and (70 mg ; 0.35 mmol) of (1,4 bis (3-pyridyl)butadiyne) (**L1)** , have been reacted at 50 °C in a flask with 15 mL of MeOH and 15 mL of $CHCl_3$ (amylene stabilized). After complete dissolving of the reagents, the reaction mixture was slowly cooled at room temperature. After twentyfour hours a green microcristalline powder of (**D3**·**L1**)$_\infty$ is precipitated from solution. (45 mg; 0.48 mmol; 89%yeld) M.p.: 180 °C (m). Green crystals suitable for X-ray analysis were obtained by preparing a solution of **D3** (20 mg; 0.458 mmol) in 5 mL of $CHCl_3$ (amylene stabilized) in a small vial wich was then introduced into a bigger one containing solution of **L1** (17.5 mg; 0.08 mmol) in 10 mL of MeOH, and left to stand at room temperature for a week. FT-IR (KBr, 4000-400cm^{-1}): 1598 vs, 1568 w, 1531 vw, 1500 s, 1455 w, 1440 w, 1389 w, 1297 ms, 1259 s, 1216 mw, 1178 mw, 1114 vs, 1064 w, 1029 vs, 949 s, 830 w, 810 mw, 646 s, 628 mw, 545 ms, 521 w, 500 vw, 472 mw, 438 vs, 383 vs, 383 s, 326 vw, 301 w, 287 vw, 235 s, 199 mw, 167 vs, 112 ms, 102 s cm^{-1}.

3.4.4 [MeO-C_6H_4)(EtO))$PS_2)_2$Ni] ·(1,4 bis (3-pyrdyl)butadiyne)]$_\infty$,(D4·L1)$_\infty$

(35.6 mg, 0.65 mmol) of [$((EtO)_2PS_2)_2$Ni] (**D4**) and (25.1 mg, 0.12 mmol) of (1,4 bis (3-pyridyl) butadiyne) (**L1)**, have been reacted at 50 °C in a flask with 13 mL of EtOH and 15 mL of $CHCl_3$ (amylene stabilized). After complete dissolving of the reagents, the reaction mixture was slowly cooled at room temperature. After twentyfour hours a green microcristalline powder of (**D4·L1**)$_\infty$ was filtered from solution (60 mg; $0.06\cdot10^{-3}$mmol; 32% yield) M.p: 180 °C (m). Green crystals suitable for X-ray analysis have been obtained by reacting in Aldrich high pressure tube the same quantity of reagents and solvents. After complete reagent dissolving, the reaction mixture was transferred in a vial and slowly cooled at room temperature diffusion. FT-IR (KBr,$^{-1}$4000-400 cm^{-1}): 3445 w, 2933 w, 2831w, 1500 s, 1567 w, 1499 m, 1473 m, 1461 m, 1295 m, 1032 s, 801 m, 776 m, 692 w, 659 w, 545 m, 520 w, 439 m, cm^{-1}.

3.4.5 [Ni($(MeO)_2PS_2)_2$·(1,4-bis(4-pyridylethynyl)benzene)]$_\infty$,(D1·L2)$_\infty$

A solution of [Ni($(MeO)_2PS_2)_2$](**D1**) (18.6 mg, 0.05 mmol) in 10 mL of $CHCl_3$ (amylene stabilized) was added dropwise to a solution of 1,4-bis(4-pyridylethynyl) benzene (**L2**) (14.0 mg, 0.05 mmol) in 15 mL of MeOH. The mixture was reacted in a flask at 100° C for 1h and after twentyfour hours a green powder of (**D1·L2**)$_\infty$ was filtered from the solution (12.16 mg; 0.020 mmol; 40 % yield). M.p. 165-170 °C (d). Elemental analysis found (calc. for $C_{24}H_{24}N_2O_4P_2S_4Ni$; formula mass = 653.3 uma): C, 44.12 (44.10); H, 3.47 (3.70); N, 4.36 (4.29); S, 17.33 (19.63). FT-IR (KBr, 4000-350 cm^1): 3455 w, 2224 w, 1638 m, 1604 s, 1508 w, 1449 w, 1413 w, 1384 w, 1215 mw, 1167 mw, 1036 m, 1010 s, 848 w, 833 w, 779 s, 737 w, 682 m, 663 m, 547 vw, 528 w cm^{-1}. FT-Raman (4000-0 cm^{-1}, 50 mW, solid state, relative intensities between parentheses related to the highest peak taken equal to 10.0): 3365 (1.9), 3067 (1.9), 2657 (1.3), 2220 (10.0), 1919 (1.0), 1596 (3.4), 1140 (1.1) cm^{-1}.

3.4.6 [Ni($(EtO)_2PS_2)_2$·(1,4-bis(4-pyridylethynyl)benzene)]$_\infty$,(D2·L2)$_\infty$

A solution of [Ni($(EtO)_2PS_2)_2$](**D2**) (21.3 mg, 0.05 mmol) in 10 mL of $CHCl_3$ (amylene stabilized) was added to a solution of 1,4-bis(4-pyridylethynyl) benzene (**L2**) (14.0 mg, 0.050 mmol) in 15 mL of EtOH. The resultant solution it was placed into a straight sample tube and left to stand at room temperature for two weeks. Crystals of (**D2·L2**)$_\infty$ suitable for X-ray analysis have been obtained (2.0 mg, 0.003 mmol, 6% yield). M.p.: 225-226 °C (d). Elemental analysis found (calc.for $C_{28}H_{32}N_2O_4P_2S_4Ni$; formula mass = 709.5 uma): C, 45.37(47.40); H, 5.19 (4.55); N, 3.47 (3.95); S, 14.30 (18.08). FT-IR (KBr, 4000-400 cm^{-1}): 3463 vw, , 2974 w, 2218 w, 1603 s, 1541 vw, 1509 w, 1438 w, 1408 w, 1385 m, 1261 s, 1214 m, 1157 w, 1098 w, 1017 s, 942 s, 800 s, 770 s, 680 s, 540 s

cm^{-1}. FT-IR (KBr, 4000-400 cm^{-1}): 3463 vw, , 2974 w, 2218 w, 1603 s, 1541 vw, 1509 w, 1438 w, 1408 w, 1385 m, 1261 s, 1214 m, 1157 w, 1098 w, 1017 s, 942 s, 800 s, 770 s, 680 s, 540 s cm^{-1}.

3.4.7 [Ni(MeOdtp)2·(1,4-bis(4-pyridylethynyl)benzene)]$_\infty$,(D3·L2)$_\infty$

[Ni(MeOdtp)$_2$] (**D3**) (26.3 mg, 0.05 mmol) and 1,4-bis(4-pyridylethynyl)benzene (**L2**) (14.0 mg, 0.05 mmol) were reacted at 130 °C in a high pressure Aldrich tube in 15 mL of MeOH and 15 mL of $CHCl_3$ (amylene stabilized). After complete dissolving of the reagents, the reaction mixture was trasferred in a vial and slowly cooled at room temperature. After two weeks was obtained a green precipitate of (**D3·L2**)$_\infty$ (17.3 mg, 0.021 mmol, 43 % yield) M.p 187 (d), 198-200 °C (f). Crystals suitable for X-ray analysis have been obtained by purifing the green precipitate of (**D3·L2**)$_\infty$ in a high pressure Aldrich tube in 15 mL of MeOH and 15 mL of $CHCl_3$ (amylene stabilized) (11.3 mg, 0.014 mmol, 28 % yield). Elemental analysis found (calc. for $C_{36}H_{32}N_2O_4P_2S_4Ni$; formula mass = 805.5 uma): C, 52.94 (53.68); H, 4.33 (4.00); N, 3.54 (3.48); S, 17.81 (15.92). FT-IR (KBr, 4000-400 cm^{-1}): 1648 m, 1600 vs, 1565 s, 1542 w, 1515 w, 1498 s, 1456 m, 1407 m, 1321 vw, 1303 w, 1292 m, 1255 vs, 1213 m, 1176 m, 1112 vs, 1066 vw, 1027 vs, 1014 vs, 842 w, 827 vs, 800 m, 779 vs, 736 w, 715 w, 659 m, 644 vs, 628 s, 345 vs, 520 m cm^{-1}. FT-Raman (4000-0 cm^{-1}, 50 mW, solid state, relative intensities between parentheses related to the highest peak taken equal to 10.0): 2221 (10.0), 1598 (5.5), 1140 (2.3) cm^{-1}.

3.4.8 [Ni(EtOdtp)2·(1,4-bis(4-pyridylethynyl)benzene)]$_\infty$,(D4·L3)$_\infty$

[Ni(EtOdtp)2] (27.7 mg, 0.05 mmol) (D4) and 1,4-bis(4-pyridylethynyl)benzene (L2) (14.2 mg, 0.05 mmol) were reacted at 150 °C in a high pressure Aldrich tube in 30 mL of EtOH and 5 mL of CHCl3 (amylene stabilized). After complete dissolving of the reagents, the reaction mixture was transferred in a big vial and slowly cooled at room temperature. After one week a green powder of (D4·L3)∞ was filtered from the solution (13.8 mg, 0.017 mmol, 33 % yield). M.p.: 204-205 °C (m). Elemental analysis found (calc. for C38H36N2O4P2S4Ni; formula mass = 833.6 uma): C, 54.74 (54.81); H, 4.35 (4.36); N, 3.48 (3.37); S, 15.82 (15.37). FT-IR (KBr, 4000-400 cm–1): 1604 vs, 1598 vs, 1565 s, 1542 m, 1517 m, 1498 s, 1457 m, 1442 m, 1411 m, 1386 m, 1303 w, 1290 m, 1255 vs, 1213 m, 1176 m, 1157 w, 1135 vw, 1110 s, 1068 w, 1025 s, 1018 s, 991 w, 981 vw, 964 vw, 937 s, 898 vw, 889 vw, 877 vw, 867 vw, 856 vw, 844 w, 827 s, 800 w, 771 m, 750 w, 738 w, 717 vw, 673 vw, 655 m, 636 s, 626 m, 617 w, 547 s, 518 w, 443 w cm-1. FT-Raman (4000-0 cm-1, 28 mW, solid state, relative intensities between parentheses related to the highest peak taken equal to 10.0): 2238 (10.0), 1603 (8.8), 1150 (7.3), 1012 (4.1) cm-1.

3.4.9 $[Ni((MeO)_2PS_2 \cdot$(R-2,2′-dimethoxy-1,1′-binaphthyl-3,3′-bis(4-pyridyl-amido))$]_\infty$, $(\mathbf{D1 \cdot L3})_\infty$

A solution of $[Ni((MeO)_2PS_2)_2]$ (**D1**) (10.5 mg, 0.05 mmol) and (R)-2,2′-dimethoxy-1,1′-binaphthyl-3,3′-bis(4-pyridyl-amido) (**L3**) (11.0 mg, 0.05 mmol) was prepared in 0.5 mL of CH_2Cl_2 and placed into a straight sample tube. On to this solution were layered carefully 2 mL of distilled EtOH. The sample tube was sealed with parafilm and left to stand at room temperature for eight weeks. $(\mathbf{D1 \cdot L3})_\infty$ (4.1 mg, $0.41 \cdot 10^{-2}$ mmol, 22 % yield) was obtained as green crystal suitable for X-ray analysis. M.p: 208-210 °C (d), 229-230 °C (m). Elemental analysis found (calc. for $C_{38}H_{38}N_4O_8P_2S_4Ni$; formula mass = 927.6 uma): C, 47.41 (49.20); H, 4.10 (4.13); N, 5.91 (6.04); S, 14.05 (13.82). FT-IR (KBr, 4000-40 $0cm^{-1}$): 2939 vw, 2836 vw, 1686 s, 1588 s, 1509 s, 1456 w, 1420 m, 1350 vw, 1330 m, 1298 m, 1270 s, 1016 s, 919 w, 788 ms, 675 m, 539 mw cm^{-1}.

3.4.10$[Ni((EtO)_2PS_2) \cdot$(R-2,2′-dimethoxy-1,1′-binaphthyl-3,3′-bis(4-pyridyl-amido))$]_\infty$, $(\mathbf{D2 \cdot L3})_\infty$

A solution of $[Ni((EtO)_2PS_2)_2]$ (**D2**), (8.6 mg, 0.02 mmol) and (R-2,2′-dimethoxy-1,1′-binaphthyl-3,3′-bis(4-pyridyl-amido))]$_\infty$, (**L3**) (11.1 mg, 0.02 mmol) was prepared in 0.5 mL of CH_2Cl_2 and placed into a straight sample tube. On to this solution were layered carefully 2 mL of pure EtOH. The sample tube was sealed with parafilm and left to stand at room temperature for eight weeks. $(\mathbf{D2 \cdot L3})_\infty$ (6.5 mg, 0.007 mmol, 33 % yield) was obtained as green crystals. M.p.: 204-206 °C (d). Elemental analysis found (calc. for $C_{42}H_{46}N_4O_8P_2S_4Ni$; formula mass = 983.7 uma): C, 51.15 (51.28); H, 4.77 (4.71); N, 5.77 (5.70); S, 13.75 (13.04). FT-IR (KBr, 4000-400 cm^{-1}): 1678 s, 1590 s, 1510 s, 1458 vw, 1422 m, 1388 vw, 1332 s, 1297 m, 1199 m, 1157 w, 1018 s, 943 s, 835 w, 756 m, 660 m, 623 vw, 543 m cm^{-1}.

3.4.11[Ni(MeOdtp)2·(R-2,2′-dimethoxy-1,1′-binaphthyl-3,3′-bis(4-pyridyl-amido))]$_\infty$, $(\mathbf{D3 \cdot L3})_\infty$

A solution of $Ni(MeOdtp)_2$ (**D3**) (10.4 mg, 0.02 mmol) and R-2,2′-dimethoxy-1,1′-binaphthyl-3,3′-bis(4-pyridyl-amido) (**L3**) (11.0 mg, 0.02 mmol) was prepared in 0.5 mL of CH_2Cl_2 and placed into a straight sample tube. On to this solution were layered carefully 2 mL of pure MeOH. The sample tube was sealed with parafilm and left to stand at room temperature for eight weeks. $(\mathbf{D3 \cdot L3})_\infty$ (0.004 mg, mmol, 18 % yield) was obtanined as green powder. M.p.: 208-209 °C (d). Elemental analysis found (calc. for $C_{50}H_{46}N_4O_8P_2S_4Ni$; formula mass = 1079.8 uma): C, 58.54 (55.62); H, 4.52 (4.29); N, 6.43 (5.19); S, 6.52 (11.88). FT-IR (KBr, 4000-400 cm^{-1}): 2936 vw, 2834 vw, 1685

vs, 1589 s, 1509 s, 1456 w, 1417 m, 1350 m, 1330 m, 1296 mw, 1209 m, 1112 m, 1068 w, 1017 s, 919 w, 863 s, 827 w, 753 m, 649 m, 623 m, 543 s cm^{-1}.

3.4.12[Ni(MeOdtp)$_2$·(R-2,2′-dimethoxy-1,1′-binaphthyl-3,3′-bis(4-pyridyl-amido))]$_\infty$, (D4·L3)$_\infty$

A solution of [Ni(EtOdtp)$_2$] (**D4**) (11.1 mg, 0.02 mmol) and R-2,2′-dimethoxy-1,1′-binaphthyl-3,3′-bis(4-pyridyl-amido) (**L3**) (11.1 mg, 0.02 mmol) was prepared in 0.5 mL of CH_2Cl_2 and placed into a straight sample tube. On to this solution were layered carefully 2 mL of pure EtOH. The sample tube was sealed with parafilm and left to stand at room temperature for eight weeks. (**D4**·**L3**)$_\infty$ (2.1 mg, $0.2\cdot10^{-2}$mmol, 10 % yield) was obtained as a green precipitate. M.p.: 184-187 °C (d). Elemental analysis found (calc. for $C_{52}H_{50}N_4O_8P_2S_4Ni$; formula mass = 1107.9 uma): C, 56.76 (56.38); H, 4.69 (4.55); N, 5.39 (5.06); S, 9.78 (11.58). FT-IR (KBr, 4000-400 cm^{-1}): 1604 vs, 1565 m, 1517 w, 1498 s, 1459 w, 1442 w, 1411 w, 1386 vw, 1303 vw, 1290 w, 1255 vs, 1213 w, 1176 w, 1157 vw, 1110 s, 1068 vw, 1022 s, 935 m, 842 w, 827 s, 798 w, 771 w, 655 w, 636 s, 626 m, 545 vs, 520 vw cm^{-1}.

3.4.13[Ni((MeO)$_2$PS$_2$)$_2$·(2,5-bis(4-pyridyl)-4-thia-1,3-thiazolidine)]$_\infty$,(D1·L4)$_\infty$

[Ni((MeO)$_2$PS$_2$)$_2$] (18.6 mg, 0.05 mmol) (**D1**) and 2,5-bis(4-pyridyl)-4-thia-1,3-thiazolidine (**L4**) (12.0 mg, 0.05 mmol) were reacted at 130 °C in a high pressure Aldrich tube in 30 mL of MeOH. After complete dissolving of the reagents, the reaction mixture was tranferred in a small vial and slowly cooled at room temperature. After five days (**D1**·**L4**)$_\infty$ few green crystals suitable for X-ray analysis were obtained. M.p.:170 °C (d). Elemental analysis found (calc. for $C_{16}H_{20}N_4O_4P_2S_5Ni$; formula mass = 611.9 uma): C, 31.63 (31.33); H, 2.38 (3.29); N, 9.31 (9.14); S, 21.75 (26.14). FT-IR (KBr, 3000-300 cm^{-1}): 2938 w, 2834 vw, 2361 vw, 1608 m, 1462 m, 1411 m, 1335 m, 1290 w, 1210 w, 1176 w, 1130 vs, 827 s, 798 s, 709 m, 691 s, 675 s, 665 m, 530 m, 439 vw, 398 w, 324 m cm^{-1}. FT-Raman (3500-100 cm^{-1}, 600 mW, solid state, relative intensities between parentheses related to the highest peak taken equal to 10.0): 1922 (6.0), 1894 (6.4), 1877 (6.0), 1811 (6.4), 1758 (4.6), 1612 (10.0), 1513 (8.6), 1459 (9.3), 1410 (9.3), 1335 (6.1), 1293 (6.0), 1020 (6.2) cm^{-1}.

3.4.14 [Ni((EtO)$_2$PS$_2$)$_2$·(2,5-bis(4-pyridyl)-4-thia-1,3-thiazolidine)]$_\infty$,(D2·L4)$_\infty$

[Ni((EtO)2PS2)2] (21.4 mg, 0.05 mmol) (**D2**) and 2,5-bis(4-pyridyl)-4-thia-1,3-thiazolidine (**L4**) (12.0 mg, 0.05 mmol) were reacted at 160 °C in a high pressure Aldrich tube in 30 mL of EtOH. After complete dissolving of the reagents, the reaction mixture was slowly cooled at room temperature. After a few days (D2·L4)∞ (4.1 mg, 0.6·10-2 mmol, 12 % yield) was obtained as green crys-

tals suitable for X-ray analysis by slow evaporation of the solvent. M.p.: 155 °C (d). Elemental analysis found (calc. for C20H28N4O4P2S5Ni; formula mass = 668.0 uma): C, 36.31 (35.89); H, 4.17 (4.22); N, 8.46 (8.37); S, 24.12 (23.95). FT-IR (KBr, 3000-350 cm–1): 3054 vw, 3032 w, 2934 w, 2893 vw, 2459 vw, 2285 vw, 1931 vw, 1609 s, 1496 vs, 1440 m, 1412 m, 1336 m, 1121 m, 1019 vs, 945 vs, 848 w, 830 m, 805 m, 773 s, 713 m, 673 s, 657 s, 644 m, 620 w, 546 w, 410 w cm–1. FT-Raman (3500-0 cm-1, 150 mW, solid state, relative intensities between parentheses related to the highest peak taken equal to 10.0): 3075 (4.8), 3027 (4.2), 2933 (5.1), 2888 (5.0), 1981 (4.1), 1611 (10.0), 1513 (5.7), 1413 (8.5), 1338 (5.9), 1229 (5.3), 1215 (5.5), 1095 (7.7), 1015 (7.7) 999 (5.7), 729 (4.2), 650 (6.1) 548 (8.8), 376 (7.5) cm–1.

3.4.15 $[Ni(MeOdtp)_2 \cdot (2,5\text{-bis}(4\text{-pyridyl})\text{-}4\text{-thia-}1,3\text{-thiazolidine})]_\infty$,$(\mathbf{D3}\cdot\mathbf{L4})_\infty$

$[Ni(MeOdtp)_2]$ (**D3**) (26.2 mg, 0.05 mmol) and 2,5-bis(4-pyridyl)-4-thia-1,3-thiazolidine (**L4**) (12.0 mg, 0.05 mmol) were reacted at 100 °C in a high pressure Aldrich tube in 30 mL of MeOH. After complete dissolving of the reagents, the reaction mixture was slowly cooled at room temperature. After a week, $(\mathbf{D3}\cdot\mathbf{L4})_\infty$ (29.5 mg, 0.39 mmol, 77 % yield) was obtained as green crystals suitable for X-ray analysis. M.p.: 160 °C (d). Elemental analysis found (calc. for $C_{28}H_{28}N_4O_4P_2S_5Ni$; formula mass = 764.0 uma): C, 44.73 (43.98); H, 3.38 (3.69); N, 7.53 (7.32); S, 21.08 (20.94). FT-IR (KBr, 1800-300): 1214 w, 1179 mw, 1130 vw, 1114 s, 1065 w, 1029 vs, 1020 vs, 909 vw, 851 vw, 830 ms, 779 vs, 754 w, 733 vw, 709 w, 690 vw, 654 ms, 640 s, 625 mw, 546 vs, 520 mw, 508 w, 457 vw, 442 w, 398 vw, 369 vw, 326 ms cm^{-1}. FT-Raman (3500-100 cm^{-1}, 150 mW, solid state, relative intensities between parentheses related to the highest peak taken equal to 10.0): 3054 (2.8), 2924 (2.8), 1615 (10.0), 1582 (5.7), 1420 (7.8), 1310 (3.6), 1280 (4.2), 1110 (5.7), 1020 (5.0), 1000 (5.0), 547 (6.4), 102 (6.4) cm^{-1}.

3.4.16 $[Ni(EtOdtp)_2 \cdot (2,5\text{-bis}(4\text{-pyridyl})\text{-}4\text{-thia-}1,3\text{-thiazolidine})]_\infty$,$(\mathbf{D4}\cdot\mathbf{L4})_\infty$

$[Ni(EtOdtp)_2]$ (**D4**) (27.7 mg, 0.05 mmol) and 2,5-bis(4-pyridyl)-4-thia-1,3-thiazolidine (**L4**) (12.4 mg, 0.05 mmol) were reacted at 100 °C in a high pressure Aldrich tube in 30 mL of EtOH. After complete dissolving of the reagents, the reaction mixture was slowly cooled at room temperature. After a week, $(\mathbf{D4}\cdot\mathbf{L4})_\infty$ was obtained as green crystals suitable for X-ray analysis (34.9 mg, $4.4\cdot10^{-2}$ mmol, 88 % yield). M.p.: 170-188 °C (m). Elemental analysis found (calc. for $C_{30}H_{32}N_4O_4P_2S_5Ni$; formula mass = 792.0 uma): C, 45.61 (45.41); H, 4.25 (4.06); N, 7.14 (7.06); S, 19.20 (20.20). FT-IR (KBr, 4000-350 cm^{-1}): 3457 w, 2973 w, 1595 s,1569 m, 1498 w,1460 m, 1435w, 1407 s, 1384 w, 1330 w, 1288 s, 1256 s, 1208 w, 1175 s, 1112 s, 1027 vs, 941 s, 825 m, 800 m, 772 s,735 w, 706 w, 670 m, 623 m, 549 s, 516 m cm^{-1}.

3.4.17 $[Ni((MeO)_2PS_2)_2 \cdot (2,5\text{-bis}(3\text{-pyridyl})\text{-}(4\text{-thia-}1,3\text{-thiazolidine})]_2$, $(D1 \cdot L5)_2$

[Ni((MeO)2PS2)2] (**D1**) (18.6 mg, 0.05 mmol) and 2,5-bis(3-pyridyl)-4-thia-1,3-thiazolidine (**L5**) (18.0 mg, 0.07 mmol) were reacted at 140 °C in a high pressure Aldrich tube in 30 mL of MeOH. After complete dissolving of the reagents, the reaction mixture was slowly cooled at room temperature. After a few days (D1·L5)2 ,(5.5 mg, 8.0·10-3 mmol, 18 % yield) was obtained as green crystals suitable for X-ray analysis by slow evaporation of the solvent. M.p.: 180 °C (d). Elemental analysis found (calc. for $C_{16}H_{20}N_4O_4P_2S_5Ni$; formula mass = 611.9 uma): C, 31.55 (31.33); H, 2.21 (3.29); N, 9.13 (9.14); S, 24.69 (26.14). FT-IR (KBr, 4000-400 cm–1): 2938 w, 2834 vw, 2361 vw, 1608 m, 1462 vm, 1411 m, 1335 m, 1290 w, 1210 w, 1176 w, 1130 vs, 827 s, 798 s, 709 m, 691 s, 675 s, 665 m, 530 m, 439 vw, 398 w, 324 m cm-1.FT-Raman (4000-0 cm-1, 200 mW, solid in KBr, relative intensities between parentheses related to the highest peak taken equal to 10.0): 1922 (6), 1894 (6.4), 1877 (6), 1811 (6.4), 1758 (4.6), 1612 (10), 1513 (8.6), 1459 (9.3), 1410(9.3), 1335 (6.1), 1293 (6), 1020 (6.2) cm-1.

3.4.18 $[Ni((EtO)_2PS_2)_2 \cdot (2,5\text{-bis}(3\text{-pyridyl})\text{-}(4\text{-thia-}1,3\text{-thiazolidine})]_\infty$,$(D2 \cdot L5)_2$

A solution of $[Ni((EtO)_2PS_2)_2]$ (**D2**) (10.3 mg, 0.02 mmol) was prepared in 0.5 mL of CH_2Cl_2 in a small vial. This vial was then introduced into a bigger one containing a solution of 2,5-bis(4-pyridyl)-4-thia-1,3-thiazolidine (**L5**) (10.0 mg, 0.04 mmol) in 10 mL of MeOH, and left to stand at room temperature for several weeks. Green crystals of $(\mathbf{D2 \cdot L5})_2$ (16.9 mg, $2.5 \cdot 10^{-2}$ mmol, 50 % yield) suitable for X-ray analysis have been obtained. M.p.: 159-162 °C (m). Elemental analysis found (calc. for $C_{20}H_{28}N_4O_4P_2S_5Ni$; formula mass = 668.0 uma): C, 34.84 (35.89); H, 4.53 (4.22); N, 8.11 (8.37); S, 24.15 (23.95). FT-IR (KBr, 4000-50 cm^{-1}): 3054 vw, 3032 w, 2934 w, 2893 vw, 2459 vw, 2285 vw, 1931 vw, 1609 s, 1496 vs, 1440 m, 1412 m, 1336 m, 11215 m, 1019 vs, 945 vs, 848 w, 830 m, 805 m, 773 s, 713 m, 673 s, 657 s, 644 m, 620 w, 546 w, 410 w cm^{-1}. FT-Raman (3500-0 cm^{-1}, 600 mW, solid state, relative intensities between parentheses related to the highest peak taken equal to 10.0): 3075 (4.8), 3027 (4.2), 2933 (5.1), 2888 (5), 1981 (4.1), 1611 (10), 1513 (5.7), 1413 (8.5), 1338 (5.9), 1229 (5.3), 1215 (5.5), 1095 (7.7), 1015 (7.7), 999 (5.7), 729 (4.2), 650 (6.1), 548 (8.8), 376 (7.5) cm^{-1}.

3.4.19 $[Ni(MeOdtp)_2 \cdot (2,5\text{-bis}(3\text{-pyridyl})\text{-}4\text{-thia-}1,3\text{-thiazolidine})]_\infty$,$(D3 \cdot L5)_\infty$

$[Ni(MeOdtp)_2]$ (**D3**) (26.3 mg, 0.05 mmol) and 2,5-bis(3-pyridyl)-4-thia-1,3-thiazolidine (**L5**) (24.0 mg, 0.1 mmol) were reacted at 100 °C in a high pressure Aldrich tube in 25 mL of MeOH. After complete dissolving of the reagents, the reaction mixture was slowly cooled at room temperature. After a week, $(\mathbf{D3 \cdot L5})_\infty$ (29.5 mg, 0.03 mmol, 62 % yield) was obtained as green crystals suit-

able for X-ray analysis. M.p.: 160 °C (d). Elemental analysis found (calc. for $C_{28}H_{28}N_4O_4P_2S_5Ni$; formula mass = 764.0 uma): C, 44.73 (43.93); H, 3.38 (3.69); N, 7.53 (7.32); S, 21.08 (20.94). FT-IR (KBr, 1600-350 cm^{-1}): 1593 s, 1569 mw, 1499 s, 1474 ms, 1432 w, 1406 m, 1331 w, 1294 s, 1254 vs, 1175 ms, 1113 vs, 1021 vs, 827 mw, 775 vs, 730 w, 654 vs, 623 s, 545 vs, 525 w, 436 w, 406 vw, 327 ms cm^{-1}. FT-Raman (4000-0 cm^{-1}, 100 mW, solid in KBr, relative intensities between parentheses related to the highest peak taken equal to 10.0): 3054 (0.7), 2850 (0.4), 2670 (0.3), 1618 (5.2), 1477 (2.6), 1418 (2.0), 1199 (6.0), 1156 (10.0), 1031 (2.6), 642 (0.8), 545 (1.2), 125 (4.2), 104 (2.4) cm^{-1}.

3.4.20 [Ni(EtOdtp)$_2$·(2,5-bis(3-pyridyl)-4-thia-1,3-thiazolidine)]$_\infty$,(D4·L5)$_\infty$

[Ni(EtOdtp)$_2$] (**D4**) (27.7 mg, 0.05 mmol) and 2,5-bis(3-pyridyl)-4-thia-1,3-thiazolidine (**L5**) (12.0 mg, 0.05 mmol) were reacted at 130 °C in a high pressure Aldrich tube in 15 mL of EtOH and 25 mL of $CHCl_3$ (amylene stabilized). After complete dissolving of the reagents, the reaction mixture was slowly cooled at room temperature. After a week, (**D4·L5**)$_\infty$ (21.3 mg, 0.03 mmol, 54 % yield) was obtained as green crystals suitable for X-ray analysis. M.p.: 148-151 °C (d), 154-166 °C (m). Elemental analysis found (calc. for $C_{30}H_{32}N_4O_4P_2S_5Ni$; formula mass = 792.0 uma): C, 46.78 (45.41); H, 4.31 (4.06); N, 6.91 (7.06); S, 19.32 (20.20). FT-IR (KBr, 4000-400 cm^{-1}): 2973 vw, 2835 vw, 1593 vs, 1569 vs, 1499 m, 1473 s, 1461 w, 1418 m, 1405 w, 1386 mw, 1304 m, 1293 s, 1254 vs, 1189 m, 1174 m, 1114 vs, 1026 vs, 943 s, 826 m, 801 mw, 778 s, 690 m, 652 vs, 547 vs, 524 w cm^{-1}.

3.4.21 [Ni((MeO)$_2$PS$_2$)$_2$·(1,3,5-tris(3-pyridylethynyl)benzene)]$_\infty$, (D1·L6)$_\infty$

A solution of [Ni((MeO)$_2$PS$_2$)$_2$] (**D1**) (7.6 mg, 0.02 mmol) and 1,3,5-*tris*(3-pyridylethynyl)benzene (**L6**) (7.3 mg, 0.02 mmol) was prepared in 0.5 ml of MeOH and placed into straight sample tubes. On to this solution was layered 1 mL of CH_2Cl_2. The sample tubes were sealed with parafilm and left to stand at room temperature for 3 weeks. (**D1·L6**)$_\infty$ (3.2 mg, $0.4\cdot10^{-2}$ mmol, 21 % yield) was obtained as green crystals suitable for X-ray analysis M.p.: 167-168 °C (d). Elemental analysis found (calc. for $C_{31}H_{27}N_3O_4P_2S_4Ni$; formula mass = 754.5 uma): C, 34.12 (49.35); H, 3.64 (3.61); N, 3.17 (5.57); S, 20.66 (17.00). FT-IR (KBr, 4000-400 cm^{-1}): 3442 vw, 2940 w, 1637 m, 1580 ms, 1480 m, 1453 m, 1419 m, 1384 vw, 117 w, 1106 vw, 1016 vs, 881 w, 788 s, 697 w, 670 s, 648 m, 530 w, 438 w cm^{-1}.

3.4.22 [Ni((EtO)2PS2)2·(1,3,5-tris(3-pyridylethynyl)benzene)]$_\infty$,(D2·L6)$_2$

[Ni((EtO)$_2$PS$_2$]$_2$ (**D2**) (42.8 mg, 0.1 mmol) and 1,3,5-*tris*(3-pyridylethynyl)benzene (**L6**) (19.2 mg, 0.05 mmol) were reacted at 150 °C in a high pressure Aldrich tube in 30 mL of EtOH. After com-

plete dissolving of the reagents, the reaction mixture was slowly cooled at room temperature. After three weeks no product has been obtained. Green crystals of (**D2·L6**)$_2$ (2.1 mg, $0.3\cdot10^{-2}$ mmol, 5 % yield) suitable for X-ray analysis have been obtained by evaporating the solution under vacuum and slow diffusion of ether into a solution of the precipitate in CH_2Cl_2. M.p.: 174-176 °C. Elemental analysis found (calc. for $C_{35}H_{35}N_3O_4P_2S_4Ni$; formula mass = 810.6 uma): C, 42.90 (51.86); H, 4.04 (4.35); N, 3.76 (5.18); S, 14.11 (15.82). FT-IR (KBr, 4000-400cm^{-1}): 3456 vw, 2977 w, 1639 w, 1582 m, 1551 w, 1478 m, 1404 mw, 1385 m, 1262 w, 1191 m, 1156 w, 1099 w, 1016 s, 943 s, 876 w, 806 , 785 m, 760 ms, 695 m, 676 s, 647 w, 582 w, 537 vw cm^{-1}.

3.4.23 [Ni(MeOdtp)$_2$·(1,3,5-tris(3-pyridylethynyl)benzene)]$_\infty$,(D3·L6)$_\infty$

[(Ni(MeOdtp)$_2$] (**D3**) (26.2 mg, 0.050 mmol) and 1,3,5-*tris*(3-pyridylethynyl)benzene (**L6**) (19.1 mg, 0.050 mmol) were reacted at 120 °C in a high pressure Aldrich tube in 30 mL of MeOH and 5 mL of $CHCl_3$ (amylene stabilized). After complete dissolving of the reagents, the reaction mixture was slowly cooled at room temperature. After two weeks (**D3·L6**)$_\infty$ (18.9 mg, 0.021 mmol, 42 % yield) was obtained as green crystals. Crystals suitable for X-ray analysis have been obtained by preparing a solution of **D3** (10.5 mg, 0.020 mmol) and **9** (7.6 mg, 0.020 mmol) in 0.5 ml of MeOH and placed into straight sample tubes. On to this solution was layered 1 ml of CH_2Cl_2. The sample tubes were sealed with parafilm and left to stand at room temperature for 4 weeks. M.p.: 167-168 °C (d). Elemental analysis found (calc. for $C_{43}H_{35}N_3O_4P_2S_4Ni$; formula mass = 906.7 uma): C, 54.12 (56.97); H, 3.88 (3.89); N, 4.48 (4.63); S, 13.12 (14.14). FT-IR (KBr, 4000-400 cm^{-1}): 3449 vw, 1594 s. 1571 ms, 1498 s, 1479 w, 1460 w, 1416 w, 1404 vw, 1205 w, 1292 m, 1255 vs, 1177 s, 1113 s, 1031 vs, 890 mw, 826 w, 812 m, 761 m, 696 ms, 625 m, 547 s, 522 w, 439 mw cm^{-1}. FT-Raman (4000-0 cm^{-1}, 600 mW, solid in KBr, relative intensities between parentheses related to the highest peak taken equal to 10.0): 2217 (10.0), 1578 (2.6), 1174 (1.7), 1129 (0.9), 1032 (1.4) 993 (0.8) cm^{-1}.

3.4.24 [Ni(EtOdtp)$_2$·(1,3,5-tris(3-pyridylethinyl)benzene)]$_\infty$,(D4·L6)$_\infty$

[Ni(EtOdtp)2](D4) (27.7 mg, 0.05 mmol) and 1,3,5-tris (3-pyridylethynyl)benzene (L6) (19.1 mg, 0.05 mmol) were reacted at 120 °C in a high pressure Aldrich tube in 15 mL of EtOH. and 15 mL of CHCl3 (amylene stabilized). After complete dissolving of the reagents, the reaction mixture was slowly cooled at room temperature. After two weeks (D4·L6)∞ (5.2 mg, 0.006 mmol, 11 % yield) was obtained as green crystals suitable for X-ray analysis M.p.: 135-141 °C (d) at 160-162 °C (m). Elemental analysis found (calc. for C45H39N3O4P2S4Ni; formula mass = 934.7 uma): C, 48.77(57.83); H, 3.85 (4.21); N, 5.04 (4.50); S, 13.28 (13.72). FT-IR (KBr, 4000-400 cm–1): 3449

vw, 2971 w, 2834 vw, 1594 s, 1569 w, 1499 s, 1477 m, 1459 w, 1439 vw, 1428 w, 1405 w, 1385 w, 1293 m, 1254 vs, 1177 s, 1113 vs, 1030 vs, 938 s, 872 w, 827 m, 802 m, 777w, 754 w, 695 s, 651 s, 624 s, 546 vs, 521 w, 490 vw, 446 w cm-1.

3.4.25 $[Ni((MeO)_2PS_2)_2 \cdot (N,N',N''\text{-tris(3-pyridin)benzene-1,3,5-tricarboxamide})]_\infty$, $(\mathbf{D1 \cdot L7})_\infty$

A solution of $[Ni((MeO)_2PS_2)_2]$ (**D1**) (30.4 mg, 0.08 mmol) in 10 $CHCl_3$ was added dropwise to a solution of N,N',N''-tris(3-pyridin)benzene-1,3,5 tricarboxamide) (**L7**) (29.2 mg, $6.7 \cdot 10^{-2}$ mmol) in 20 ml of MeOH. The resultant solution was placed into a vial and slowly cooled at room temperature for ten days. A green powder was obtained (25mg, $3.8 \cdot 10^{-2}$ mmol; 43%). Green crystals of $(\mathbf{D1 \cdot L7})_\infty$ suitable for X-ray analysis have been obtained by reacting **(**7.6 mg, 0.02 mmol) of **D1** and 7.3mg, ($1.67 \cdot 10^{-2}$ mmol) in 15 mL of EtOH. and 15 mL of $CHCl_3$ (amylene stabilized) at 130 °C in a high pressure Aldrich tube, but they did diffract. (3.2 mg, $0.4 \cdot 10^{-2}$ mmol, 21 % yield) M.p.: 170 °C (d). FT-IR (KBr, 4000-400 cm^{-1}): 3492 w, 2901 vw, 1642 w, 1489 w, 1209 w, 1030 w, 1420 m, 1380 w, 1277w 1248 w, 1168 w, 1118 m, , 801 w, 708 w, 650 w, 513 w cm^{-1}.

3.4.26$[Ni((EtO)_2PS_2)_2 \cdot (N,N',N''\text{-tris(3-pyridin)benzene-1,3,5-tricarboxamide})]$, $[\mathbf{D2(L7)_2}]$

$[Ni((EtO)_2PS_2]_2$ (**D2**) (42.8 mg, 0.09 mmol) and (N,N',N''-tris(3-pyridin)benzene-1,3,5 tricarboxamide) (**L7**) (19.2 mg, 0.04 mmol) were reacted at 130 °C in a high pressure Aldrich tube in 10 mL of $CHCl_3$ (amylene stabilized) and 20 mL of EtOH. After complete reagents dissolving, the reaction mixture was slowly cooled at room temperature. Twentyfour hours after, was obtained a green powder of **$[D2(L7)_2]$** (30 mg, $0.03 \cdot 10^{-3}$ 24% yeld) and few green crystals were obtained by high pressure Aldrich tube in 15 mL of EtOH. and 15 mL of $CHCl_3$.) M.p.: 174-176 °C. FT-IR (KBr, 4000-400cm^{-1}): 3456 vw, 2908 w, 1639 w, 1482 m, 1250 w, 1412 m, 1401 mw, 1385 m, 1262 w, 1191 w, 1156 w, 1016 s, 943 s, 896 w, 785 w, 665 m, , 647 w, 525 w, 531 vw cm^{-1}.

3.4.27$[Ni(MeOdtp)_2 \cdot (N,N',N''\text{-tris(3-pyridin)benzene-1,3,5-tricarboxamide})]$,$[D3(L7)_2]$

$[(Ni(MeOdtp)_2]$(D3) (26.2 mg, 0.04 mmol) and (N,N',N''-tris(3-pyridin)benzene-1,3,5 tricarboxamide) (L7) (19.0 mg, 0.04 mmol) were reacted at 120 °C in a high pressure Aldrich tube in 30 mL of MeOH and 5 mL of $CHCl_3$ (amylene stabilized). After complete dissolving of the reagents, the reaction mixture was trasferred in a vial and slowly cooled at room temperature. After two weeks $[D3(L7)_2]$ (18.9 mg, 0.02 mmol, 20 % yield) green crystals suitable for X-ray analysis have been

obtained. M.p.: 175°C (d). FT-IR (KBr, 4000-400 cm^{-1}): 3485 w, 3110 w, 2998 w, 1585 vs, 1579 s, 1450m, 1421 m, 1386 m, 1281s 1238 vs, 1170 m, 1110 s, 1035 s, 943 m, 820 w, 811 m, 768 w, 648 m, 612 m, 530 m, 512 w cm^{-1}.

3.4.28 $[Ni(EtOdtp)_2$·(N,N',N''-tris(3-pyridin)benzene-1,3,5- tricarboxamide)$]_\infty$,$(D4·L7)_\infty$

$[Ni(EtOdtp)_2]$(D4) (43.7 mg, $0.09·10^{-2}$mmol) and N,N',N''-tris(3-pyridin)benzene-1,3,5 tricarboxamide (L7) (44.1 mg, 1.02 mmol) were reacted at 120 °C in a high pressure Aldrich tube in 15 mL of EtOH. and 15 mL of $CHCl_3$ (amylene stabilized). After complete dissolving of the reagents, the reaction mixture was slowly cooled at room temperature. After two weeks $(D4·L7)_2$ was obtained as a few green crystals suitable for X-ray analysis that did not diffracted, instead. M.p.: 170 °C (m). FT-IR (KBr, 4000-400 cm^{-1}): 3490 w, 3112 w, 3002 w, 1599 vs, 1583 s, 1452 m, 1420 m, 1385 m, 1280s 1250 vs, 1182 m, 1116 s, 1038 s, 942 m, 810 w, 801 m, 758 w, 651 m, 615 m 550 m cm^{-1}.

3.4.29$[Ni((MeO)_2PS_2)_2$·(N,N',N''-tris(4-pyridin)benzene-1,3,5-tricarboxamide)$]_\infty$, $(D1·L8)_\infty$

A solution of $[Ni((MeO)_2PS_2)_2]$ (**D1**) (22.8 mg, 0.06 mmol) in 10 $CHCl_3$ was added dropwise to a solution of N,N',N''-tris(4-pyridin)benzene-1,3,5 tricarboxamide) (**L8**) (21.9 mg, 0.05 mmol) in 20 mL of MeOH. The resultant solution was left to evaporate at room temperature. After two days $(D1·L8)_\infty$ (16 mg, $1.9·10^{-2}$ mmol, 16 % yield) was obtained as a green powder. Very few green crystals of $(D1·L8)_\infty$ suitable for X-ray analysis have been obtained by reacting (**D1**) (7.6 mg, 0.02 mmol) and (7.3 mg, 0.02 mmol) at 130 °C in a high pressure Aldrich tube in 15 mL of MeOH and 15 mL of $CHCl_3$ (amylene stabilized), but they were solvent loss sensitive and did not diffract. M.p.: 170 °C (d) FT-IR (KBr, 4000-400 cm^{-1}): 3225 w, 2995 w, 1695 vs , 1601 vs, 1512 s, 1430 m, 1315 m, 1308 m, 1212 w 1248 w, 1119 w, 1127 vw, 806 m, 730 w, 703 w, 680 w 528 w cm^{-1}.

3.4.30$[Ni((EtO)_2PS_2)_2$·(N,N',N''-tris(4-pyridin) benzene-1,3,5-tricarboxamide)$]_\infty$, $(D2·L8)_\infty$

$[Ni((EtO)_2PS_2]_2$ (**D2**) (42.8 mg, 0.09 mmol) and (N,N',N''-tris(4-pyridin)benzene-1,3,5 tricarboxamide) (**L8**) (32.1 mg, 0.07 mmol) were reacted at 130 °C in a high pressure Aldrich tube in 15 mL of $CHCl_3$ (amylene stabilized) and 10 mL of EtOH. After complete reagents dissolving, the reaction mixture was slowly cooled at room temperature. Twentyfour hours after, precipitated a green powder of $(D2·L7)_2$ (26 mg, 0.03 mmol, 32 % yield). M.p.: >250 °C. FT-IR (KBr, 4000-400cm^{-1}): 3423 vw, 3082 w, 2118 w, 1682 m, 1604 s, 1512 s, 1415 m, 1332 m, 1292 m, 1191 w, 1056 w, 1007 m, 940 w, 866 vw, 830 m, 665 m, , 715 m, 585 w, 527 m, cm^{-1}.

3.4.31 [Ni(EtOdtp)$_2$·(N,N',N''-tris(4-pyridin)benzene-1,3,5 tricarboxamide]$_\infty$,(D4·L8)$_\infty$

[Ni(EtOdtp)$_2$] (**D4**) (27.7 mg, 0.05 mmol) and (N,N',N''-tris(4-pyridin)benzene-1,3,5 tricarboxamide) (**L8**) (22.1 mg, 0.05 mmol) were reacted at 120 °C in a high pressure Aldrich tube in 20 mL of EtOH and 10 mL of $CHCl_3$ (amylene stabilized). After complete dissolving of the reagents, the reaction mixture was trasferred in a vial and slowly cooled at room temperature. After two weeks (**D4·L8**)$_\infty$ (11 mg; 0.01 mmol; 10%) green crystals suitable for X-ray analysis were obtained. M.p.: 172 °C (m). FT-IR (KBr, 4000-400 cm^{-1}): 3426 w, 3016 w, 1686 w, 1608 s, 1522 m, 1452 m, 1335 m, 1291 m 1231 m, 1192 m, 1056 s, 1008 m, 941 m, 830 s, 711 m, 581 w, 524 m 550 m cm^{-1}.

3.4.32[Ni((MeO)$_2$PS$_2$)$_2$·(1,3-benzenetricarboxylic acid, 1,3-bi-3-pyridinyl ester)]$_\infty$, (D1·L9)$_\infty$

A solution of [Ni((MeO)$_2$PS$_2$)$_2$] (**D1**) (47 mg; 0.12 mmol) in 10 ml of $CHCl_3$ (amylene stabilized) was added dropwise to a solution of (**L9**) of (1,3-Benzenetricarboxylic acid, 1,3-bi-3-pyridinyl ester) (50 mg 0.12 mmol) in 20 mL of MeOH. The resultant solution was left to evaporate at room temperature. After twentyfour hours a green powder of (**D1·L9**)$_\infty$ was filtered from the solution and washed with 5ml of methanol (47mg, 0.038 mmol, 33 % yield) M.p.: >250°C °C. FT-IR (KBr, 4000-400 cm^{-1}): 3403 w, 2938 w, 1747 m, 1616 m, 1559 m, 1480 w, 1433 m 1297 w, 1261 vw, 1200 s 1192 w, 1093 m, 1014 m, 796 w, 697 w, 732w w, 659 vw, 640 vw, 615 vw cm^{-1}.

3.4.33 [Ni((EtO)$_2$PS$_2$)$_2$·(1,3-benzenetricarboxylic acid, 1,3-bi-3-pyridinyl ester)Ni]$_\infty$, [2D2·2L9b·Ni(EtOH)$_2$]$_\infty$

[Ni((EtO)2PS2]2 (D2) (10.8 mg, 0.025 mmol) and (1,3-Benzenetricarboxylic acid, 1,3-bi-3-pyridinyl ester) (L9b) (10.2 mg, 0.025 mmol) were reacted at 100 °C in a flask in 10 mL of CHCl3 (amylene stabilized) and 20 mL of EtOH. After complete reagents dissolving, the reaction mixture was slowly cooled at room temperature. Twenty-four hours after, was obtained a green powder of [2D2·2L9b·Ni(EtOH)2]∞ (90 mg, 0.067 mmol, 34% yield). Very few green crystals of [2D2·2L9b·Ni(EtOH)2]∞suitable for X-ray analysis have been obtained by reacting the same quantities of starting materials at 130 °C in a high pressure Aldrich tube in 15 mL of EtOH and 15 mL of CHCl3 (amylene stabilized) M.p.: >250°C. FT-IR (KBr, 4000-400cm–1): 3419 vw, 2901 w, 1749 s, 1615 m, 1577 m, 1479 m, 1432 m, 1389 m, 1298 w, 1186 s, 1091 w, 1013 m, 944 m, 788 w, 733 w, 696 w, , 665 w, cm-1.

3.4.34 [Ni(MeOdtp)$_2$·(1,3-benzenetricarboxylic acid,1,3-bi-3-pyridinyl ester)]$_\infty$, (**D3·L9**)$_\infty$

[(Ni(MeOdtp)$_2$](**D3**) (50.1 mg, 0.09 mmol) and 1,3-Benzenetricarboxylic acid, 1,3-bi-3-pyridinyl ester (**L9**) (10.0 mg, 0.02 mmol) were reacted at 120 °C in a high pressure Aldrich tube in 10 mL of MeOH and 10 mL of $CHCl_3$ (amylene stabilized). After complete dissolving of the reagents, the reaction mixture was transferred in a vial and slowly cooled at room temperature. After twenty-four hours a green powder of (**D3·L9**)$_\infty$ was filtered from the solution. (42mg, 0.035 mmol, 31 % yield) M.p.: >250°C °C M.p.: 175°C (d). FT-IR (KBr, 4000-400 cm^{-1}): 3373 vw, 1747 m, , 1615 m, 1563 m, 1434 m, 1370 m, 1266 m, 1214 m, 1154 w, 1106 vw, 793 w, 717 w, 699 m, 643 w, cm^{-1}.

3.4.35 [Ni(EtOdtp)$_2$·(1,3-benzenetricarboxylic acid, 1,3-bi-3-pyridinyl ester)]$_\infty$, (**D4·L9**)$_\infty$

[Ni(EtOdtp)$_2$] (**D4**) (54.7 mg, 0.012 mmol) and 1,3-Benzenetricarboxylic acid, 1,3-bi-3-pyridinyl ester (**L9**) (50.1 mg, 1.0 mmol) were reacted at 120 °C in a flask in 15 mL of EtOH. and 15 mL of CHCl3 (amylene stabilized). After complete dissolving of the reagents, the reaction mixture was slowly cooled at room temperature. Twenty-four hours after, it was observed the precipitation of a green solid of (D4·L9)$_\infty$, (49.1 mg, 0.034 mmol 38% yield) from the solution that it was filtered and washed with 5mL of methanol. M.p.:>250°C. FT-IR (KBr, 4000-400 cm–1): 2971 w, 1746 s, 1593 s, 1499 m, 1430 w, 1293 w, 1256 s 1250 vs, 1197 s, 1113 s, 1022 s, 938 m, 800 w, 696 w, 660 w, 621 w, 547 m cm-1.

3.4.36 [Ni((MeO)$_2$PS$_2$)$_2$·(1,3-benzenetricarboxylic acid, 1,3-bi-4-pyridinyl ester)]$_\infty$, (**D1·L10**)$_\infty$

A solution of [Ni((MeO)$_2$PS$_2$)$_2$] (**D1**) (100 mg, 0.26 mmol) in 10 ml of $CHCl_3$(amylene stabilized) was added dropwise to a solution of (**L10**) (1,3-Benzenetricarboxylic acid, 1,3-bi-3-pyridinyl ester) (99.0 mg, 0.23 mmol) in 20 ml of MeOH. The resultant solution ~~it~~ was left to evaporate at room temperature. After twenty-four hours a green powder of (**D1·L10**)$_\infty$ was filtered from the solution and washed with 5ml of methanol (85 mg, 0.067 mmol, 29 % yield) M.p.: >250°C °C. FT-IR (KBr, 4000-400 cm^{-1}): 3443 w, 2963 w, 1434 m, 1538 m, 1612 m, 1370 m, 1261 s, 1380 w, 1095 m 1192 w, 1021 m, 800 m, 751 m, 715 m, 601 w, 592 vw, 504 vw cm^{-1}.

3.4.37 $[Ni((EtO)_2PS_2)_2$·(1,3-benzenetricarboxylic acid, 1,3-bi-4-pyridinyl ester)$Ni]_2$, $(D2·L10)_\infty$

$[Ni((EtO)_2PS_2]_2$ (**D2**) (66.8 mg, 0.15 mmol) and (1,3-Benzenetricarboxylic acid, 1,3-bi-3-pyridinyl ester) (**L10**) (67.2 mg, 0.14 mmol) were reacted at 100 °C in a flask in 10 ml of $CHCl_3$ (amylene stabilized) and 20 ml of EtOH. After complete reagents dissolving, the reaction mixture was slowly cooled at room temperature. Twenty-four hours after, was obtained a green powder of $(D2·L10)_\infty$ (56 mg,0.043 mmol 30% yield). M.p.: >250°C. FT-IR (KBr, 4000-400cm^{-1}): 3448 vw, 1610 m, 1521 m, 1476 s, 1434 s, 1374 s, 1261 w, 1103 w, 755 w, 724 w, cm^{-1}.

3.4.38 $[Ni(EtOdtp)_2$·(1,3-benzenetricarboxylic acid, 1,3-bi-4-pyridinyl ester)$]_2$, $(D4·L10)_\infty$

$[Ni(EtOdtp)_2]$ (D4) (10.8 mg, 0.019 mmol) and 1,3-Benzenetricarboxylic acid, 1,3-bi-3-pyridinyl ester (L10) (15.1 mg, 0. 035 mmol) were reacted at 120 °C in a flask in 15 mL of EtOH. and 15 mL of $CHCl_3$ (amylene stabilized). After complete dissolving of the reagents, the reaction mixture was slowly cooled at room temperature. Twenty-four hours after, it was observed the precipitation of a green solid of $(D4·L9)_\infty$, (97.1 mg, 0. 043 mmol) from the solution that it was filtered and washed with 5ml of methanol. M.p.:>250°C. FT-IR (KBr, 4000-400 cm^{-1}): 3449 m, 1609 s, 1522 m, 1477 m, 1435 s, 1375 s, 951 w, 745 w, 726 s cm^{-1}.

4.1 Conclusions

By using the synthetic approaches described in § 3.4, 38 new coordination polymers have been synthesize of which 20 structural characterized. The use of organodithiophosphorous complexes has confirmed their tendency to be axially coordinate by polypyridyl donors, yielding coordination polymers with different geometrical and topological features. The coordination of the donor determines an expansion of the nickel coordination sphere from square planar to distorted octahedral. In all cases the donor molecules act as spacers bridging two adjacent dithiophosphoric units thus forming monodimensional infinite chains. All polymers show a primary structure directly dependent on the nature of the spacer used and linear, waved, zig-zag, or helical shapes, with different Ni-Ni distances have been prepared confirming the fundamental role of the nitrogen donors in the design of the coordination polymers. In fact depending on the ligand rigidity, number, distance and position of donor atoms, various structural topologies and coordination environment of the metal ions may be observed. This notwithstanding, the predictable construction of coordination polymers with predetermined topologies is still a challenging goal. This is the reason why one of the aims of this work was that of finding and outlining which elements can be employed to predict the final structure of the resulting coordination polymer with a certain grade of confidence. On the basis of the result above discussed we can state that the use of rigid spacers or semi-rigid spacers characterized by a unique conformation of the donor atoms confers an elevate grade of predictability. This is case, for example of the rigid bidentate ligands **L1** and **L2** that yielded exclusively the expected monodimensional polymers with almost linear or zig-zag primary motifs depending on the position of the endocyclic nitrogen atoms of the pyridyl rings: ligands featuring *para*-positioned nitrogens lead to linear or almost linear polymers (Fig. 4.1 a), whilst ligands featuring *meta*-positioned nitrogens confer a zig-zag shape to the resulting polymer (Fig. 4.1 b).

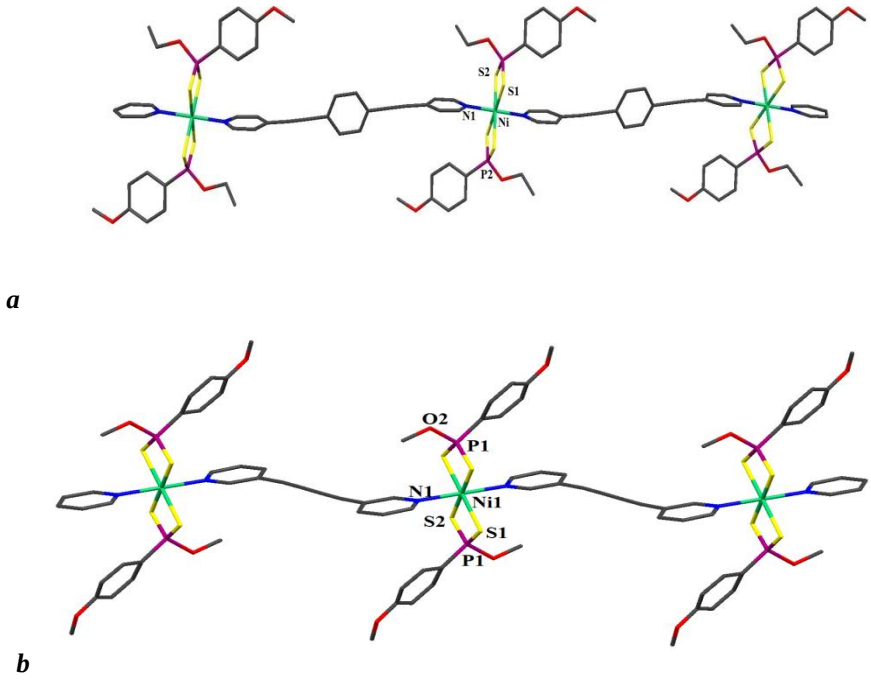

Figure 4.1 Examples of linear (a) and zig-zag (b) Polymers chains obtained with Ligands **L1** and **L2**

We have demonstrated also that helical shapes can be conferred to the coordination polymers by using appropriate ligands, such as **L3**, capable to transfer or impart chiral information. Fig. 4.2 shows the chiral helical coordination polymers obtained by reacting the dithiophosphato complexes **D1** and **D2** with ligand **L3**.[70]

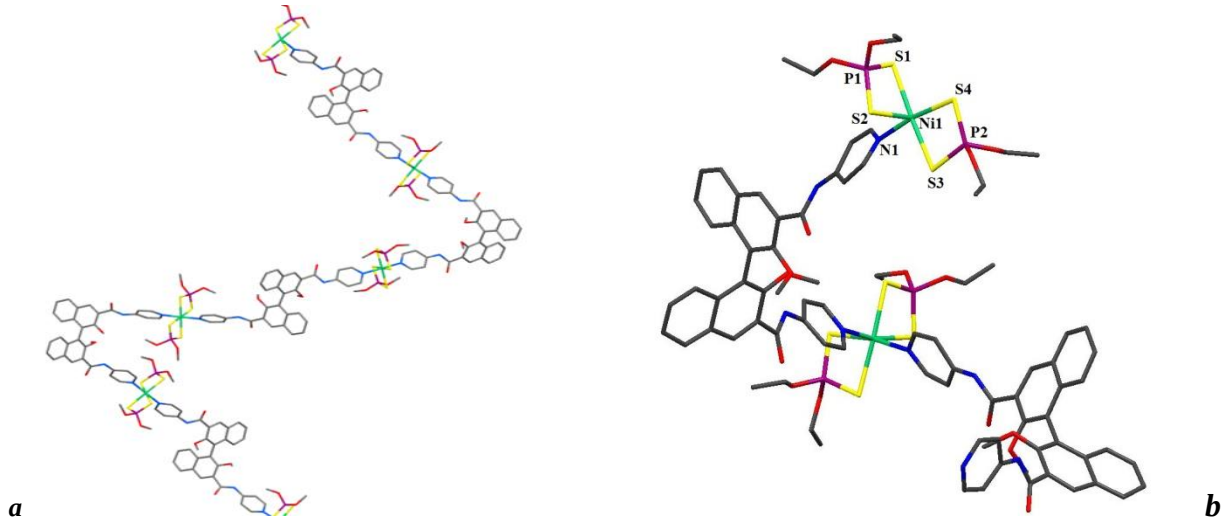

Figure 4.2 Homochiral Helical Chains obtained by using **L3** as spacer: (a) right-handed spiral of Compound $(\mathbf{D1}\cdot\mathbf{L3})_{\infty}$, (b) left-handed spiral of Compound. $(\mathbf{D2}\cdot\mathbf{L3})_{\infty}$.

The case of the less rigid ligands **L4** and **L5** exemplifies how another important factor that affect the predictability of the coordination polymers is the existence of different conformations available

for a certain ligand. The thiadiazolidine **L4** and **L5** are structural isomers which differ for the position of the endocyclic nitrogen atoms in the pyridyl appendages (see § 2.3.2.2). In the case of **L4** an unique conformation is available whilst for **L5**, due to the different position of the nitrogen atoms as a consequence of the different rotational conformations allowed for the pyridyl rings, two planar isomers, cissoid and transoid, and several orientations of the binding sites are achievable. As a consequence, ligand **L4**, even if less rigid if compared with **L1** and **L2**, has proved to lead to highly predictable linear coordination polymers due to the unique coordination conformation available. On the contrary, a convergent and a divergent coordination can be expected for **L5** leading to either dimeric or polymeric constructs as shown in Fig. 4.3.

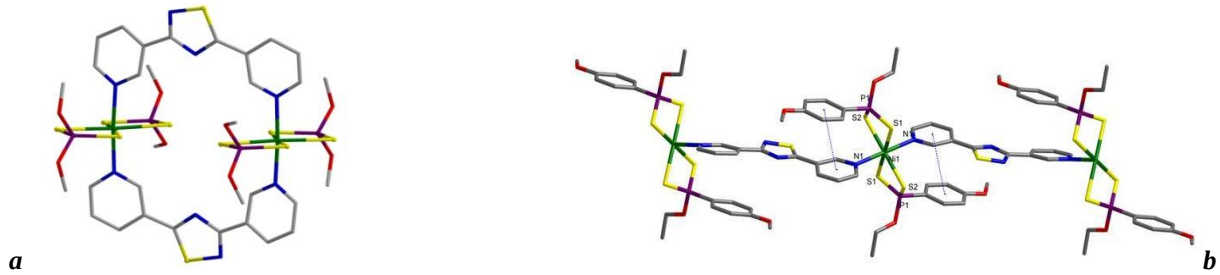

Figure 4.3 Different Products obtained by using **L5** as Spacer: (a) Dimeric Structure of $(\mathbf{D1{\cdot}L5})_2$; (b) Polymeric Chain of Compound $(\mathbf{D4{\cdot}L5})_\infty$.

Many tridentate ligands have been employed with the intent of expand the network dimensionality as a second goal of the research. However, the obtaining of coordination tridimensional networks through the use of Polypyridyl ligands is resulted complicated for two reasons:

- Solvent competition: the used Polypyridyl ligands were insoluble in low polar solvents and appreciably soluble only in methanol and chloroform/methanol mixtures. Unfortunately, the formation of strong H-bonds involving the solvents and the pyridine nitrogen atoms hindered the coordination bond formation and consequently the polymerization of compound, Fig. 4.4.

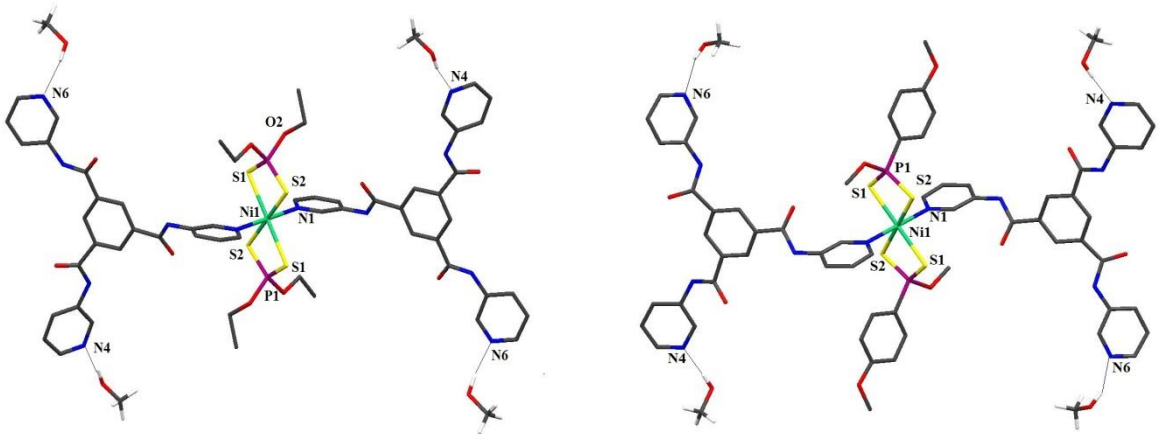

Figure 4.4 Methanol Interactions in [**D2(L7)$_2$**] and [**D3(L7)$_2$**] Complexes.

- Donor atom protonation: in many cases, reaction solvents promote the protonation of the pyridine nitrogen (involving the formation of counter ion interactions) as observed in (**D4·L8**) competing with the coordination bond formation and hindering in this way the tridimensional expansion of the polymer, Fig. 4.5.

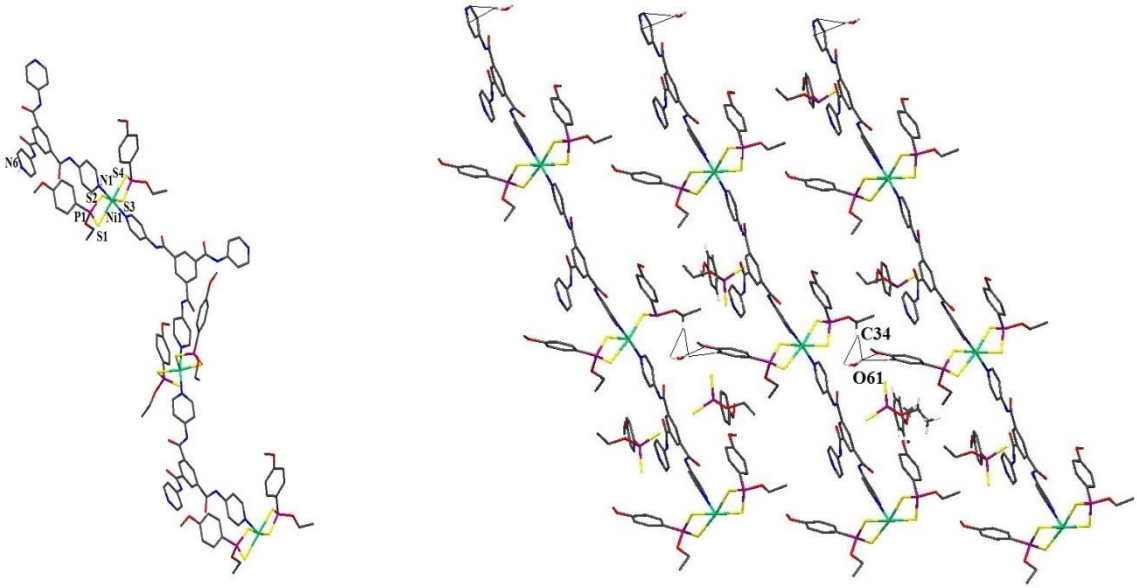

Figure 4.5 Polymeric Chain and main Interaction involving the Dithiophosphonato Anion and Water co-crystallized molecules for (**D4·L8**)$_\infty$.

Finally, some words must be spent on the role of the P-substituents in the phosphorodithioato nickel complexes used as metal nodes. In fact they have been proved to play a crucial role in determining the final network through secondary intermolecular interactions involving the polymeric chains. Depending on the nature of substituents, either H-bonding or aromatic interactions have been found (Fig. 4.6).

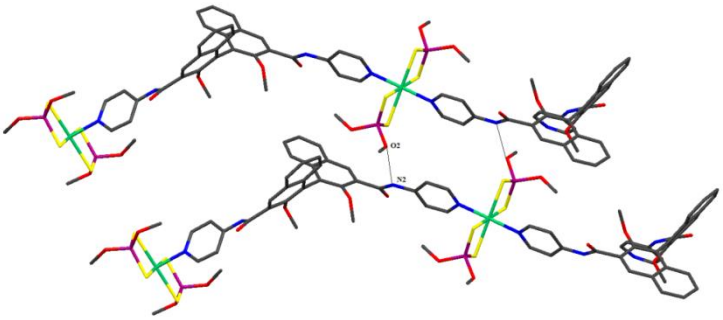

Figure 4.6 Examples of Intermolecular Interactions between the polymeric Chains involving the P-substituents: (a) Hydrogen Bond Interaction (N2-H2··O2; 2.9 Å) between Polymeric Chain of Compound (**D1**·**L3**)$_\infty$

Moreover, the presence of aromatic substituents leads to π···π intramolecular face-to-face and/or edge-to-face interactions, with the pyridyl rings of the Polypyridyl ligands, Fig. 4.7.

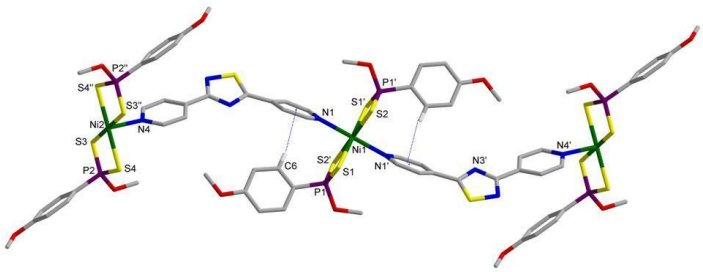

(**D3**·**L4**)$_\infty$

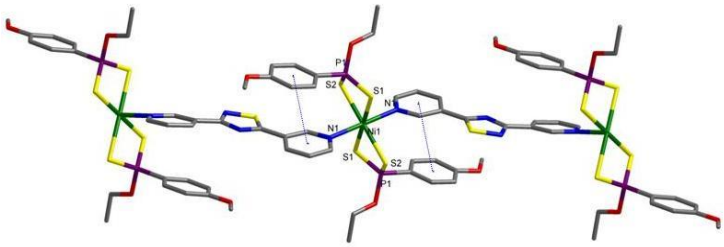

(**D4**·**L5**)$_\infty$

Figure 4.7 Examples of Intramolecular Aromatic Interactions: (a) Edge to Face Interactions in Compound (**D3**·**L4**)$_\infty$; (b) Edge to Face Interactions in Compound (**D4**·**L5**)$_\infty$.

In the most of cases, the polymeric structures are organized in very compact crystal pickings, with the exception of few polymers that showed small cavities in the crystal structure often occupied by solvents, Fig. 4.8

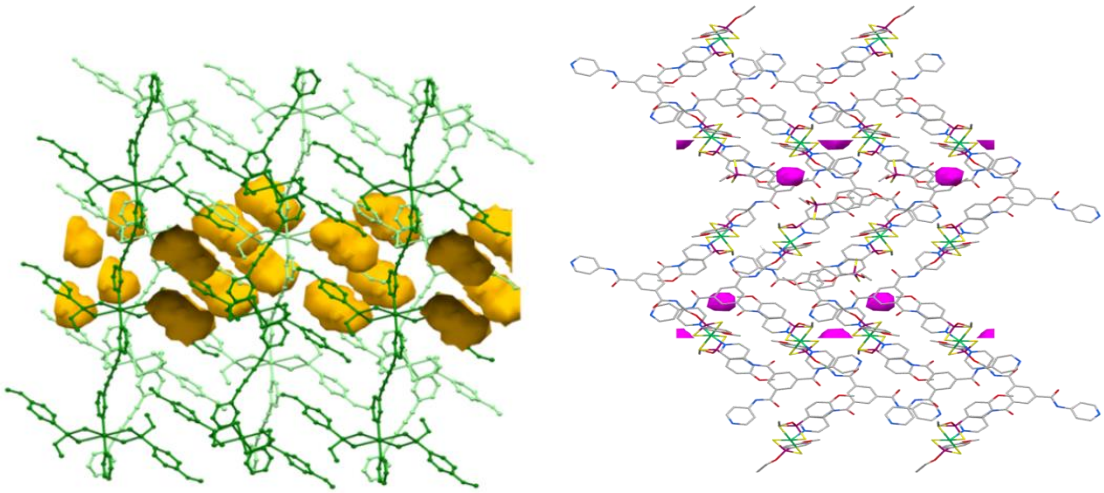

(**D3·L1**)$_\infty$ (**D4·L8**)$_\infty$.

Figure 4.8 Crystal Packing Views of (**D3·L1**)$_\infty$ and (**D4·L8**)$_\infty$ showing the presence of small voids 206.1Å^3 that occupy 5.5% of the unit cell.

4.1 New Perspectives in Coordination Polymers Building-up

The three dimensional network serendipity obtained corresponding to the formulation of [2**D2**·2**L9b**·Ni(EtOH)$_2$]$_\infty$ (Fig. 4.9) containing nickel ions featuring different coordination environments, gave us the inspiration for the design and synthesis of new coordination polymers. Starting from these results new synthetic strategies will be explored combining the use of Ni^{II} phosphorodithioato complexes with different Ni^{II} nodes that can act as building blocks in order to exploit the different coordination behavior of coordinatively unsaturated and free metal ions.

Figure 4.9 Views of [2**D2**·2**L9b**·Ni(EtOH)$_2$]$_\infty$ evidencing the two different coordination environment of Ni0A and Ni1.

References

[1] J.M. Lehn, *Chem. Soc. Rev.*, **2007**, 36, 151-160.
[2] G.V. Oshovsky, D.N. Reinhoudt, W. Verboom, *Angew. Chem. Int. Ed.*, **2007**, 46 (14) 2366–2393.
[3] L.F. Lindoy, I. M. Atkinson, "Self Assembly in Supramolecular Systems", Cambridge, UK, **2000**
[4] G.D. Braga and F. Grepioni Eds, "*Making Crystal by Design: Methods, Techniques and Applications*", Weinheim, **2007**.
[5] R. Pepinsky, Phys. Rev., **1955**, 100, 971.
[6] V.R. Thalladi, B.S. Goud, V.J. Hoy, F.H. Allen, J.A.K. Howard ,G.R. Desiraju, *Chem. Comm*., **1996**, 401-402.
[7] G.R. Desiraju, *Angew. Chem. Int. Ed.,* **2007** ,46, 8342–8356.
[8] G.R. Desiraju, *J. Chem. Sci*., **2010**, 122, 667–675.
[9] J.M. Lehn , *Science*, **2002**, 295, 2400-2403.
[10] C. M. Drain, A. Varotto, I. Radivojevic, *Chem Rev*. **2009**,109(5),1630–1658.
[11] J.W. Steed, J.L. Atwood, "*Supramolecular chemistry"*, 2nd Edition John Wiley & Sons, England, **2009**.
[12] E.D. Glowacki, M.I. Vladu, S. Bauerb, N. S. Sariciftcia, *J. Mater. Chem*., **2013**, 1, 3742-3753.
[13] G.A. Jeffrey, "An Introduction to Hydrogen Bonding", Oxford University Press, Oxford, **1997**.
[14] L.J. Prins, D. N. Reinhoudt, P. Timmerman, *Angew. Chem. Int. Ed. Engl.,* **2001**, 40, 2382-2426.
[15] R. Taylor , O. Kennard, *Acc. Chem. Res.,* **1984**, 17, 320-326.
[16] E.R Tiekink, J. Zukerman Schpector, "*The importance of Pi-Interaction in Crystal Engineering: Frontiers in Crystal Engineering"*, Wiley and Sons, England, **2012**.
[17] C.A. Hunter, K.R. Lawson, J. Perkins, C. J. Urch, J. *Chem. Soc., Perkin Trans*., **2001**, 2, 651-669.
[18] C.G. Claessens, J.F. Stoddart, *Phys. Org. Chem*., **1997**, 10, 254-272
[19] S. Dalai,*Journal of Phys. Sci.*, **2011**, 15, 223-230.
[20] I. Boldog, E.B. Rusanov, A.N. Chernega, J. Sieler, Konstantin V. Domasevitch, *Chem. Soc., Dalton Trans*., **2001**, 893-897.
[21] R.J. Kuppler, D.J. Timmons, Q.R. Fanga, J.R Li, T.A. Makal, M.D. Younga, D. Yuana, D. Zhaoa, W. Zhuanga, H.C. Zhoua, *Coord. Chem. Rev*., , **2009**, 253, 3042–3066.
[22] P. M. Forster, P. M. Thomas, A. K. Cheetham, *Chem. Mater*., **2002**, 14, 17-20.
[23] U. Mueller, M. Schubert, F. Teich, H. Puetter, K. Schierle-Arndt, J. Pastre, *J. Mater. Chem.,* **2006**, 16, 626-636.
[24] A. Y. Robin, K. M. Fromm*, Coord. Chem. Rev*., **2006**, 250, 2127-2157
[25] D. Braga, F. Grepioni, L. Maini, M. Polito, *Struct Bond*, **2009,** 132, 27-49.
[26] T.L Hennigar, D.C MacQuarrie, P. Losier, R.D. Rogers, M. J. Zaworotko, Angew. Chem., Int. Ed. Engl., **1997**, 36, 972-973.
[27] B. Moulton, M.J. Zaworotko, Chem. Rev.,**2001**, 101, 1629–1658.
[28] J.R. Li, R.J. Kuppler, *Chem. Soc. Rev.*, **2009**, 38, 1477-1504.
[29] O.M. Yaghi, M.O'Keeffe, N.W. Ockwig, H.K. Chae, M. Eddaoudi, J. Kim, *Nature*, **2003**, 423*,* 705-714
[30] H. Li, M. Eddaoudi, M.O'Keeffe, O.M. Yaghi, *Nature*, **1999**, 402, 276-279.
[31] D.J Collins, H.C Zhou, *J. Mater. Chem*., **2007**,17, 3154-3160.
[32] Z. Li , G. Zhu , X. Guo , X. Zhao , Z. Jin , S. Qiu, *Inorg. Chem*., **2007**, 46, 5174–5178.
[33] A. Corma, H. García and F. X. Llabrés i Xamena, *Chem. Rev*., **2010**, 110, 4606–4655.
[34] J. Fritsch, M. Rose, P. Wollmann, W. Böhlmann, S. Kaskel, Materials, **2010**, 3, 2447-2462
[35] M. Ohba, H. Okawa, *Coord. Chem. Rev.*, **2000**, 198, 313–328.
[36] I. Goldberg, *Chem. Com*., **2002**, 38, 1243–1254.
[37] M. Arca, A. Cornia, F. Devillanova, A. Fabretti, F. Isaia, V. Lippolis, G. Verani, *Inorg. Chim. Acta*, **1997**, 262, 81-84.
[38] M.C. Aragoni, M. Arca, F. Demartin, F. Devillanova, C. Graiff, F. Isaia, Vito Lippolis, A. Tiripicchio, G. Verani, *J. Chem. Soc., Dalton Trans.*, **2001**, 18, 2671-2677.
[39] M.C. Aragoni, M. Arca, N.R. Champness, M. De Pasquale, F. Devillanova, F. Isaia, V. Lippolis, N.S. Oxtoby, C. Wilson, *CrystEngComm.*, **2005**, 7, 363-369.
[40] P.G. Harrison, M.J. Begley, T. Kikabhai, F. Killer, *J. Chem. Soc., Dalton Trans*., **1986**, 925-928 ; Y. Lin, *Lubr. Eng*., **1995**, 51(10), 855-860.

[41] R.B. Fearing, E.N. Walsh, J. J. Menn, A.H. Freiberg, *J. Agric. Food Chem*., **1969**, 17(6), 1261-1264; D.A. Wustner, J. Desmarchelier, T.R. Fukuto, *Life Sci*., **1972**, 11(11), 583-588; N. K. *Roy, Chemistry of Pesticides*, **1990**.
[42] I. Haiduc, D. B. Sowerby, S.F. Lu, *Polyhedron*, **1995**, 14, 3389-3472.
[43] W.E. Van Zyl, J. D. Woollins, *Coord. Chem. Rev*., **2013**, 257, 718–731.
[44] M. Arca, A. Cornia, F. A. Devillanova, A. C. Fabretti, F. Isaia,V. Lippolis, G. Verani, *Inorg. Chim. Acta*, **1997**, 262, 81-84.
[45]M. C. Aragoni, M. Arca, F. Demartin, F. .Devillanova, C. Graiff, F. Isaia, V. Lippolis, A. Tiripicchio G. Verani, *Eur. J. Inorg. Chem*., **2000**, 10, 2239–2244.
[46] S. F. Martin, A. S. Wagman, G.G. Zipp, M.K. Gratchev, *J. Org. Chem*.,**1994**, 59, 7957-7958.
[47] (a)M.C. Aragoni, M. Arca, F. Demartin, F. A. Devillanova, A. Garau, F. Isaia, F. Lelj, V. Lippolis, S. Pedraglio, G. Verani, J. Chem. Soc. **1999**, 121, 7098-7107; (b) M. Arca, F. Demartin, F. A. Devillanova, A. Garau, F. Isaia, F. Lelj, V. Lippolis, S. Pedraglio, G. Verani. J. Chem. Soc. **1998**, 21, 3731-3736.
[48] M. St. John Foreman, J.D. Woollins, *J. Chem. Soc., Dalton Trans*., **2000**, 10, 1533-1543.
[49] M.C. Aragoni, M. Arca, N.R. Champness, A.V. Chernikov, F.A. Devillanova, F. Isaia, V. Lippolis, N.S Oxtoby, G. Verani, S. X. Vatsadze, C. Wilson, *Eur. J. Inorg. Chem*., **2004**, 2008-2012.
[50] M.C. Aragoni, M. Arca, F. Demartin, F. A. Devillanova, C. Graiff, F. Isaia, V. Lippolis, A. Tiripicchio, G. Verani, *Dalt. Trans*., **2001**, 2671-2677.
[51] M.C. Aragoni, M. Arca, N.R. Champness, Al. V. Chernikov, F. Devillanova, F. Isaia, V. Lippolis, N.S. Oxtoby, Gaetano Verani, Sergey Z. Vatsadze, Claire Wilson, *Eur. J. Inorg. Chem*., **2004**, 2008-2012.
[52] B. Yde, N.M. Yuosif, U. Pedersen, I. Thomsen, S.O. Lawesson, *Tetrahedron*, **1984**, 40, 2047-2052.
[53] A. Beheshti, W. Clegg, V. Nobakht, and R. W. Harrington, Cryst. Growth Des., **2013**, 13 (3), 1023–1032.
[54] M.C. Aragoni, M. Arca, M. Crespo Alonso , F. A. Devillanova, M. Hursthouse, S. L. Huth, F. Isaia, V. Lippolis, G. Verani, *Dalton Trans*., **2009**, 14, 2510-2520.
[55] X. Chen, G. Zhou, X. Pengand, J. Yoon, *Chem. Soc. Rev*., **2012**, 41, 4610- 4630.
[56] F.H. McMillan, F. Leonard, R.I. Meltzer, J.A. King, *J. Pharm. Sci*.,**1953**, 42 (8), 457-464.
[57] M.C. Aragoni, M. Arca, C. Caltagirone, C. Castellano, F. Demartin, A. Garau, F. Isaia, V. Lippolis, R. Montis, A. Pintus, *CrystEngComm*, **2012**, 14, 5809-5823.
[58] S. Hasegawa, S. Horike, R. Matsuda, S.Furukawa, K. Mochizuki, Y. Kinoshita, S. Kitagawa., *J. Am. Chem. Soc*. **2007**, 129, 2607-2614.
[59] T. M. Fasina, J. C. Collings, D. P. Lydon, D. Albesa-Jove, A.S. Batsanov, J. A. K. Howard, P.Nguyen, M.Bruce, A. J. Scott, W. Clegg, S.W. Watt, C. Vineye, T. B. Marder, *J. Mater. Chem.* , **2004**, 14 , 2395–2404
[60] M. J. Thompson, Jennifer C. Louth, G. K. Greenwood., Fiona J. Sorrell, S. G. Knight, N. B. P. Adams, Beining Chen, *Chem.Med.Chem*.,**2010,** 5,1476-1488.
[61] 118688-56-5 1,3,5-Tris(phenylethynyl)benzene.
[62] S.Naien, Y.Gui, H.Min, X.Zheng, *Colloids and Surfaces B: Biointerfaces*, **2008**, 66, 84-89
[63] B.Li, L.Tang, L.Qiang, K.Chen, *Soft Matter,* **2011**, 7, 963-969.
[64] M. C. Aragoni, M.Arca, F.. A. Devillanova, J. R. Ferraro, F. Isaia, F. Lelj, V. Lippolis, G. Verani *Can. J. Chem. Vol*., **2001**,79,1483-1491.
[65] H.Gampp , M.Maeder , CJ Meyer , AD Zuberbühler *, Talanta* ,**1985**,32,257-264.
[66] J.G. Rodríguez, R. Martín-Villamil, F.H. Cano, I. Fonseca, *J. Chem. Soc., Perkin Trans.*, **1997**, 1, 709-714.
[67] (a) D.J. Cram, R. Helgeson, S.C. Peacock, L.J. Kaplan, L.A. Domeier, P. Moreau, K. Koga, J. M. Mayer, Y. Chao, M.G. Siegel, D.H. Hoffman, G.D.Y Sogah, *J. Org. Chem*., **1978**, 43, 1930–1946; (b) M.Asakawa, H.M. Janssen, E.W. Meijer, D. Pasini, J.F Stoddart, *Eur. J. Org. Chem.*, **1998**, 6, 983–986; (c) C. Xin, S. Da, D. Dong, J. Liu, Wei, R. *Tetrahedron Asymm.*, **2002**, 13, 1937–1940.
[68] S. Hasegawa, S. Horike , R. Matsuda, S. Furukawa, K. Mochizuki, Y. Kinoshita, S. Kitagawa, J. Am. Chem. Soc., **2007**, 129, 2607–2614.
[69] A. Westcott, C.J. Sumby, R.D. Walshaw and M.J. Hardie, *New J. Chem*., **2009**, 33, 902-912.
[70] M. Crespo Alonso, M. Arca, F. Isaia, R. Lai, V. Lippolis, S. K. Callear, M. Caricato, D. Pasini S.J. Coles, M.C. Aragoni, *CrystEngComm*, **2014**, 16, 8582-8590.